Application of Polyelectrolytes and Polyelectrolyte Complex Nanoparticles to Improve the Stability of CO_2 Foam in Enhanced Oil Recovery

By

Nishkriya Kalyanaraman

Submitted to the graduate degree program in Chemical and Petroleum Engineering and the Graduate Faculty of the University of Kansas in partial fulfillment of the requirements for the degree of Master of Science in Petroleum Engineering

_____

Chairperson: Dr. Barati, Reza

_____

Dr. Tsau, Jyun Syung

_____

Dr. Vossoughi, Shapour

Date Defended: 01/29/2016

The Thesis Committee for Nishkriya Kalyanaraman

certifies that this is the approved version of the following thesis:

Application of Polyelectrolytes and Polyelectrolyte Complex Nanoparticles to Improve the Stability of CO_2 Foam in Enhanced Oil Recovery

_____

Chairperson: Dr. Barati, Reza

Date approved: 01/29/2016

Table of Contents

List of Figures

List of Tables

Abstract

This research focusses on the application of polyelectrolytes and polyelectrolyte complex nanoparticle system along with a nonionic surfactant to stabilize the CO_2 foam used in enhanced oil recovery applications.

The ratio and pH of the polyelectrolytes are optimized in order to generate nanoparticles that are stable. The interaction of the polyelectrolyte-surfactant CO_2 foam and the polyelectrolyte complex nanoparticle (PECNP)-surfactant CO_2 foam with crude oil in a high pressure, high temperature static view cell was studied. The view cell apparatus was useful in understanding the interfacial properties and stability of the CO_2 foam in the presence of different crude oils. The PECNP-surfactant CO_2 foam system was found to be more durable in the presence of crude oil. Additionally, the influence of polyelectrolytes on the critical micelle concentration of surfactants was also observed through the view cell tests.

A high pressure high temperature rheometer setup was used to study the bulk rheology of the foam under shear for the three different systems and the viscosity was measured with time. It was found that the viscosity of the CO_2 foams generated by these new systems of polyelectrolytes were slightly improved compared to the surfactant generated CO_2 foams.

Foam mobility tests were conducted through the design of a high pressure high temperature core flood apparatus. The setup was designed to include various flow paths for testing the durability and mobility of the foam. The different CO_2 foam systems were tested in the presence of crude oil to determine the incremental oil recovery obtained by each system. Sequential flooding that involved a series of CO_2 foam tests on a particular core presented results that further corroborated the results obtained during the view cell tests. The PECNP-surfactant foam proved to be the most

stable foam in the presence of Mississippian crude oil and resulted in the highest incremental oil recovery compared to the other CO_2 foam systems.

It is imperative to understand the effect of PECNP injection on the core and this was tested by injecting the PECNP solution into a new 3 inch core. The recovered permeability was measured and the damage to the core was found to be insignificant.

Through this research, a stable PECNP-surfactant CO_2 foam was developed and proved to enhance the oil recovery by more than 50% after water flooding.

Acknowledgements

I would like to thank my advisor Dr. Reza Barati for his continuous support, motivation and guidance throughout this project. I also appreciate the invaluable support, time and comments extended by my thesis committee members Dr. Jyun Syung Tsau and Dr. Shapour Vossoughi.

I am grateful to Mr. Alan Walker, Jeff Curly and Scott Ramskill for their help in installing the equipment and experimental setup. I would like to thank the Chemical and Petroleum Engineering Department for financing this project and the Tertiary Oil Recovery Program (TORP) at the University of Kansas for providing help and support. Special mention to Dr. Jyun Syung Tsau from TORP for allowing me to use his laboratory and training me during the initial phases of the thesis. I thank Huntsman for providing samples of the surfactant for the purpose of this research. I would also like to thank Cameron Arnold from the University of Kansas for his assistance in completing the rheology experiments.

I extend my deepest appreciation to all my friends who helped me sail through this journey.

Finally, I dedicate this thesis to my parents (Chandrika Kalyanaraman and Natarajan Kalyanaraman), brother (Nishanth Kalyanaraman) for providing their constant support and encouragement throughout the development of this thesis.

Chapter 1: Introduction

1.1 Thesis Statement

CO_2 has been used commercially as an enhanced oil recovery method for over 40 years [1]. However, CO_2 flooding has some potential weaknesses such as unfavorable mobility ratio, gravity override, early breakthrough of CO_2 and viscous fingering. Different methods have been employed industrially in order to combat these problems. Water alternating gas injection is one of the most commonly applied mobility control technique industrially. Injection of alternate slugs of water and gas improves the sweep efficiency of CO_2. The WAG process does not increase the density or viscosity of the CO_2 and also suffers from reduced injectivity [2] [3]. Thus, the implementation of CO_2 foams for mobility control could address these problems in an efficient manner.

The aim of this research is to develop a more stable CO_2 foam system for enhanced oil recovery (EOR) applications using polyelectrolytes and polyelectrolyte complex nanoparticles. Supercritical CO_2 foams stabilized by surfactants have some potential weaknesses. Surfactants tend to degrade under the high temperature reservoir conditions and they also suffer from adsorption losses to the reservoir rock. Additionally, CO_2 foams lack a stable front in the presence of crude oil as they tend to collapse on contact with the crude oil. These problems can be attributed to the dynamic instability of foam interface as they leave and enter the foam interface. Thus, the long term stability of foams during field applications are hard to maintain. [4]

The following chapters of this thesis will discuss the addition of polyelectrolytes and polyelectrolyte complex nanoparticles to the surfactant solution in order to stabilize the interface using electrostatic forces with a view to generate stronger and longer lasting foams.

The ratio and pH of the polyelectrolytes chosen for this research work was optimized in order to generate the nanoparticles. Subsequently, the interaction between the polyelectrolyte-surfactant CO_2 foam and the polyelectrolyte complex nanoparticle-surfactant CO_2 in the presence of crude oil under high pressure, high temperature conditions was studied using a static sapphire view cell.

The interfacial properties and stability of the CO_2 foam in the presence of different crude oil samples was studied using the view cell apparatus.

When bubbles in a foam come in contact with each other, the thinning of the films and their resistance to rupture are important for the ultimate stability of the foam. Thus, it becomes essential to understand the bulk and interfacial rheology of the foam [5]. The effect of shear on the viscosity of the CO_2 foam is studied through the design of a high pressure, high temperature rheometer setup.

Lastly, the foam mobility and incremental oil recovered was determined through core flood experiments. The extent of damage, if any that could be caused by the injection of nanoparticles is also reviewed in this thesis.

1.2 Layout of the Thesis

Chapter 1 introduces the research topic and its objectives.

Chapter 2 reviews the literature and background of CO_2 flooding, including the theory, mechanisms and drawbacks of using CO_2 flooding. CO_2 foam for mobility control of CO2 was discussed from the current literature available. The role of surfactants and nanoparticles in the generation of CO_2 foams was studied and finally the application of polyelectrolytes and their interactions with surfactants was reviewed.

Chapter 3 summarizes the chemicals used for this research followed by the methods and procedures implemented for the different experiments. The design of three high pressure, high temperature systems that include a rheometer, a core flood setup and a view cell setup are discussed in detail. The working principles of the ZetaPals is also explained.

Chapter 4 presents the results obtained from the tests performed and discusses them. The optimized ratios and pH values of the polyelectrolytes and polyelectrolyte complex nanoparticles are summarized and analyzed. The rheology and view cell tests provide more insight on the stability of the foam films in the presence of different types of oil. The mobility of the different foams are compared and the oil recovered from each of the foam systems are summarized.

Chapter 5 discusses the important findings of the research topic under discussion and summarizes the conclusions derived. This chapter also reviews the scope of future work that could be conducted in order to further understand the foam behavior.

Chapter 6 presents the references that were used and cited for the purpose of this research.

Chapter 7 describes some of the tests that were conducted prior to achieving the final results. This chapter also includes VBA code snippets that were used to calculate the pressure head for the vertical core flood setup.

Chapter 2: Literature Review

2.1 Enhanced Oil Recovery

Oil recovery is divided in three different stages: primary recovery, secondary recovery and tertiary recovery.

Primary production refers to the oil production when the pressure in the subsurface is sufficient enough for the oil to flow naturally to the producer wells. The natural energy for oil production during primary recovery is provided by either of the following:

- Solution gas drive
- Gas cap drive
- Natural water drive
- Fluid and rock expansion
- Gravity drainage

Typically, 15-20 % of the Original Oil in place (OOIP) is produced through primary production. As the production declines, secondary recovery techniques such as water flooding, pressure maintenance and gas injection are implemented. Gas injection for secondary recovery implies the injection of gas into the gas cap for pressure maintenance. Water flooding is the most commonly used secondary recovery method to recover additional oil. Water flooding is known to recover 20-40 % of the OOIP and thereby leaving behind around 60 % of the OOIP [6]. Tertiary oil recovery techniques involve miscible gases, chemicals or thermal energy to displace the remaining oil after secondary recovery. It is not always possible to follow the chronological order of the oil recovery mechanisms since it depends on the nature of the reservoir [6]. Therefore tertiary oil recovery

techniques are considered as enhanced oil recovery methods [6]. These methods not only provide the supplemental energy required for oil production, they also interact with the oil to lower the interfacial tension, density, and viscosity thereby facilitating the flow of oil [6] . Enhanced oil recovery methods include the following techniques:

1. Mobility control
2. Thermal
3. Miscible
4. Microbial
5. Chemical

Mobility control processes aim at improving the mobility ratio between the displacing and displaced fluid. Addition of polymers to water to enhance the viscosity of the displacing fluid and foams to replace gas as the displacing fluid are favorable methods to promote mobility control [6].

Thermal methods include steam injection or in - situ combustion. These methods depend on thermal energy or in-situ generation of heat for the alteration of oil viscosity and favorable phase behavior for the enhanced oil recovery [6].

Miscible flooding is responsible for creating miscibility between the oil and the injected fluid. Thus, the primary objective of miscible flooding is to form a single phase when mixed in all proportions which would facilitate the displacement of oil more efficiently. Common hydrocarbon solvents such as methane or CO_2 are used during this process [6].

Chemical flooding methods involve the injection of chemicals that displace the oil through their phase behavior properties that result in the reduction of the interfacial tension (IFT) between the

oil and displacing liquid. The most common chemical process is the injection of surfactants and polymers with the aqueous phase as the displacing fluid [6].

Microbial Enhanced oil recovery is the process by which microorganisms and nutrients are injected into the reservoir in order to displace the oil. These nutrients release metabolic products and bacteria which mobilizes the residual oil by reducing the IFT thereby enhancing the oil recovery [6].

The scope of this research is within the domain of mobility control process for CO_2. The next few sections will discuss about mobility control process for CO_2 through the implementation of CO_2 foam, as well as generation and stability of these foams in the presence of crude oil.

2.2 CO_2 Flooding

CO_2 flooding has been industrially practiced for over 60 years beginning from the 1950's. It is an established technique that improves oil recovery and can also be used for carbon capture and storage in the geologic formations thereby mitigating carbon emissions. A large volume of conventional oil remain in the US oil reservoirs which could be produced economically by CO_2 EOR. Based on the data from National Energy Technology Laboratory (NETL) and the oil industry, around 1673 fields and reservoirs that account for 146 billion barrels of original oil in place are candidates for CO2 flooding [7] [1]. In the US alone, CO_2 flooding has been underway for several decades in the Permian basin of West Texas and New Mexico. It is also being pursued in other parts of the US [1]. As of 2012, oil recovery from CO_2 EOR accounts for about 6% of the crude oil production which is equivalent to 280,000 barrels of oil per day in the US [1] [7].

Industrially, CO_2-EOR is often implemented as Water Alternating Gas (WAG) through the alternate injection of CO_2 and water slugs. Based on the reservoir conditions such as temperature,

pressure and oil composition, CO_2 EOR can be either miscible in which the injected CO_2 and the hydrocarbons form a single phase fluid with favorable flow properties, or immiscible in which the gas sweeps the oil but does not mix with it to form a single phase fluid [6]. The majority of CO_2 EOR floods are miscible. However, the mobility of CO2 is significantly larger compared to oil thereby resulting in CO2 channeling and early breakthrough of CO2. This increases the gas processing costs and reduces the oil output [1].

2.2.1 Theory and mechanism

CO_2 flooding is a form of miscible displacement wherein the displacing fluid is miscible with displaced fluid. Therefore the interfacial tension is significantly reduced [6]. The process could also be immiscible, but the mechanism would then be similar to water flooding with significantly larger number of viscous fingers. The two different types of miscible displacement are explained below.

First contact miscibility (FCM) - The injected slug of a specified volume is completely miscible with crude oil. The miscroscopic efficiency that can be attained in a miscible process is much higher than an immiscible process and can be as high as 100%, leaving little to no residual oil [6]. If it is implemented as a secondary recovery, a microscopic efficiency of 100% could be attained due to the absence of a water bank [6]. However, as a tertiary recovery technique, the injected slug would have to displace the water bank initially prior to contacting the residual oil. Thereby the oil bank is displaced upon contact [6].

Multiple contact miscibility (MCM) – In this process, the injected slug is not miscible with crude oil under the reservoir conditions upon first contact. The miscibility develops dynamically as the fluid/slug moves through the reservoir. The compositions of the injected slug or crude oil are modified to a certain degree such that the miscibility can be achieved eventually [6]. This

modification could be achieved by two processess known as the vaporizing gas process and the enriched gas displacement process. In the enriched gas displacement process, the injected slug consists of intermediate components ($C_2 – C_6$) and these components are condensed into the crude oil. Thus the crude oil composition is modified and becomes miscible with the injected solvent. For the vaporizing gas process, the heavier components from the crude oil are vaporized thereby making the injected dry gas enriched with these components. Thus the crude oil and the injected gas become miscible with each other [6]..

2.2.2 Advantages and Disadvantages

CO_2 as a dense fluid has many advantages, one of them being its miscibility with lighter hydrocarbon in all proportions for a wide range of temperatures and pressures. Thus the recovery efficiencies by using CO_2 as a miscible displacement fluid are higher than using water as an immiscible displacement method [5]. CO_2 is available at a relatively low cost near oil fields and hence makes it a suitable candidate for enhanced oil recovery [1]. Additionally, CO_2 has a low solubility in water and since CO_2 has been used in reservoirs that have been water flooded, a significant amount of CO_2 is not lost to the water and can be effectively used for displacing the oil [5].

The main disadvantage of CO_2 is its low viscosity compared to crude oil and hence results in a higher mobility of CO_2 compared to oil [1] [6]. Due to this instability of the front, the CO_2 fingers begin to grow and an early breakthrough of CO_2 occurs. High gravity, light crude oil is complex and may contain components that are not completely miscible with CO_2..

In summary, CO_2 flooding suffers from low displacement efficiencies and early breakthrough due to high mobility of CO_2 [6].This thesis focuses on the mobility control of CO_2 by stabilizing CO_2 foam systems using polyelectrolytes and PECNP which will be discussed in detail in later sections.

2.3 Mobility control for CO_2

2.3.1 CO_2 Foam for Mobility Control

Foaming of CO_2 can potentially reduce the mobility of the gas and can result in a favorable macroscopic sweep effeciency [8] [6] [5]. Foams are typically thermodynamically unstable and tend to collapse with time [8]. They are also known to be sensitive in the presence of crude oil and the development of a stable long lasting foam has been underway for many years [5] [9]. A lot of research has been done to find CO_2 thickening agents and other chemical additives to reduce the mobility of CO_2 [1]. However, the most promising technique for mobility control has been the use of CO_2 foams [1].

2.3.2 Foam Generation Theory and Mechanism

Foam as defined by Schramm is considered as a special colloid that comprises of two phases: a gas (internal phase) dispersed in a liquid (continuous phase) [5]. Typically the gas phase is separated from the liquid phase by an interface known as the lamella. Additionally, a foaming agent which could either be surfactants, macromolecules or finely divided solids is used to reduce the surface tension at the interface [5]. The foaming agent is also required to form a protective film at the interface to prevent the coalescence with other bubbles [5].

Foam stability can be described through coalescence (film rupturing) and film thinning [5]. Film thinning results in the thinning of the liquid film between two bubbles. This process does not result in a reduction of total surface area. The fusion of two or more bubbles to form a bigger bubble is referred to as coalescence. Contrary to film thinning, coalescence results in a reduction of total surface area and the rupture of the liquid film [5]. Foams are generally thermodynamically unstable and hence stability of the foam refers to the kinetic stability [5]. The stability of the foam depends on the following interfacial and bulk properties that include steric Repulsion, dispersion forces,

electrical double layer formation between the ions at the interface and the, surface rheology, gravity drainage and capillary suction of the foam. [5].

Foam Generation:

There are three primary mechanisms for the generation of foams in porous media:

1- Snap Off:

When the local capillary pressure is sufficiently lower than the entry pressure of the pore throat, lamellae are formed by the snap off mechanism. Thus, for the gas to enter the pore body, it needs to exceed the local capillary pressure to enter the pore throat [8].

Figure 1: Schematic of Snap off mechanism of foam generation. [9]. The above figure is reprinted with permission from Taylor and Francis Group LLC Books

2- Division: Lamella division occurs when the lamella enters a branching point. As a single mobile lamella passes by a pore throat that does not contain any liquid phase or another lamella, the mobile lamella either breaks or spans the throat [5]. Thus, a moving foam can create a lamella as they break [8]

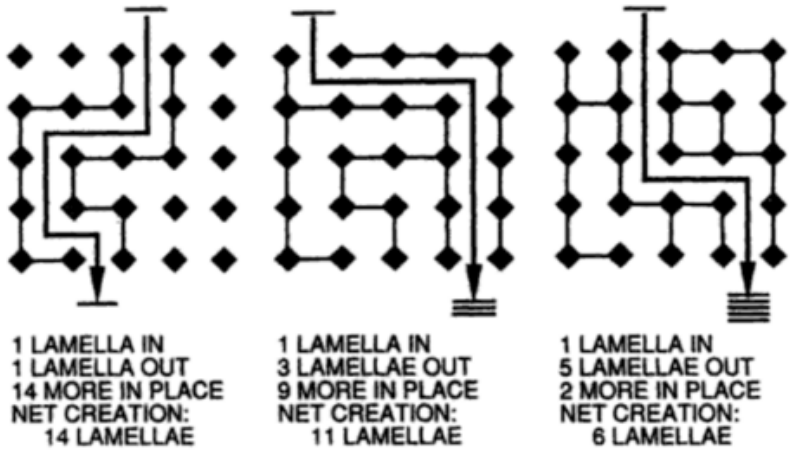

Figure 2: Schematic of Lamella Division mechanism of foam generation [9]. A lamella is created between two points as depicted in the above schematic.The above figure is reprinted with permission from Taylor and Francis Group LLC Books

3- Leave Behind: This mechanism of foam creation occurs when the gas enters a porous medium that is initially saturated with surfactant solution. The lamella is created in the pore throats when the gas enters from different directions [8]. Leave behind foam generation occurs during drainage, when the gas saturation increases [8].

Snap Off mechanism is found to be the most dominant mechanism for foam generation from experimental observations [10].

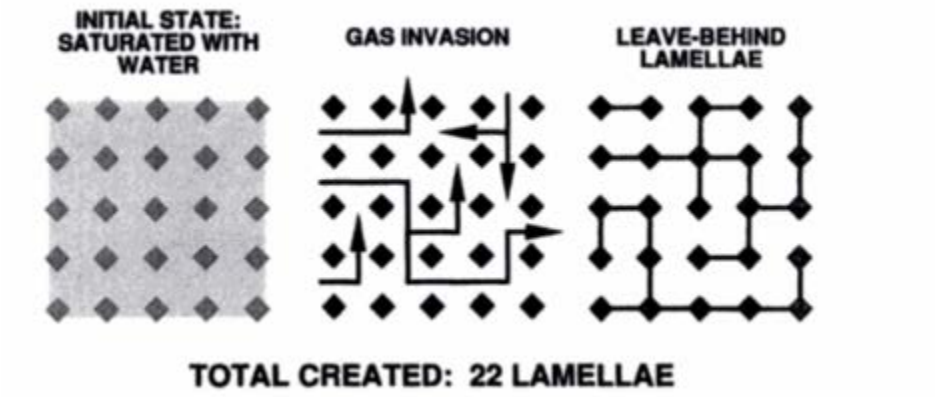

Figure 3: Schematic of Leave behind mechanism of foam generation [8]. Each lamella is created between two points as depicted in the above schematic. The above figure is reprinted with permission from Taylor and Francis Group LLC Books

2.3.3 Foam in the Presence of Oil

Foams are known to be destabilized by the presence of most oils [5]. Studies show that the stability of the foam depends on the nature of the foam and also the nature of the oil. In particular, foams in porous media also depend on the residual oil saturation [9]. The presence of residual oil saturations greater than 20% can destabilize the foam and lower the mobility reduction factor which could have been achieved at lower oil saturations [5]

The composition of crude oil also plays an important role in the destabilization of foam. A decrease in foam stability has been observed for lighter crude oil [5]. This phenomenon could also be attributed to the viscosity of the oil. The more viscous oil might emulsify slower if a stable pseudoemulsion is formed, which could possibly delay the rate of foam lamella rupture [5].

In general, the destabilization of foam by oil in a porous media are described to have the following steps according to Schramm [5]:

1. Penetration of oil into the foam lamellae is known as oil imbibition. Depending upon the stability of the pseudo emulsion film, this process could either be detrimental or in favor of the foam stability i.e. if the pseudo emulsion film is stable, the foam would be stable. Pseudo emulsion thinning is known to be the most dominant mechanism of destabilization and occurs when there is continuous injection of gas into a surfactant flooded porous media at residual oil saturation [11]. A pseudo emulsion film is formed when some of the oil is

emulsified into the aqueous phase and this new film seperates the gas and remaining oil [11].

2. Perturbation of the lamellae due to the penetration of the oil or Marangoni flow (contraction and expansion of lamella)
3. If the penetration of the oil or thinning of the pseudo emulsion does not result in the rupture of the foam lamellae, the spreading of the oil across the interface could result in the lamella destruction.

Farajzadeh et al found that if the surfactant (foaming agent) is injected into the reservoir prior to the injection of supercritical CO_2 above minimum miscibility pressure(MMP), the oil recovered is much more than a regular CO_2 flood [12]. However, there is no improvement in oil recovery if supercritical CO_2 (less than the minimum miscibility conditions) is injected when the surfactant is already present in the reservoir. Thus, the formation of CO_2 foam above MMP proves to be improve the oil recovery [12].

2.3.4 Influence of Wettability of the Rock on Foam Stability

Most petroleum reservoirs are intermediate wet, oil wet or mixed wet in nature. The addition of surfactant is known to alter the wettability of the rock formation from hydrophobic to hydrophilic.

Huh et al. [13] found that the micromodel wettability could be altered to intermediate or oil-wet as a result of crude oil saturation. Schramm and Mannhardt [5] conducted oleophilic micro visual cell experiments with different foams. They found that foams were least stable in the presence of crude oil and oleophilic surfaces compared to crude oil in hydrophilic surfaces. Suffridge et al [14] suggested the same results based on core flood tests. Thus, they concluded that foams were more stable in water wet cores than oil wet cores. It is possible for the surfactants forming the foam to

alter the wettability of the formation. It should be noted that the surfactants that alter wettability are different from typical surfactants. In the case of the CO_2 foam generated by surfactants, the wettability could be altered by the CO_2 as well [15]. The oil wet formation would then become water wet thereby resulting in a more effective and stable foam. This result is consistent with the core-flood tests of Sanchez and Hazlett [16] in which foaming surfactants caused wettability reversal in oil wet porous media. This reversal was hypothesized to be the reason that stable foams could be generated and propagated in their oil-wetted cases.

2.3.5 Surface Chemistry

The interface of the foam film carries an interfacial charge on either side of the film. Depending on the charge density and the film thickness, either van der Waals force or repulsive forces will stabilize the foam by preventing the thinning of the film [5]. Depending on the charge of the ions that are either attracted or repelled at the surface, an electric double layer is formed (EDL). The EDL has two layers, an inner layer that includes adsorbed ions and a diffuse layer that have distributed ions depending on the electrical forces and thermal motion [17]. The different forces that dominate the stability will be discussed in detail in the next few sections.

When the EDL overlaps due to the repulsion between the two charged interfaces, the foam is stabilized by repulsive forces [5]. As the thickness of the foam film decreases from the metastable common black film state, the repulsive forces dominate [5]. However as the film thickness decreases further, the attractive van der Waals forces dominate and a more stable newton black film is formed [5]. The atomic electron clouds overlap when the separation between the two charged interfaces are very small [5]. This results in a stronger repulsion and is called the born repulsion and dominates the stability of the newton black films which are extremely thin [5]. The

DVLO (Derjaguin Landau Verwey Overbeek) theory, also known as the total interaction theory includes the energy changes due to the forces of attraction and repulsion with distance [17].

In general, a system can be stabilized by steric repulsion by the addition of a suitable polymer that can adhere on to the interface thereby preventing the two interfaces from interacting with each other [18] [19]. If flocculation is desired for the final application, electrostatic or charge stabilization should be dominant and a desired chemical is required to alter the charge of the interface [19]. For the purpose of this research, the final application is to stabilize the foam film without any flocculation. Thus, polyelectrolytes are added to the surfactant to stabilize the foam film by providing a coating that is thick enough to prevent the foam lamella from interacting. In addition to just the addition of polyelectrolytes, this research studies the effect of a polyelectrolyte complex nanoparticle with surfactant on the stability of the foam film. The next few sections describe the role of the surfactants and nanoparticles in the stability of foam films and the research done in these domains so far.

2.3.6 Role of Surfactants in CO_2 Foam Generation

CO_2 foams used for mobility control of high pressure CO_2 are typically generated by surfactants [17]. Surfactants are surface active agents that are both amphiphilic and amphipathic. They are short chain fatty acids that have a hydrophilic head and a hydrophobic tail which have an affinity towards polar and non-polar media [17]. The role of surfactants in the stabilization of CO_2 foam films can be explained by the equilibrium between the capillary pressure and disjoining pressure [20]. Surfactants tend to reduce the gas-liquid interfacial tension thereby reducing the capillary pressure and surface energy. This in turn reduces the drainage. The surface charge at the interface is increased by the presence of surfactants which enhances the repulsive forces between the gas-liquid interfaces [20].

Surfactants are energetically favorable when oriented at the interface or surface since this allows the head and tail to be attached to their preferred media [17]. Surfactants help in lowering the interfacial tension due to their adsorption at the interface [17]. The adsorption of surfactants at the interface provides an expanding force against the normal interfacial tension [5]. This can also increase the interfacial viscosity thereby providing a resistance to film thinning and rupturing [5].

Types of Surfactant:

Surfactants are amphiphilic in nature as they consist of both a hydrophilic head group and a hydrophobic alkyl tail group. Figure 4 s a schematic diagram that represents the head and tail group of a surfactant.

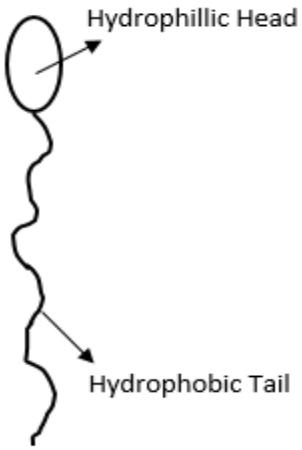

Figure 4: Structure of a surfactant [21].

The tail part may contain one or more alkane chains or ring structures which are either linear or branched. The hydrophobic tail can be a hydrocarbon, fluorocarbon or a siloxane while the hydrophilic head group can be anionic, cationic or neutral. The head group determines the properties of the surfactant. The surfactants are classified as non-ionic, ionic, or zwitterionic based on the charge carried by the head group. Figure 5 represents the different types of surfactants.

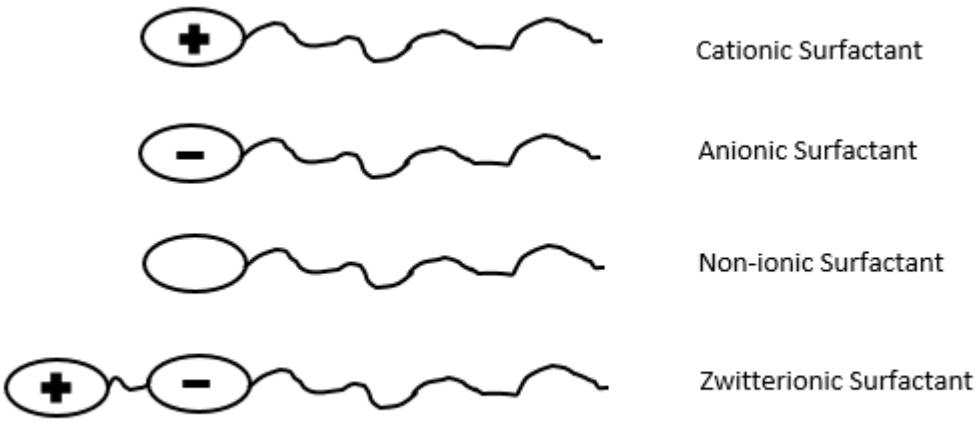

Figure 5: Classification of surfactants [22]

Critical Micellar Concentration and Foam Stability

Surfactants behave as electrolytes in dilute concentrations and at higher concentrations they form aggregates called micelles [17]. The lipophilic part of the surfactant are associated to the interior of the aggregates forming the micelles while the hydrophilic parts face the aqueous medium. The concentration at which the surfactants form micelles is termed as the critical micelle concentration (CMC) [17]. The formation of micelles is opposed by the electrostatic and thermal forces and hence it is of great importance for the formation of foams [17]. The CMC can typically be lowered by the addition of electrolytes and lowering the temperature [17].

Different mechanisms control the stability of the foam depending on weather the surfactant concentration is above or below the CMC [17]. Surface rheology controls the stability of the foam below the surfactant concentrations below CMC [17] [5]. Once the foams film attains a critical film thickness, the film either deteriorates or reaches a stable state. It was mentioned that an

increase in surface viscosity would increase the surface mobility and hence result in a longer drainage time [5]. Thus, the study of rheology becomes crucial in understanding the behavior of the foams.

At surfactant concentrations above the CMC, the surface rheological properties do not play an important role and are of secondary importance for the film stability [17]. Stratification or stepwise thinning of foam films occurs [22]. The ordering of micelles in the liquid phase as well as inside the bulk phase of the foam takes place. Foams that have a thin film, become thinner due to the phenomena of stratification and it could take many steps to attain equilibrium [17] [5]. Thus, it is ideal to maintain the surfactant concentrations below the CMC for the formation of foams.

Non-Ionic Surfactants

According to the Bancroft's rule, surfactants are more soluble in the continuously dispersed phase like brine as opposed to the gaseous phase like CO_2. Thus, foams are typically stabilized by water soluble surfactants. However, in the recent past, it was found that certain nonionic surfactants could be soluble in CO_2 as well thereby facilitating the in situ generation of CO_2 in brine foams for mobility control [23]. Huntsman's SURFONIC N, a commercially available nonionic surfactant is a nonylphenol ethoxylate that has 12-15 ethylene oxide repeat units. Additionally, from literature review [1] the use of Surfactant alternating gas (SAG) for mobility control has also been studied. In this method, alternate slugs of aqueous surfactant is injected followed by slugs of CO_2. This would require the CO_2 to flow through the same path as that of the aqueous surfactant solution injected. The use of nonionic surfactant with CO_2 directly will ensure that the surfactant is available for foam generation wherever the CO_2 flows [23]. This concept was first proposed by Bernard and Holm in their 1967 patent as well [24].

2.3.7 Role of Nanoparticles in CO_2 Foam Generation

The tendency of nanoparticles to adsorb at the fluid-fluid interface are known to stabilize drops in emulsions and bubbles [4]. This is due to the fact that they have a high adhesion energy for particle adsorption, particularly at the foam interface [4]. Thus, long term foam stability can be achieved. The equation to calculate the energy of adhesion for a particle is as follows:

$$\Delta G_{ad} = \pi\alpha^2\gamma_{ow}(1-|\cos\theta|)^2,$$

where

α is the particle radius;

γ_{ow} is the interfacial tension;

θ is the contact angle through the aqueous phase.

This equation shows that for the substitution of typical values of the above parameters, the adhesion energy is of the order of several thousands of kBT [25]. This is much larger than the adsorption and desorption energy of a typical surfactant molecule at the oil-water interface which of the order of kBT [25]. The stability and equilibrium of the solid particle layers at the fluid-fluid interface could be attributed to three factors: electrostatic repulsion, van der Waals attraction and capillary attraction forces [26] and [27].

Binks and Jameson ([28] and [29]) have reviewed the behavior of nanoparticle stabilized emulsions and foams in detail as well. Johnston et al. pioneered the use of nano-silica for the generation of Pickering emulsions of CO_2-in-water as opposed to the traditional surfactant stabilized CO_2 foam [28]. Although not explicitly stated, the work could be an application for mobility control in enhanced oil recovery processes. Espinosa et al. has also reported CO_2 in water

foams that were generated using silica nanoparticles in the absence of surfactants [4]. In another literature review, it was summarized that 50% SiOH nanoparticles could generate stronger and more stable CO_2 foams compared to PEG-coated silica nanoparticles [30]. Metal nanoparticles were used by Shah to enhance the thermal conductivity of supercritical CO_2 in order to reduce the viscosity of heavy oils rapidly [31].

Additionally, recent literature summarizes the use of fly ash to stabilize CO_2 foams, which is a cheaper and more widely available nanoparticle. Singh et al reported that thermally treated fly ash could stabilize anionic surfactants and generate a stable foam in the absence of oil in a porous media [32] . However, they observed antagonistic effects when the nanoparticles were used along with nonionic surfactants.

The process of stabilizing foams with small particles may be easier to perform in a smaller scale than injecting an aqueous dispersion of nanoparticles into a porous medium due to the requirement of high shear to generate these foams [4]. Although the nanoparticle-stabilized CO_2 foams can stabilize the foam for longer periods, the stability of these foams in the presence of crude oil in cores and their ability to recover oil have not been explored extensively. Additionally, most of the nanoparticles that are commercially available are non-surface active and would have to be surface activated in order to stabilize foams [33].

In the following sections, the advantages of adding polyelectrolyte and polyelectrolyte complex nanoparticles to surfactants in order to stabilize the CO_2 foams will be discussed from the current literature available.

2.4 Polyelectrolytes

Polyelectrolytes are polymers that have ionic groups as their repeating units. These groups dissociate in an aqueous solution (polar medium such as water) thereby making the polymer chains charged and releasing counter ions. The dissociation process results in an increase in entropy of the system which is opposed by the electrochemical potential [34]. Thus the increase in entropy is the driving force for the release of counter ions into the aqueous solution and the electrochemical potential attracts the oppositely charged counter ions to the polyelectrolyte chain [35] [36]. This process results in the creation of an equilibrium state composed of free and condensed counter ions around the polyion which is similar to the electrical double layer for dilute colloids. Ion condensation is also known as Manning theory [35] [34]. Figure 6 represents the schematic of the equilibrium state developed during the above process.

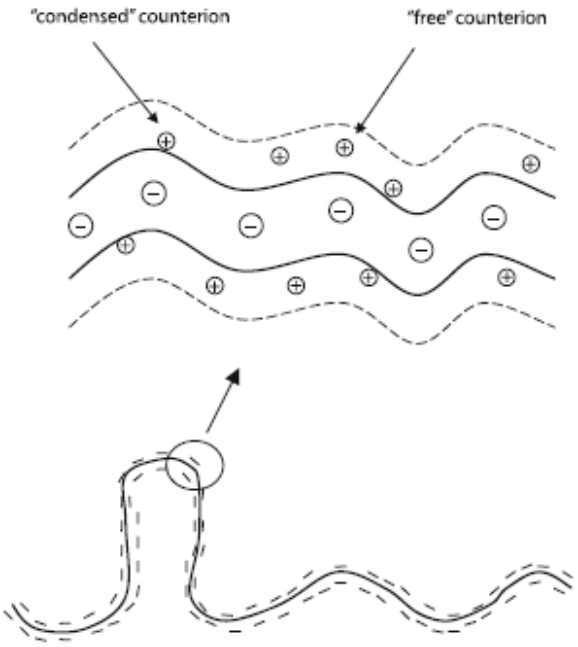

Figure 6: Schematic diagram showing the condensed and free states created around the polyion in dilute solutions [34].The above figure is reprinted with permission from Springer Science and Bus Media B.V.

Classification of Polyelectrolytes

There are different types of polyelectrolytes that can be classified based on their ability to dissociate in an aqueous solution [34]. Polyelectrolytes that can dissociate completely in macro ions and counter ions through a whole range of pH are considered to be strong polyelectrolytes (example – Sodium polystyrene) while those that do not dissociate at certain pH values are considered to be weak polyelectrolytes (polyacrylic acid) [35].

Polyelectrolytes typically have the viscosity of a polymer and the electrical properties of an electrolyte [34]. Polyelectrolytes are also classified depending on their charge:

1. Polycation – the ionic group is positively charged

2. Polyanion – the ionic group is negatively charged

3. Polyampholytes – they carry both anionic and cationic groups

Proteins are an example of polyampholytes and they become positively charged in an acidic medium, negatively charged in an alkaline medium and neutrally charged at the isoelectric point.

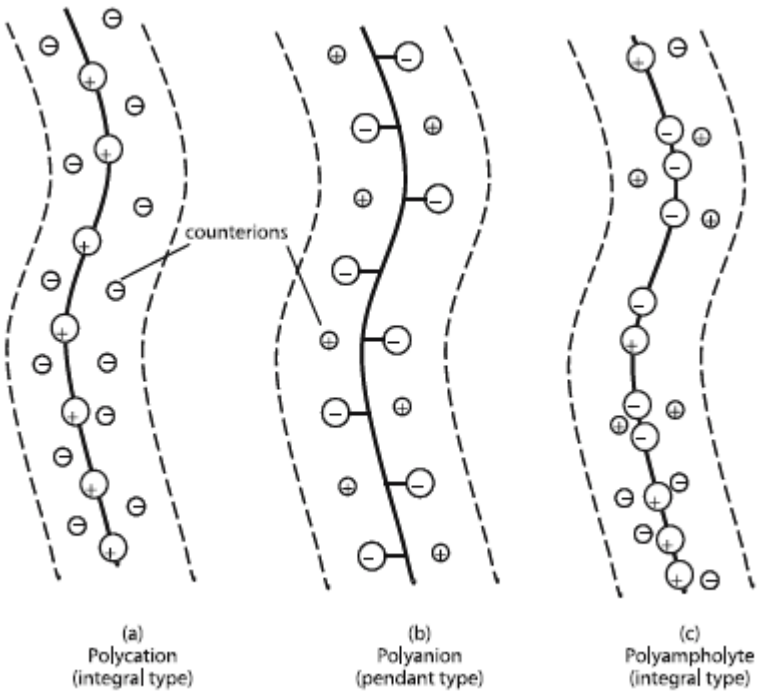

Figure 7 : Schematic diagram representing the different types of polyelectrolytes based on their charge [34]. The above figure is reprinted with permission from Springer Science and Bus Media B.V.

Polyelectrolytes that have a broad range of size, shape and mass characteristics are usually characterized by their polydispersity index [34]. Polydispersity index is the measure of the distribution of molecular mass in a given sample of polymer [34]. The next section reviews the theory behind the polyelectrolyte and surfactant interactions.

2.4.1 Polyelectrolyte and Surfactants

There are two primary forces that govern the thermodynamic stability of surfactant and polyelectrolyte binding.

1. Electrostatic forces
2. Hydrophobic forces

Electrostatic interaction is due to the coulombic attraction between the oppositely charged ions and thus results in the release of counter ions [36] [34]. Thus, the polyelectrolyte-surfactant binding results in a significant entropy gain [37]. The electrostatic interaction depends on the charge density to a great extent. Below a critical charge density, the binding is controlled by the hydrophobic forces [38].

Hydrophobic forces occur due to a large gain in the entropy of the system through the discharge of unfavorable water molecules surrounding the hydrophobic regions during the binding [39]. This hydrophobic interaction depends mainly on the surfactant hydrophobicity [39] and the ionic strength [40].

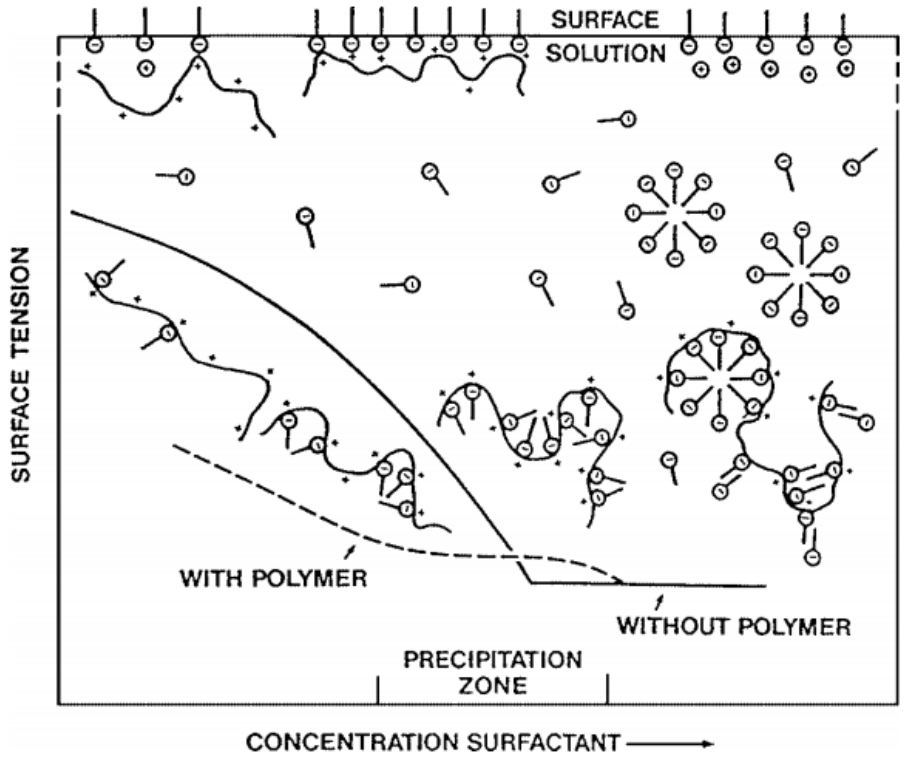

Figure 8: Surface tension and system composition change versus surfactant concentration change in polyelectrolyte/surfactant mixture [41].

Polyelectrolytes tend to bind with surfactant molecules and displace their counter ions [34] [36]. At the critical aggregation concentration (CAC), aggregation of surfactants forming polyion-mediated surfactant aggregates take place. Typically, the CAC is 1~3 orders of magnitude lower than the CMC [34]. This is due to the reduction in free energy of the double layer surrounding the surfactant aggregates since the small counterions are replaced by a polyion. Above the CAC, substantial surfactant binding occurs and this results in the formation of polyion-mediated micellar cluster [34] [36].

This ion-exchange process occurs without reducing the translational entropy that is caused by the adsorption of monovalent counterions to free surfactant micelle [36]. For highly charged

polyelectrolyte systems, the entropy gain is increased by the release of the condensed counterions on the polyelectrolyte chains [36].

Surface tension is a cohesive force between liquid molecules and this force provides resistance to external forces [17]. A reduction in surface tension is usually an indicator of the formation of surface complexes since surface tension is very sensitive to variations of the adsorbed complex at the surface [34]. It could also be indicative of the formation of polyelectrolyte-surfactant complexes at the bulk. Surface tension tends to decrease as the surfactant concentration increases till a change in slope is observed at the CMC [41]. At a constant polyelectrolyte concentration, as the surfactant concentration is increased the surface tension variation can be represented by the dashed line in Figure 8 [41]. Surface tension starts decreasing with further addition of surfactants and a plateau can be observed once the CAC is attained. A second decrease in surface tension is observed after this and results in the onset of the CMC [41].

2.4.2 Role of Polyelectrolyte-Surfactant Combinations on Foam Films

The stability of foams, emulsions or suspensions are mainly governed by the stability of the microscopic and mesoscopic thin liquid films [22]. It is important to discuss the two forces that are responsible for the stability of aqueous and non-aqueous films:

1. Electrical Double Layer (EDL) consists of a charged surface and a distribution of neutralizing counter ions near the surface. This layer comprises of two layers – an inner layer comprised of adsorbed ions (Stern layer) and a diffuse layer where the ions are distributed by the influence of electrical forces and thermal motions [17] [5].

2. Dispersion forces are weak intermolecular forces. They are attractive forces that result when the electrons in two adjacent atoms occupy positions that make the atoms form a temporary dipole [5] [17].

EDL controls the stability of the aqueous foam films while dispersion forces dominate for the stability of non-aqueous films [22]. Stratification is the phenomena of discontinuous thinning of a film. This process occurs due to an oscillation of the disjoining pressure in the film and occurs in a polyelectrolyte network that is formed in the film above the overlap concentration c* [34] [22]. Polyelectrolyte concentrations are referred to as dilute below c* and as semi dilute above c* [34]. Stratification is found to occur below the CAC (of the polyelectrolyte and surfactant) and above the overlap concentration of the polyelectrolyte [22]. Stratification is an irreversible process and as the applied pressure increases, the layers of the network are pressed out of the film [22].

The steps of thickness follow a power law [22]:

$\Delta h \propto c^{-\frac{1}{3}}$ for branched polyelectrolytes such as Polyethylenimine (PEI)

$\Delta h \propto c^{-\frac{1}{2}}$ for linear polyelectrolytes

Disjoining pressure is the pressure that keeps two opposing surfaces apart from each other and conjoining pressure brings the two surfaces together. It is an excess pressure within the film with respect to the pressure outside the bulk liquid [22].

2.4.3 Polyethylenimine-Surfactant System

For the purpose of this research, the interaction between a cationic polyelectrolyte (branched Polyethylenimine (PEI)) and a nonionic surfactant (N120 surfonic from Huntsman) are studied and their application for the formation of stable CO2 foam for enhanced oil recovery is tested. PEI is widely investigated for its extensive use in pharmaceutical formulation, personal care products,

food products and detergents. PEI is commercially available as a linear or branched polyelectrolyte. However, linear PEI is only soluble in hot water while branched PEI is water soluble at room temperature [42]. Branched PEI comprises of 25% primary ammines, 50% of secondary ammines and 25% tertiary ammines whereas the linear PEI comprises of 100% of secondary ammines only. At low pH values of PEI, the amine groups are protonated thereby making it positively charged and at higher pH values it is almost a neutral polymer [21]. The next section reviews the nanoparticle complex formed by PEI and their current applications.

2.4.4 Polyelectrolyte Complex Nanoparticles

Polyelectrolyte complexes are formed by the strong electrostatic interaction between two oppositely charged polyelectrolytes [35]. The process of forming a complex is considered as a cooperative process between electrostatic and hydrophobic forces [36]. An anionic polyelectrolyte, Dextran sulphate is known to reduce the toxicity of the cationic PEI by creating polyelectrolyte complex nanoparticles (PECNP) [43]. Dextran sulphate (DS) is soluble in water and insoluble in ethanol and ether. PEI and DS are both biodegradable and biocompatible polyelectrolytes [44]. This system was introduced by Tiyaboonchai as a delivery vehicle for pharmaceutical applications [42]. Her study indicated that the cationic density of PEI is pH dependent and that PEI exhibits a high buffering capacity above pH 7 [42].

Tiyaboonchai found that the ratio of PEI over DS controlled the particle size of the nanoparticles generated [43]. As the ratio increased, the mean particle size decreased. She believed that this behavior was due to the colloidal protective nature of PEI which prevents the aggregation of the nanoparticles. The optimal ratio of cationic to anionic polyelectrolytes was found to be 2:1 along with a pH of PEI of 8 [42].

The PEI/DS nanoparticle system developed by Tiyaaboonchai [43] was used by Barati [45] for the purpose of entrapping the enzymes used as breakers in fracturing fluids. Owing to the harsh pH and temperature conditions in the reservoir, a nano sized carrier to carry the enzyme to the filter cake was developed by him to protect the enzyme from being denatured and delayed its release [45]. He also found that the PECNP loaded with enzyme was stable under shear and thus could be used in the flow lines and well bores during injection [45]. Bose et al [46] used the same PECNP system as Barati's [44] fluid loss additive for hydraulic fracturing applications.

The above mentioned advantages and preparation methods of PECNP could be implemented to stabilize the surfactant interface in CO_2 foams thereby generating longer lasting foams under shear and in the presence of crude oil. The application of PECNP to surfactants to stabilize the CO_2 foam for enhanced oil recovery applications has not been researched to the best of this author's knowledge.

Chapter 3: Methods and Materials

This chapter describes the methodologies implemented and chemicals used in order to achieve a stable CO_2 foam using PE and PECNP. The following high pressure, high temperature experimental setups were used:

1. Zeta Potential measurements through Zeta Pass.
2. Sapphire View Cell setup for CO_2 foam durability and stability measurements.
3. Rheology setup to study the bulk rheology of the CO_2 foam.
4. Core flood setup to measure the foam mobility and incremental oil recovery.

The chemical and physical properties of the substances purchased, along with their product specifications are summarized below.

3.1 Chemicals Used:

3.1.1 Polyethylenimine (PEI)

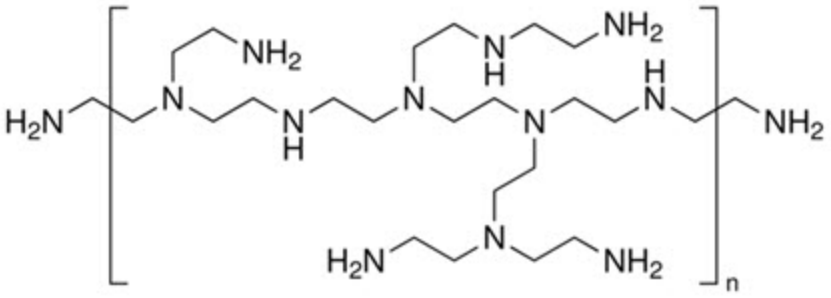

Figure 9: Chemical structure of PEI (obtained from MSDS sheet from Sigma Aldrich)

A branched PEI is used for this thesis, which is a polycation with an average molecular weight of 25,000 as reported by Sigma Aldrich. Figure 9 shows the chemical structure of the branched PEI. The density is 1.03 g/ml at 25 degrees Celsius and the viscosity is between 13,000 -18,000 cP at

50 degrees Celsius. PEI was purchased from Sigma Aldrich (Lot# MKBN3988V, CAS# 9002-98-6)

3.1.2 Dextran Sulphate (DS)

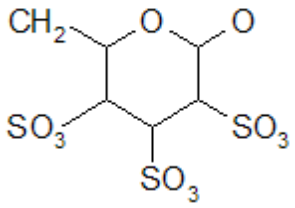

Figure 10: Chemical structure of Dextran Sulphate [44].

Dextran Sulphate (Sodium salt) is a polyanion with an average molecular weight of 500,000. It was purchased from Sigma Aldrich (Lot# 116614, CAS# 9011-18-1). The chemical structure of DS is shown in Figure 10.

3.1.3 N-120 –Huntsman Surfonic (Surfactant)

The chemical name of N120 is Poly (oxy-1, 2-ethanediyl), alpha-(nonylphenyl-omega-hydroxy). N120 is a non-ionic surfactant which was provided by Huntsman (Lot # E312D33, CAS# 9016-45-9). It has 12 Ethylene oxide (EO) groups. The theoretical molecular weight of the surfactant is 748 and the density was reported to be 1.066g/ml at 25 degrees Celsius. Hydroxyl number for this nonionic surfactant is 75.

3.1.4 Brine

2wt% potassium chloride (KCl) was prepared using water purified by the reverse osmosis (RO) method and deionized. Potassium chloride used for these experiments were purchased from Sigma Aldrich (Lot # 0134C127, ACS Grade, CAS# 7447-40-7)

3.1.5 Crude Oil

Mississippian crude oil is used for the view cell and core flood experiments. The viscosity and density were measured to be 3.88 cP and 0.82 g/cc, respectively, at 40 degrees Celsius.

Lansing Kansas City (LKC) crude oil is used for the view cell tests only. The measured viscosity and density are 5.86 cP and 0.83 g/cc respectively at 40 degrees Celsius.

3.1.6 Light Mineral Oil

Light mineral oil was used for the view cell tests to observe the interaction between the CO_2 foam system and oil. The viscosity and density of the light mineral oil are 15 cP and 0.84 g/cc, respectively, at 40 degrees Celsius.

3.1.7 Cores

Indiana limestone outcrop cores were purchased from Kocurek Industries. The length and diameter of the cores were 12 inches and 1.5 inches, respectively. The cores were cut to the desired length before the experiments. The permeability for these cores were typically between 100-350 mD.

3.2 Preparation of samples

3.2.1 PEI and DS

PEI obtained from Sigma Aldrich is highly viscous and PEI of different concentrations ranging from 0.01% - 10% by weight are prepared in 2wt% KCl solution. PEI of different concentrations are also prepared in RO water for the initial set of tests. The solutions are allowed to stir at a 600 revolutions per minute (RPM). The average pH of the PEI solution is 11 which is highly basic. An optimized weight percent based on the overlap and critical aggregate concentration is chosen and the pH of this solution is further reduced to 9, 8.5 and 8 using 6N HCl. Table 1 shows the volume of 6N HCl required to reduce the pH of the PEI solution to the desired pH. The different batches

of the PEI are further analyzed based on the pH using the zeta potential and DLS measuring device and the most favorable pH of the PEI is used for the tests moving forward.

Table 1: Summary of the titration of PEI (1wt %) in 2wt% KCl using 6N HCl

pH of PEI	Volume of 6N HCl (ml)
7.5	4.1
8	3.4
8.5	3.2
9	2.2

DS is available as a powder and 1wt% DS is prepared in two batches, one in RO water and the other in 2wt% KCl and are also stirred at 600 RPM. The pH of the DS solution is measured to be 7.

3.2.2 Synthesis of PECNP

The PECNP is self-synthesized in the laboratory before the start of each experiment. PEI of different pH (8, 8.5 and 9) is mixed with DS. During the synthesis of the nanoparticle, PEI should be released into the beaker containing DS solution instantaneously to avoid precipitation. One batch of PECNP was prepared with Reverse Osmosis (RO) water and the other batch was prepared using 2wt% KCl.

PECNP in RO water is prepared in the ratio 2:1:0.1 of PEI (pH 8, 1wt %): DS: RO water. The optimized ratio for a given a pH and concentration of PEI was obtained from Reza Et Al [47]. The PECNP was further diluted in RO water in the ratio 1:9 of PECNP: RO water.

The table below summarizes the different ratios that were used to prepare the PECNP in 2wt% KCl.

Table 2: Summary of the ratio of the PEI: DS along with the different pH of PEI used for each batch of PECNP synthesis.

Batch	pH of PEI	Ratio of PEI:DS: 2wt% KCl
1	8	1:1:0.1
1	8.5	1:1:0.1
1	9	1:1:0.1
2	8	2:1:0.1
2	8.5	2:1:0.1
2	9	2:1:0.1
3	8	3:1:0.1
3	8.5	3:1:0.1
3	9	3:1:0.1
4	8	4:1:0.1
4	8.5	4:1:0.1
4	9	4:1:0.1

Four different batches of PECNP were synthesized for each pH of PEI with a total of 12 PECNP samples as shown in Table 2. The zeta potential and the particle size of the 12 samples were further analyzed to estimate the best ratio and pH of PEI required for the synthesis of PECNP which was later used for the tests.

3.2.3 Surfactant

Different concentrations of N120 ranging from 0.025 – 0.25 wt% are prepared in 2wt% KCl or RO water. The interfacial tension (IFT) of the different batches of the surfactant is measured in order to determine the critical micelle concentration (CMC). The final surfactant concentration is maintained below the CMC for all the tests.

3.2.4 PECNP-Surfactant System

The surfactant- PECNP solution are mixed in 1: 9 ratios. The final concentration of the surfactant in the solution is maintained at 0.1wt% which was determined through the CMC tests. The final pH of the solution mainly depends on the pH of the PEI used to prepare the PECNP.

3.2.5 PEI-Surfactant System

The surfactant and PEI (1wt% and pH of 8, 8.5 or 9) are mixed in the ratio 1:9 of surfactant over PEI. The final pH of the solution depends on the pH of the PEI used and the final surfactant concentration in the solution is maintained at 0.1wt%.

3.2.6 Foam Quality

The supercritical CO_2 foam quality is maintained at 90% for the view cell tests and core flood tests. The bulk rheology tests were conducted at 80% and 90% foam quality to understand the influence of the foam quality on the rheology of the foam. This implies that either 80% or 90% of the fluid injected is supercritical CO_2 and the remaining volume is the the aqueous solution,.

3.3 Experimental setup

3.3.1 Zeta Potential and DLS Particle Size Measurements

In order to determine the optimized ratio for the preparation of the nanoparticles as well as the most optimized pH of PEI (1wt %), mean particle size and zeta potential were measured for different samples using the Brookhaven ZetaPALS instrument.

Working Principle:

This instrument works on the principal of Brownian movement. The diameter and electrical double layer are measured by the DLS particle measurement. Zeta potential or the electrophoretic

potential is the measure of the electro kinetic motion of the particles away from the charged inner surface within the electrical double layer.

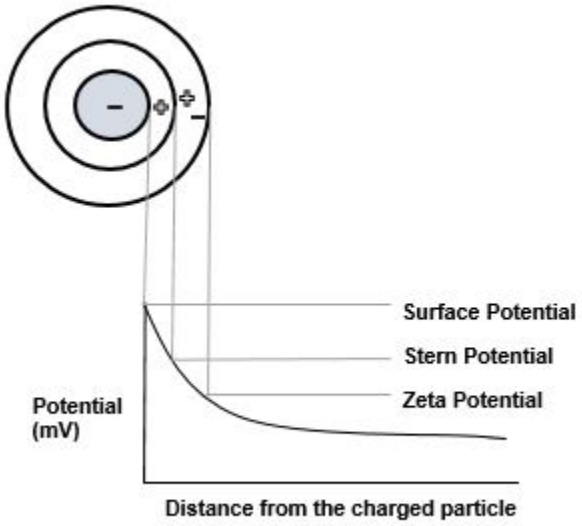

Figure 11. Schematic diagram representing the potential difference as a function of distance from the charged particle suspended in a dispersion medium [17].

Stability of the system depends on the zeta potential values. High zeta potential values correspond to stronger electrostatic repulsion which results in a more stable system.

Procedure

The particle diameter for each sample was measured by taking the average of the three readings. The measurements were recorded by detecting the light scattering at 90 degrees. The mean particle size of each sample along with the electrophoretic mobility is used for determining the zeta potential of the given sample. For the zeta potential measurements, the samples were diluted 10 times using 1mM KCl before taking the average of three readings.

3.3.2 Operating Conditions

In the upcoming sections, the same operating conditions are maintained through the completion of the experiments. The view cell, rheology and core flood tests are conducted at 1300 psi and 40 ˚C. These conditions are at the supercritical state for CO_2. These conditions were chosen relevant to the real well conditions. For example, the Lansing Kansas City and Mississippian formations in Kansas have similar pressure and temperatures in most parts.

3.3.3 View Cell

The experimental setup is designed using a sapphire view cell and is designed to withstand high temperatures and pressures. The pressure and temperature is maintained at 1300 psi and 40 degrees Celsius for all the experiments. The view cell setup was used to determine two important parameters, the interfacial tension (IFT) of the different CO_2 foam systems and their stability/durability in the presence of crude oil.

Working Principle for IFT Measurements:

The calculations involved in the IFT measurements are analogous to that of the drop weight method. The size of the drop rising from a capillary tube depends on the surface tension of the liquid. The view cell is initially filled with the pressurized surfactant being tested. Bubbles of dense CO_2 are then introduced through the central tube of connection at the lowest end of the tube and the surfactant solution is withdrawn through the annulus. Because all the fluids in the apparatus are at the same high pressure, the CO_2 enters at the same rate that surfactant is withdrawn. Since the CO_2 rate is set by the ISCO pump and the bubble volume detachment is determined by the IFT between the surfactant solution and the dense CO_2, the IFT can be computed from the interval between the releases of bubbles from the needle. A considerable portion of the bubble (up to 40%)

may remain attached to the capillary tip after the drop detaches. This effect is compensated with Harking-Brown correction factor, f as described by Adamson [48] and is tabulated in Table 24.

Procedure for IFT measurements:

The frequency of produced bubbles is recorded, which is used to determine the volume and radius of each bubble. The correction factor takes into account effects of attraction to the end of the tube and imperfections in the system, generally ranging from 0.5 to 1.0. The correction factor in most of the experiments in this study ranges from 0.5 to 0.7 and further details about the calculation and correction factor are described in chapter 7, (7.6). The durability of the foam can also be calculated by observing the time it takes for foam to decay into a simple layer of dense CO_2 at the top of the tube. The ISCO pump B was used to inject the desired aqueous phase (surfactant, PEI-surfactant or PECNP-surfactant) through the bottom of the view cell. Valve #4 is kept open to release air bubbles that may have been present in the view cell. By keeping Valve #4 closed, the view cell is pressurized to the required pressure using the ISCO pump B. For the purpose of this experiment a pressure of 1300 psi was maintained. Another ISCO pump A was used to maintain the CO_2 at supercritical state. The oven was maintained at a temperature of 40 degrees Celsius at all times. The view cell with the surfactant solution was allowed to stabilize to 40 degrees Celsius by leaving it inside the oven for a couple of hours before the start of the experiment. Once a stabilized pressure of 1300 psi is maintained between the view cell and the CO_2, the ISCO pump B was used to withdraw surfactant solution from the view cell at the rate of 0.04 cc per minute while the CO_2 is injected from the bottom of the view cell at the same rate. The first bubble of CO_2 is viewed after about 6-8 minutes. Readings for the purpose of calculating the interfacial tension were taken after 1 hour from the formation of the first bubble. Foam decay is calculated after stopping the foam generation by stopping the ISCO pump A and B and isolating the view cell. Figure 12 is a

schematic diagram of the view cell setup that is used to measure the interfacial tension for the CO_2 foam generated by surfactant, PEI-surfactant and PECNP-surfactant.

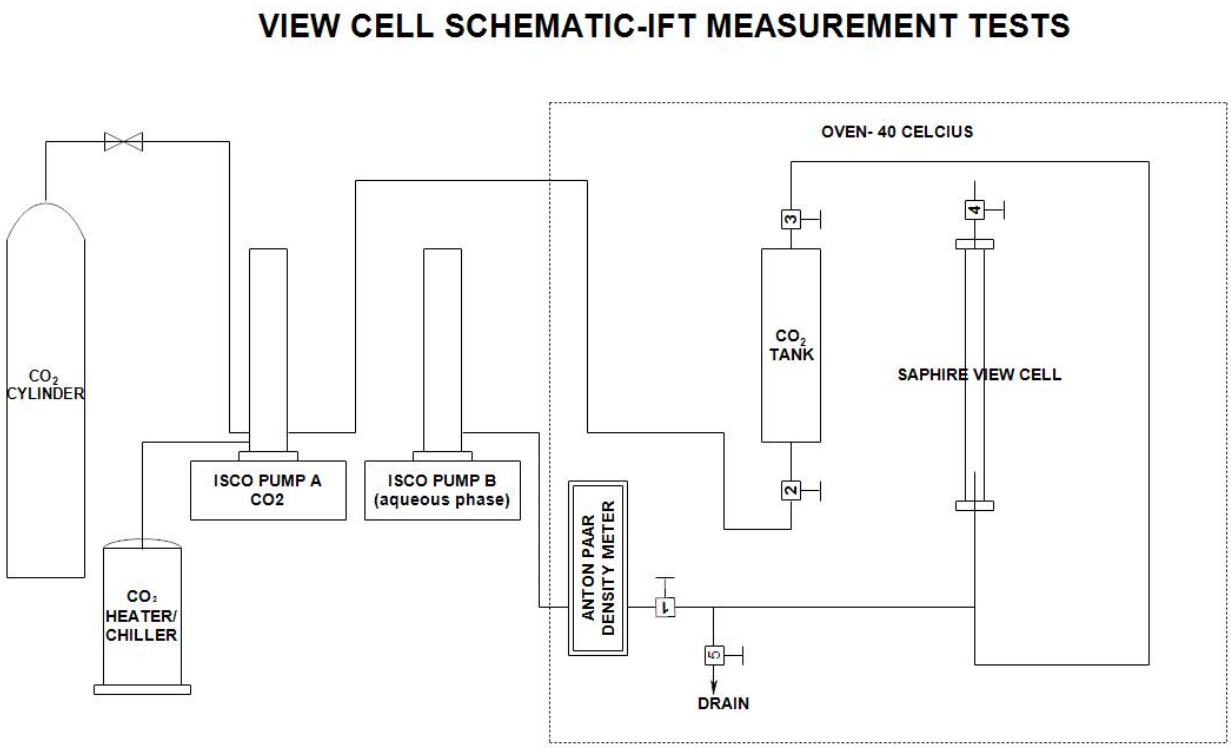

Figure 12: Schematic diagram showing the flow path for the measurement of interfacial tension for the surfactant , PEI-surfactant and PECNP-surfactant systems.

Procedure for Foam durability Tests:

Initially the original view cell setup (Figure 12) was used without any modifications to test the durability of the CO_2 foam systems with light mineral oil. ISCO pump B was filled with the surfactant solution. The lines were flushed with the surfactant solution and allowed to enter the view cell from the bottom. About 2 cm from the top of the view cell is remained unfilled for the light mineral oil to be filled. The surfactant solution was prepared in RO water for the purpose of this test. The entire system was pressurized using the ISCO pump B up to 1300 psi. The sapphire view cell is placed in an oven which was allowed to reach a stable temperature of 40 degrees

Celsius. Once the desired pressure and temperature were reached, CO_2 was allowed to enter the view cell from the bottom and the foam is generated by the drop weight method similar to the IFT measurements. The ISCO pump B withdrew the surfactant solution at 0.04 cc/minute and CO_2 was injected at the same rate by ISCO pump A. The foam generation was allowed to take place for an hour with a standard volume of 2.4 cc of CO_2 injected. Foam decay was observed by discontinuing the CO_2 supply and ISCO pump B simultaneously. Valve #5 was closed to isolate the view cell in order to observe the foam decay. The outcome of this test is discussed in the next chapter and the setup required slight modifications for a more satisfactory result.

Figure 13 describes the modified process flow diagram for the foam durability testing. The experimental setup used to measure the interfacial tension of the different CO_2 foam systems, is slightly modified by the insertion of a 7 micron inline mixer to pre generate the foam before it enters the sapphire view cell. A sight glass is added prior to the entrance of the sapphire view cell to preview the foam generated.

Baseline tests were conducted with no oil in the system initially, by filling the cell with the corresponding aqueous phase, surfactant or PEI (1wt%, pH 8)-surfactant or PECNP-surfactant using ISCO pump B. The aqueous phase and CO_2 were passed through the inline filter to pre-generate the foam at 90% foam quality. The generated foam is allowed to pass through a sight glass for 10 minutes or until 30 ml of foam is generated. Valve #6, #7, #8, #9 and #11 are closed to bypass the foam flow through the sight glass during this period. Once 30 ml of foam is generated, Valve #9 and #11 are opened to allow the foam to enter the view cell and fill up half view cell. The foam decay between the generated CO_2 foam column and aqueous phase are monitored there after by closing valve #9 and #11. CO_2 at supercritical conditions (1300 psi and 40 degrees Celsius) is used for these experiments.

After the baseline tests, the CO_2 foam systems were tested with light mineral oil and crude oil. A gear pump was used to fill the view cell with crude oil or light mineral oil initially. The system was then pressurized up to 1300 psi. The aqueous phase which comprises of surfactant or PEI (1wt%, pH 8)-surfactant or PECNP-surfactant, and the supercritical CO_2 were allowed to flow through the 7 micron inline mixer and allowed to pass through the sight glass for about 10 minutes or till 30 ml of foam was generated. The foam was then bypassed into the view cell and once it fills up half the cell, valve #9 and #11were closed to isolate the view cell. The foam decay was observed thereafter.

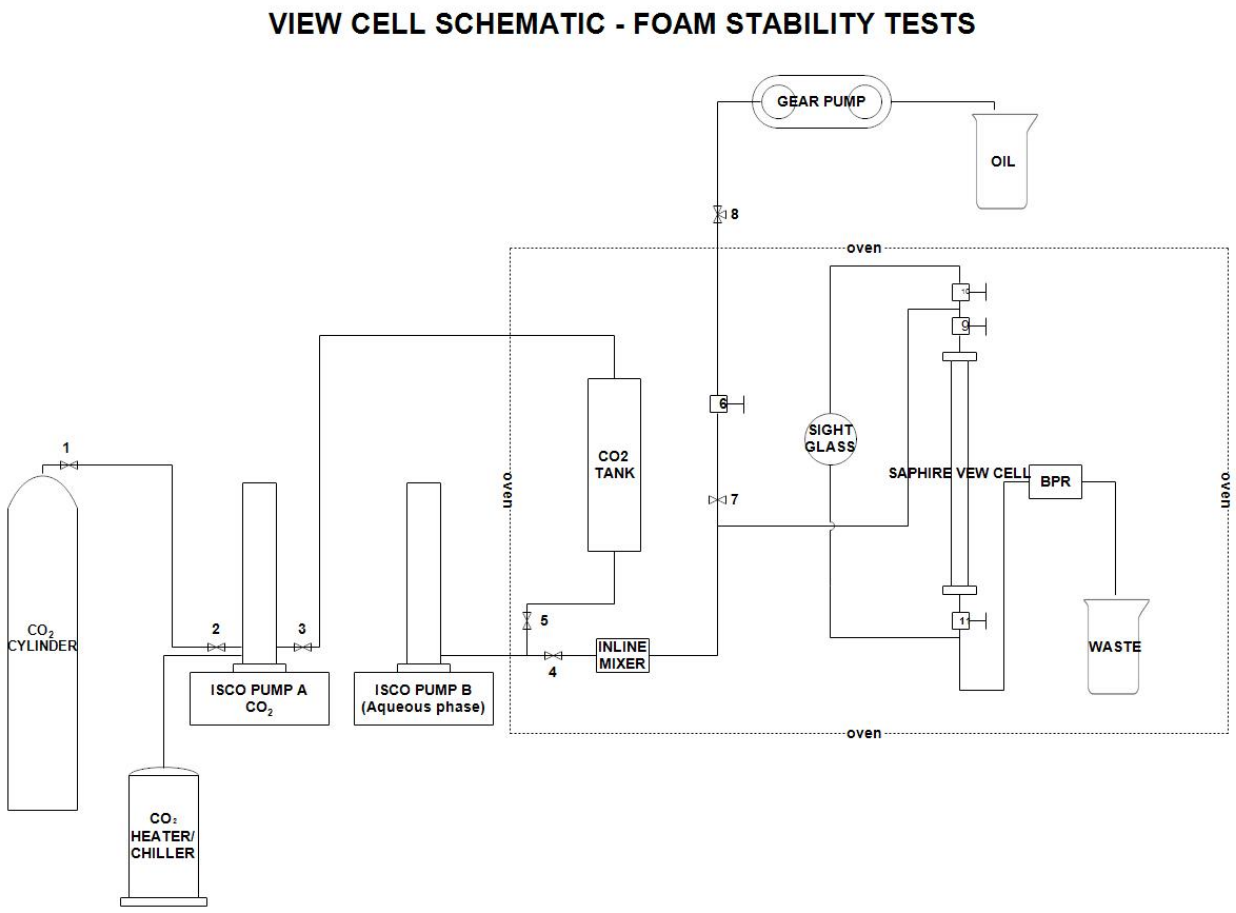

Figure 13: Schematic diagram showing the flow path for the foam durability tests in the presence and absence of light mineral and crude oil.

3.3.4 Rheology

CO_2 foams are considered to be Non- Newtonian fluids. The apparent viscosity of the foam decreases as the shear rate increases and is characterized as a pseudo plastic fluid. The measuring cup in the rheometer comprises of two co-axial cylinders and the annulus between these cylinders is filled with CO_2 foam. The outermost cylinder is rotated by a magnetic motor that provides torque values up to 300 mNm.

Experimental Procedure

The CO_2 pump is filled at 8 Degrees C and the pressure is raised depending on the required temperature. There are three ISCO pumps required for this setup. One is used for CO_2, one for the aqueous phase and the last one is for refilling the solution to maintain the pressure in the system. All the lines are taped with Teflon to prevent heat loss to the surrounding. The three pumps are also maintained at uniform temperature using the chiller/heater setup. The system is pressurized up to 1300 psi. For all the tests a shear rate of 2000 s^{-1} was used. All tests are conducted under constant shear rate. Ramp tests are conducted by ramping the shear step wise from 2000 s^{-1} to 100 s^{-1} and ramped back up to 2000 s^{-1}. Once the tests are completed the setup is de- pressurized section-wise and rinsed with RO water. Figure 16 is a schematic representation of the flow diagram for the rheology setup.

Different Types of Tests Conducted using the Rheometer

Dynamic Test:

Under this test different foam qualities are used and is continuously sheared at a given shear rate (2000 s^{-1}). The foam is generated continuously at a given flow rate and the refill pump maintains the pressure by withdrawing the foam into the pump and leaving sufficient foam in the rheometer as well. All the parameters are as follows: 140 measuring points at 30 second intervals for a total of 70 minutes. Figure 14 is a screen shot describing the parameters that were input into the Rheoplus software to run the dynamic test as well as the static test.

Static Test:

Different foam quality tests that were conducted during the dynamic tests are allowed to stay in the measuring cup for the static tests. The foam is sheared at the same rate (2000 s^{-1}) and the

parameters are the same as described in Figure 14. However, valve #9 and #10 are closed to isolate the measuring cup. The foam generation is halted by stopping the ISCO pumps. This test measures the viscosity of the foam that is already present in the measuring cup and does not require continuous foam generation.

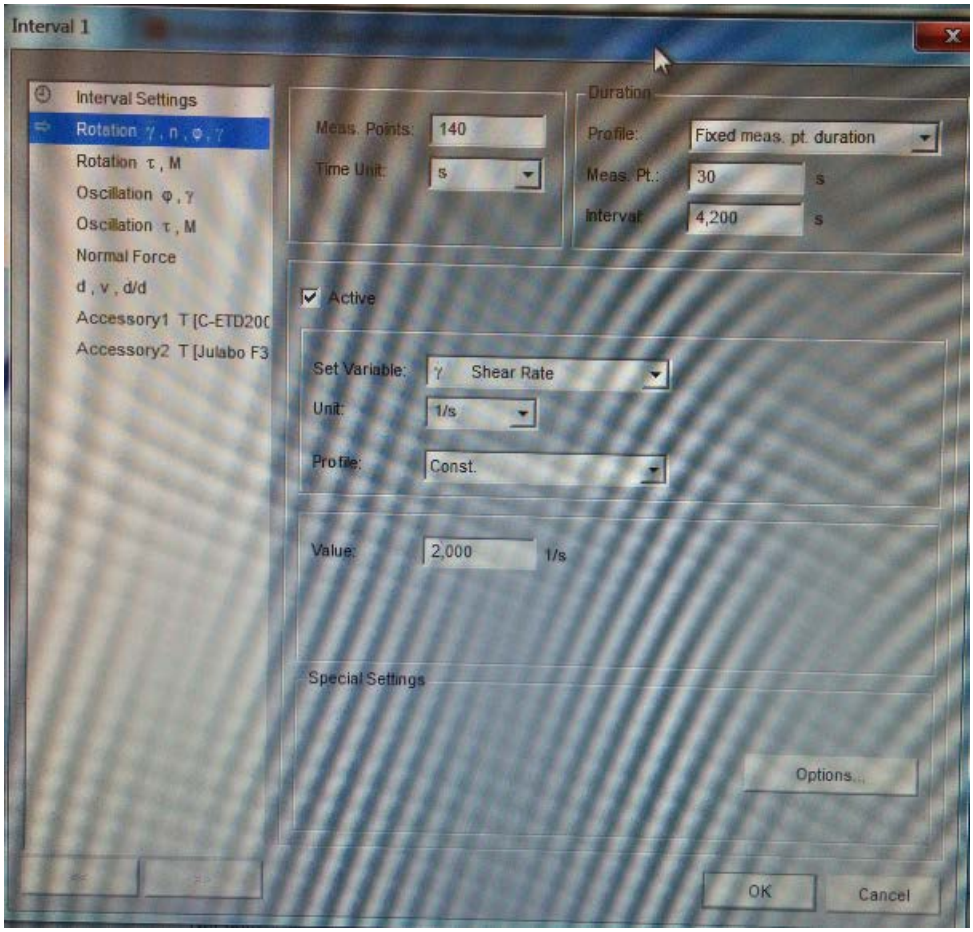

Figure 14: Screen shot of the parameters used for the static and dynamic test for the rheology testing.

Ramping Test:

Different shear rates are applied to the foam inside the measuring cup during the ramp tests. A new dynamic test at 3 cc/minute flow rate was conducted and the foam generation was halted prior to

the ramp tests. Valve #9 and #10 are closed and the pressure is maintained. The system is sheared from 2000 s^{-1}100 s^{-1} and ramped back up to 2000 s^{-1}. This test is used to determine whether the fluid is shear thinning or shear thickening. Fifteen measuring points were used at 30 second intervals for both ramps, which totals to 15 minutes. Figure 15 represents the parameters used for the ramp tests.

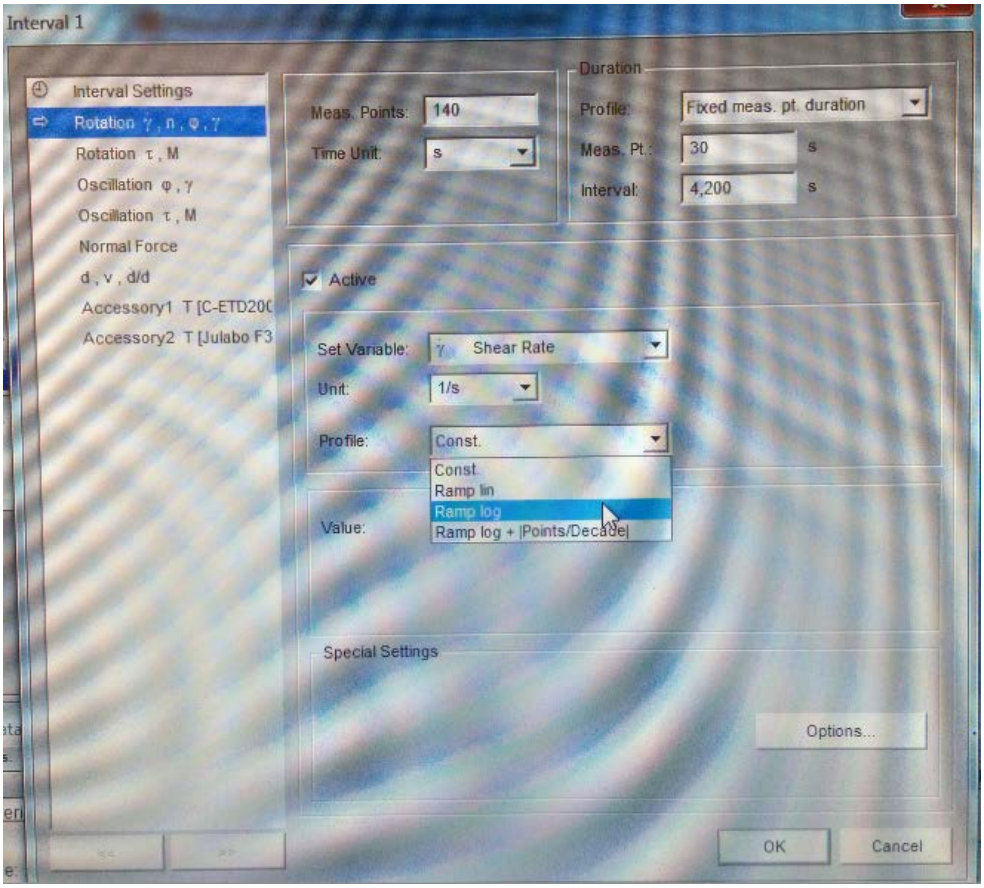

Figure 15: Screen shot of the parameters used for the ramp tests.

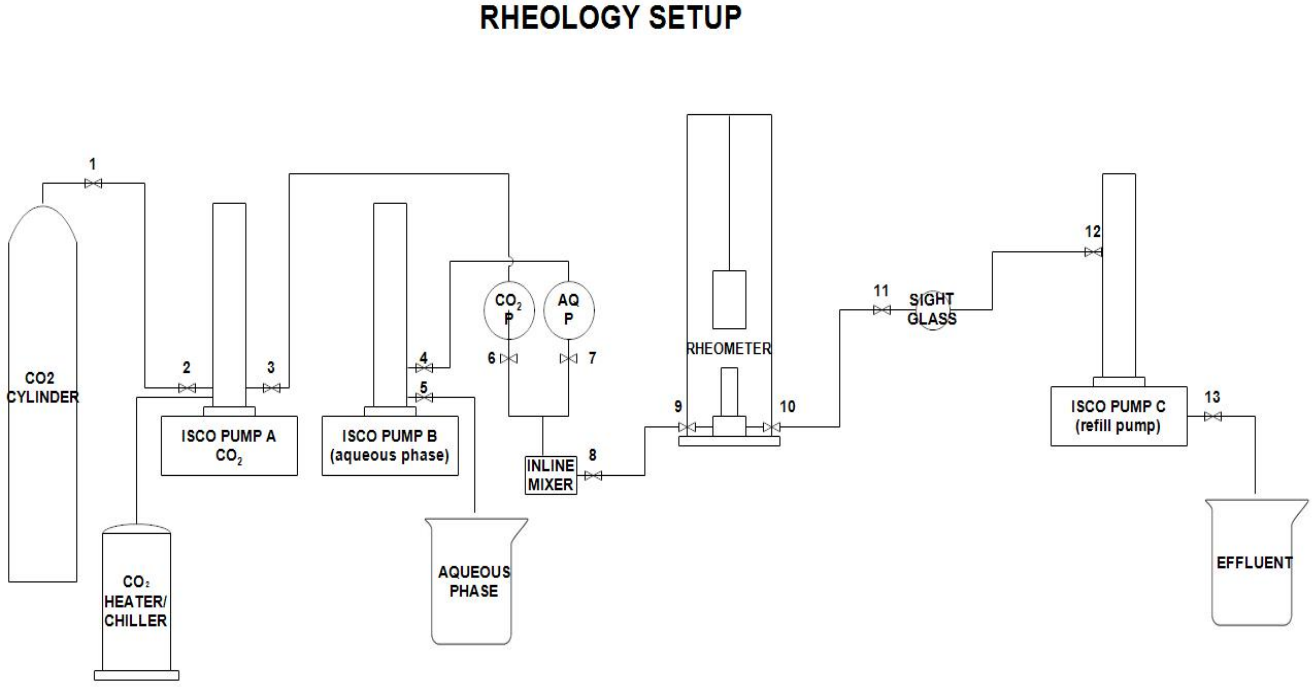

Figure 16: Schematic diagram representing the flow path of the rheology setup.

3.3.5 Core Flood for CO_2 Foam Flooding

A 12 inch vertical core holder is used in a core flood setup in order to conduct CO_2 foam flooding experiments. The setup was designed to perform different experiments apart from the CO2 foam experiments. The core flooding apparatus is represented as a schematic diagram in Figure 17.

There are three pressure taps measuring the pressure drop across different sections of the core. Validyne differential pressure transducers of 125 psi rating are used for measuring the pressure drops across these sections of the core. The pressure drop across the whole core is measured using a 500 psi rating Validyne differential pressure transducer. A heater/cooler unit is used to attain the supercritical state of CO_2. The setup is designed to divert the CO_2 foam to three different flow paths. The first flow path allows the aqueous phase and the supercritical CO_2 to pass through a 7 micron inline filter into the core holder. The second flow path allows the CO_2 foam to pass through

the inline filter and then through a series of loops into a sapphire view cell. The foam from this flow path can either be diverted into the core or to the outlet directly. This flow path can be used to study the effect of shearing the foam using a series of loops. Lastly, the CO_2 foam can flow through the inline filter into a sapphire view cell and into the core or to the outlet directly. The pre generated foam can be observed in the view cell and foam durability tests could be conducted through this setup as well. For the experiments that are described in the following sections, the first flow path is used and the CO_2 foam is injected at a superficial velocity of 12.4 feet/day (3ml/minute). The CO_2 foam quality is also maintained at 90% for all the CO_2 foam tests. The flow diagram is further simplified and the flow path for the different tests are described using the green lines showing the path of flow.

Figure 18 and Figure 19 represent the flow path for filling the left and right transfer cylinders or accumulators inside the oven before the start of each experiment. The left transfer cylinders are usually filled with either brine or any aqueous phase and the right transfer cylinder is always filled with crude oil. The ISCO pump, containing Soltrol 130 is used to bring the piston in the transfer cylinders to the top. Since the transfer cylinders can not be manually dismantled to fill the required phase (either crude oil or aqueous phase), a gear pump is used to inject it into the transfer cylinder by opening valve #6 and #11 for crude oil and valve #1 and #10 for the aqueous phase. The remainng valves are kept closed. The Soltrol 130 present on the other side of the piston inside the transfer cylinder is collected at the bottom using a beaker.

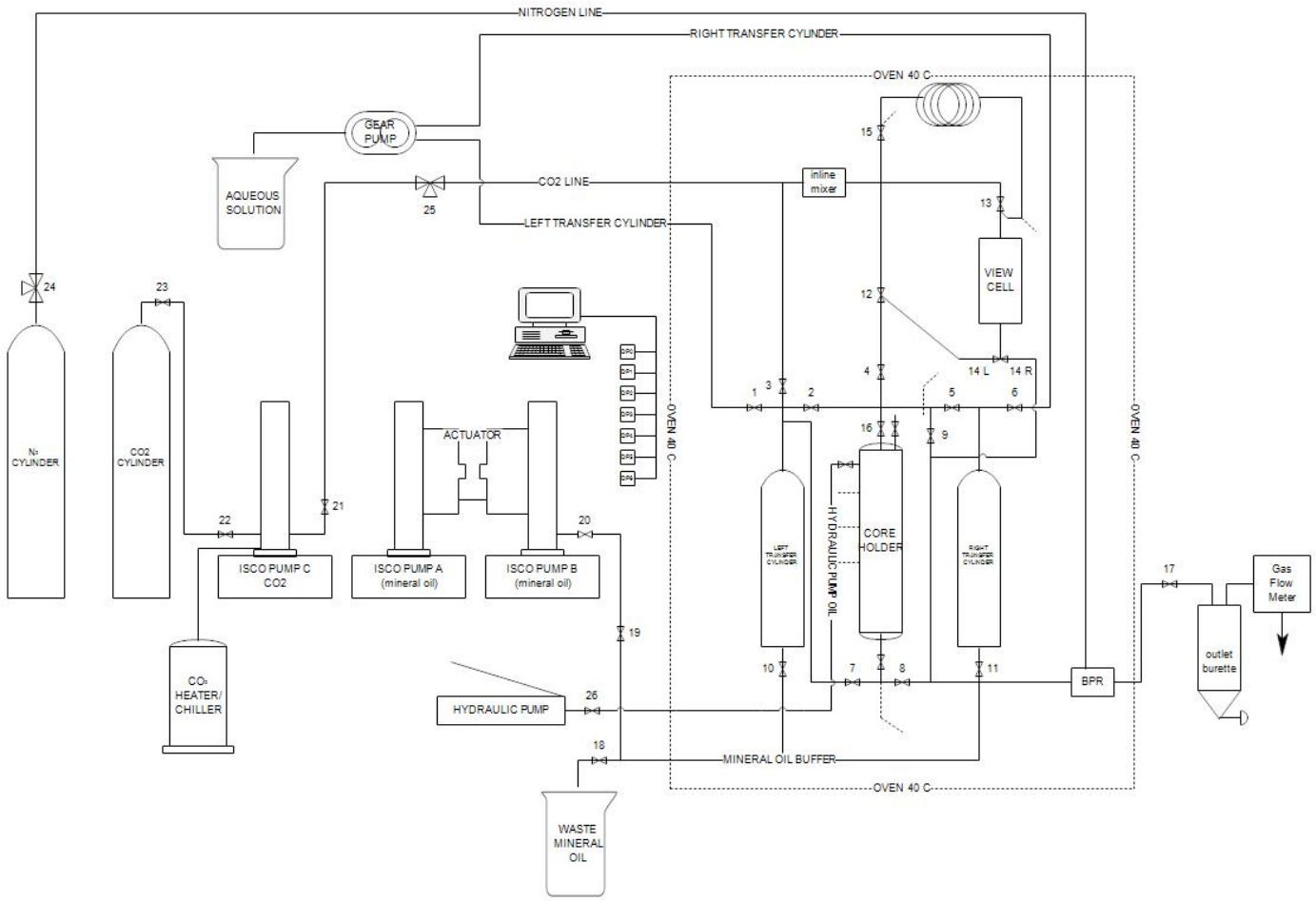

Figure 17: Schematic of the Core flood setup designed for the CO_2 foam tests [49].

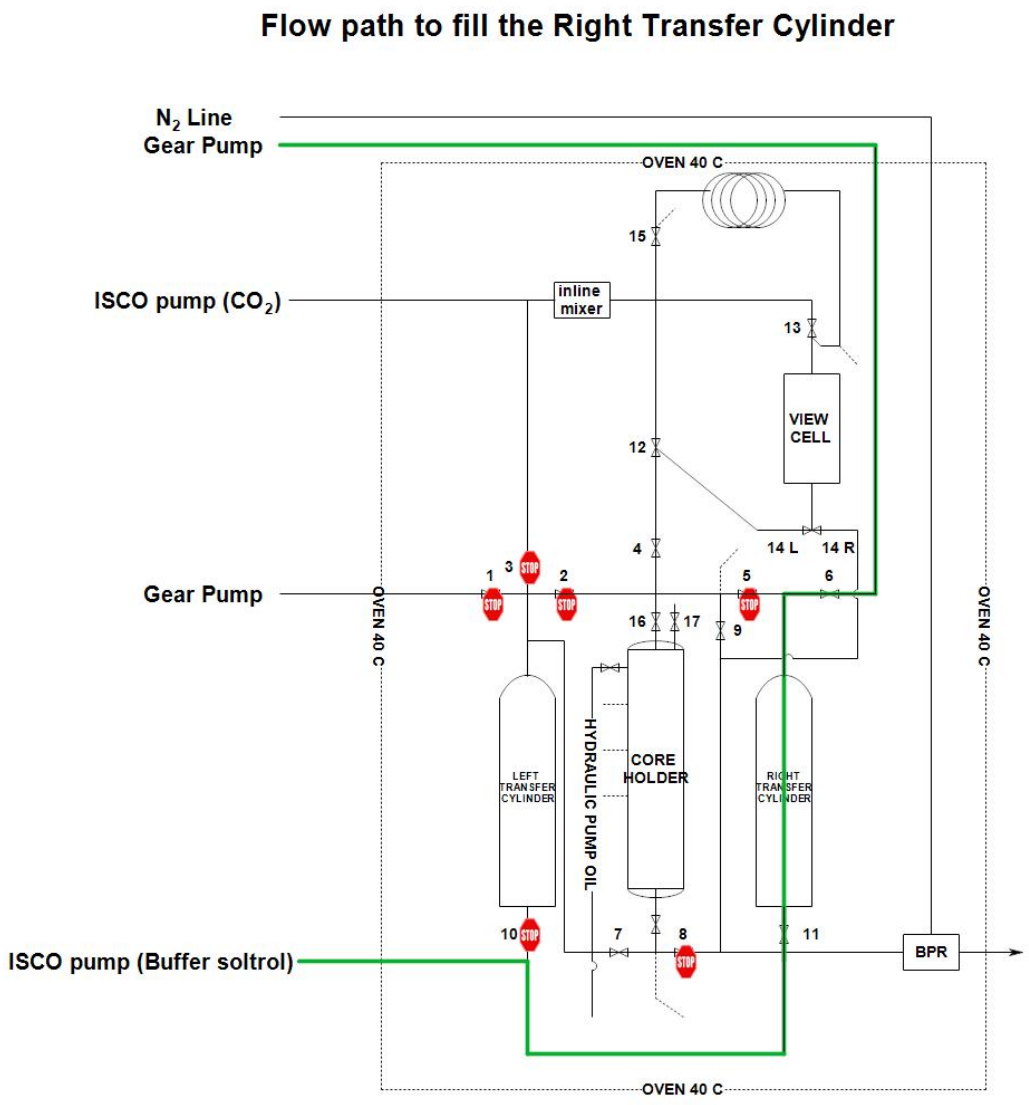

Figure 18: Flow sheet providing the flow path in green to fill the right transfer cylinder with crude oil.

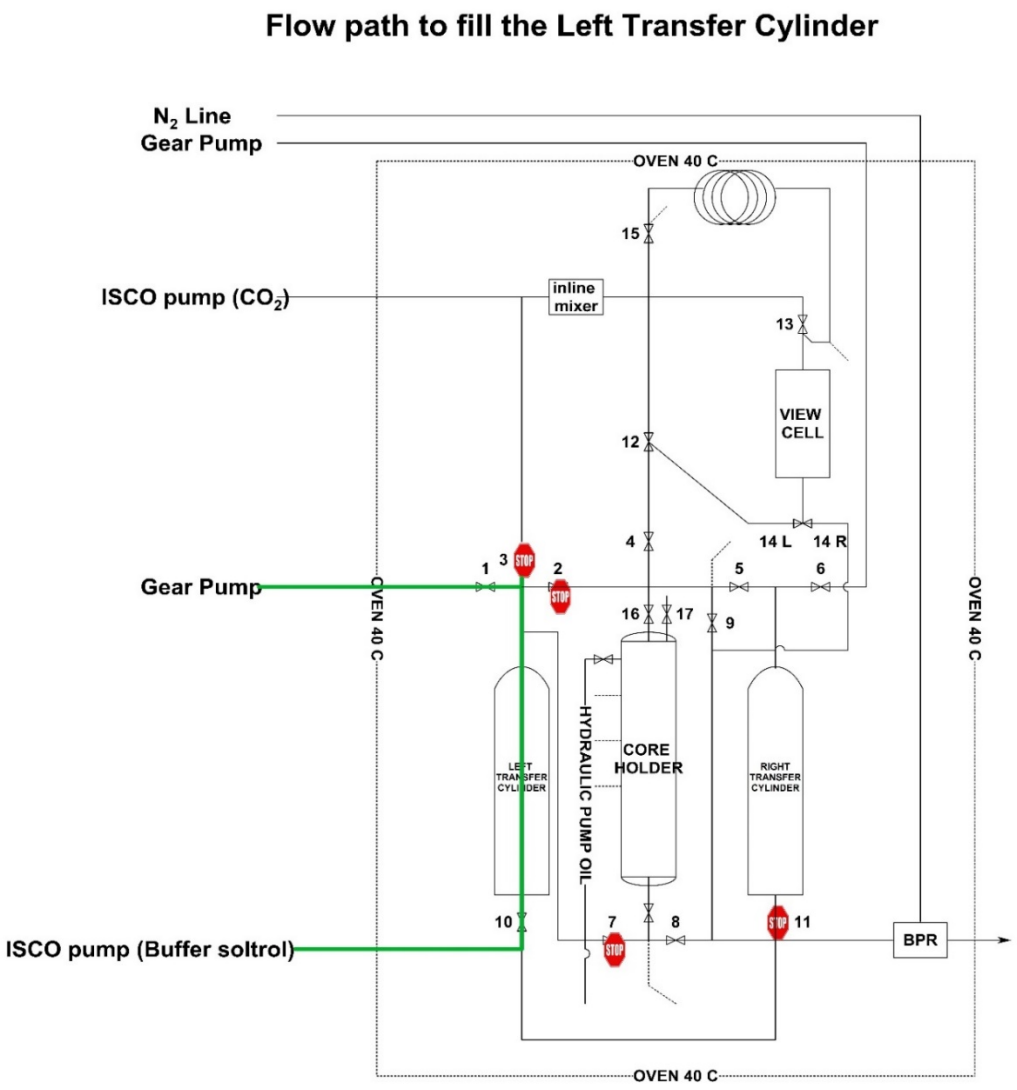

Figure 19: Flow sheet providing the flow path in green to fill the left transfer cylinder with aqueous phase.

Core Saturation

The wet core is cut to the desired length and diameter and is dried in the oven at 75 Degrees Celsius for 48 hours. The dry weight of the core is measured every hour after that until the weight remains a constant. The dry core is allowed to cool for some time and is placed in the core holder. The core is vacuumed using a vacuum pump till a pressure reading of -30 psi is reached and is allowed to

stay for 35 minutes. Figure 20 represents the flow path for the core saturation with brine. A vacuum pump is connected to the bottom of the core holder and the rest of the valves are closed during this step till the pressure reading of -30 psi is attained. Following this step, brine is allowed to saturate the core through suction by opening valve # 17.

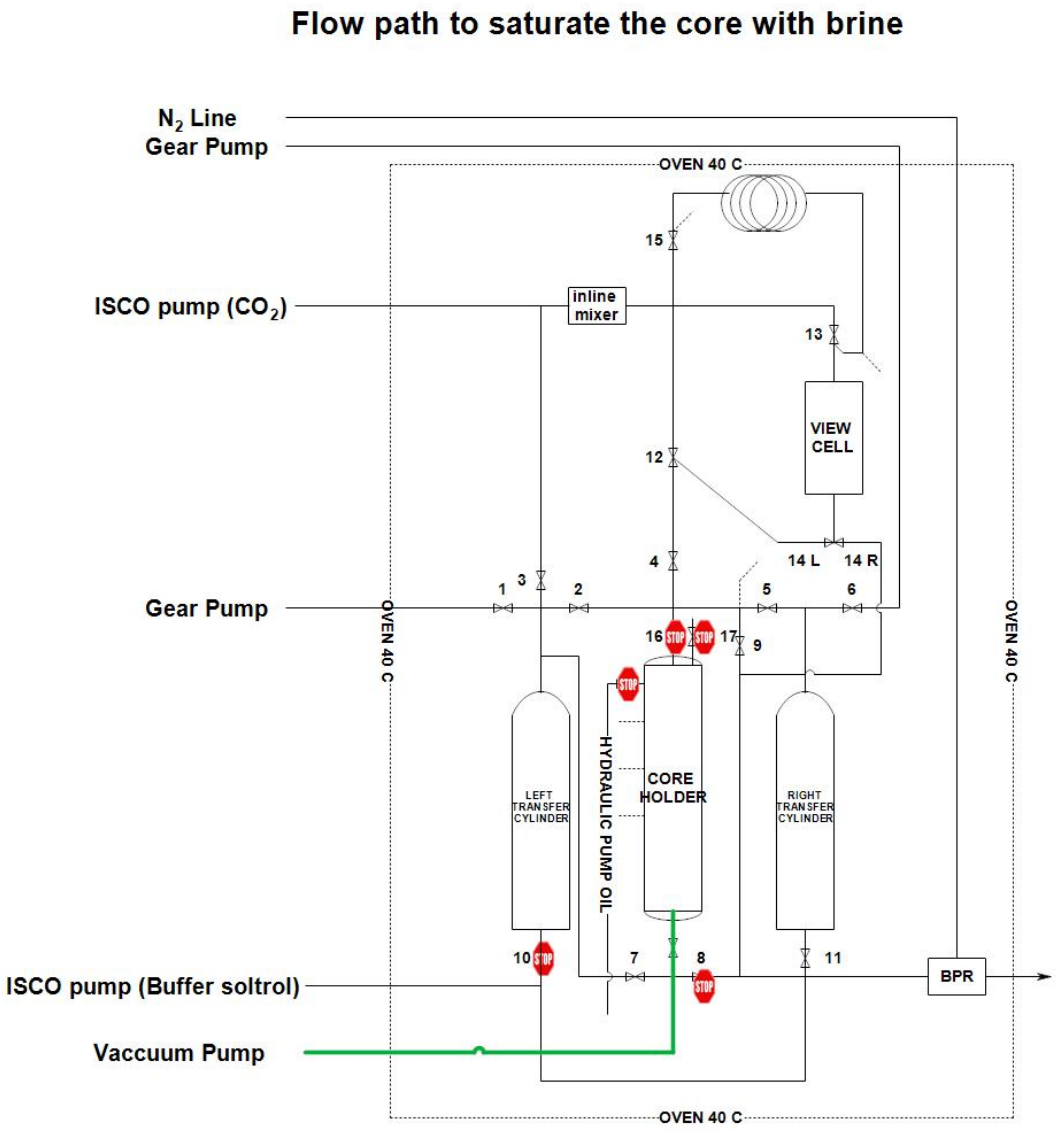

Figure 20: Flow diagram that shows the process for saturating the core using a vacuum pump.

Calibration of Validyne Pressure Transducers

The transducers are calibrated by inserting 0's and 1's to the x and y axis of the table shown below. The demodulator is then adjusted to read a differential pressure of close to 0 for all the transducers. Once this step is completed, the 0's and 1's in the x and y axis are replaced with the maximum transducer voltage reading.

Table 3: Summary of the LABVIEW excel sheet used for calibrating the transducers

Input	Raw Data	x	y	Calibrated Data	Config	Name	mode
Ain 8	0.030401	0	12.5	0.02	1	Val 0	NFSE
Ain 9	0.005948	0	12.5	0.01	1	Val 1	NFSE
Ain 10	0.002192	0	12.5	0.03	1	Val 2	NFSE
Ain 11	0.005311	0	12.5	0.03	1	Val 3	NFSE
Ain 12	0.021889	0	50	0.02	1	Val 4	NFSE
Ain 13	0.010934	0	300	0.05	1	Val 5	NFSE
Ain 14	0.006097	0	300	0.03	1	Val 6	NFSE
Ain 15	0.053932	0	5	0.06	1	Val 7	NFSE

Permeability Measurement with Brine

The core is inserted into the vertical core holder. The top and bottom parts of the core holder are tightened to ensure a complete seal for the core inside. The transfer cylinder containing brine is pressurized to remove any air bubble present inside. Before applying any overburden pressure, hydraulic pump oil is used to bleed any air between the core sleeve and the core holder manually by opening the release valve located on the left side of the core holder. An overburden pressure of 500 psi is initially applied in order to bleed the lines of the setup with the desired brine solution. The pressure transducer lines are flushed with brine solution. Once the setup is ready, Brine is allowed to flow through the core and the backpressure regulator and collected through the outlet.

This is carried out for at least 25 – 30 minutes at any desired flow rate. This ensures that there is fluid inside the backpressure before applying Nitrogen gas on the dome side. The system pressure is then gradually increased in steps of 100 psi through a pressure regulator connected to the nitrogen cylinder, while the overburden pressure is increased in steps of 500 psi till the desired system pressure is reached. At all times, the difference in pressure between the system pressure and overburden pressure is maintained at 500 psi. The pressure drops across the cores are monitored using the validyne transducers. The pressure drops at different flow rates are observed and noted. The permeability is measured using different flow rates after measuring pressure drops and by substituting those values in the Darcy equation.

Supercritical CO_2 Foam Preparation

The piston of the ISCO pump is lowered by closing Valve #21 and #22 of the pump. The temperature of the chiller is set to 8 Degrees Celsius. Once the temperature is attained by the chiller, valve #21 and # 23 is opened to the CO_2 tank for about 30 minutes. The valves are closed and the temperature is increased to 40 degrees Celsius as desired. Before running the tests using the high pressure CO_2, the lines are flushed with CO_2 and released before the entrance to the core holder by unscrewing the inline filter fitting. It takes about 1.5 hours for the chiller to reduce the temperature from 40 degrees Celsius to 8 degrees Celsius and then to refill the CO_2 pump.

CO_2 WAG Without Crude Oil

The core is installed into the core holder after the core has been saturated and aged in brine for 48 hours. Brine in the transfer cylinder is pressurized to release air if any. Supercritical carbon dioxide is kept ready at 40 degrees Celsius and 1300 psi using the heater to maintain the temperature. The CO_2 loop is flushed with CO_2 before the start of the experiment.The inline filter is also flushed with the supercritical CO_2 to remove any residue from the previous experiements. The cores are

flooded with brine till the desired system pressure is attained (1300 psi). At all times the over burden pressure is 500 psi above the system pressure. The back pressure regulator is used to provide the system pressure using the nitrogen supply. Fluid is always allowed to flow through the back pressure regulator first for at least 30 minutes before the nitrogen is applied to the dome side. At 1300 psi, the brine flow is halted for about 1 hour 45 minutes. At this point, the transducers are calibrated again if they have drifted. The slug size of WAG is calculated and the time of injection for each slug size is determined. Brine is allowed to flow at the desired flow rate based on the slug size calculations and for the desired cycle time. Once the brine cycle is complete, the valves are closed and the CO_2 valves are opened to the core holder and flow of supercritical CO_2 begins. This change between the two cycles should take around 30 seconds. CO_2 breakthrough is observed and once the desired number of pore volumes is injected, brine injection begins to flush out the CO_2. Depending on the gas flow meter reading, around 6 – 10 Pore volumes (or more) of Brine is injected until no gas is observed in the outlet. While depressurizing the system, the nitrogen supply to the back pressure regulator is closed and the lab view is continued to allow logging data to determine the gas ejected during this time.

CO_2 Foam Flooding Without Crude Oil

The required surfactant solution is prepared and the transfer cylinder is filled with the solution using the flow path similar to Figure 19. The lines are rinsed with the new solution to flush out the previous one. The system is pressurized using the surfactant solution and the transducers are calibrated at 1300 psi. At three different flow rates, the pressure drops are determined in order to observe the permeability changes using surfactant alone before the foam test. Based on the foam quality (90 %, 80% or 70 % foam) the flow rates of the surfactant solution and gas are pre-determined. The foam is pre generated before injecting into the core. The pressure drop across the

core is observed. Once the system is flooded with CO_2 foam, the core is flushed with brine. The core is re-dried and re-saturated in surfactant solution and flooded again with surfactant solution to measure the change in permeability if any. The lines to the transducers and the core holder were always flushed before the start of any experiment in order to prevent contamination of the new solution. Figure 23 describes the schematic flow diagram for the flow path of the CO_2 foam through the core. The green lines in the flow sheet represent the exact flow path for this experiment.

For the purpose of this research, the following series of tests were conducted on the 10 inch Indiana limestone core whose permeability was initially measured and described in

Table 17. Brine was injected at three different flow rates to measure the pressure drops corresponding to these flow rates, which could further be translated to permeability using Darcy's Law. After measuring the permeability of the core, five pore volumes of surfactant was injected at different flow rates to measure the pressure drops across the core. Supercritical CO_2 (90% foam quality) was injected along with the surfactant and was allowed to foam inside the inline mixer before entering the core. Volume of CO_2 foam injected through the period of the test is 113ml. Brine was injected after this test to clean the core and the permeability is measured again.

Five pore volumes of PEI (1wt%, pH 8) -surfactant solution was injected into the same core once the permeability was measured again. This was followed with CO_2 foam generated by PEI (1wt%, pH 8) -surfactant. After injecting 113ml of foam, the core was cleaned with brine and the permeability was measured once again.

Following the above tests, PECNP-surfactant was injected into the same core for five pore volumes after which CO_2 foam generated by PECNP-surfactant was injected. Lastly, the core was cleaned with brine and the permeability was measured again.

Core Flooding with Crude Oil in Place:

1. Primary Drainage

Crude oil was injected into the brine saturated core till no more brine was produced in the outlet. The volume of crude oil used was approximately 2.4 PV. The volume of brine collected was noted and this was the volume that was replaced by crude oil inside the core. Ambient pressure and 500 psi of overburden pressure was applied. The temperature of the oven was maintained at 40 degrees Celsius.

Figure 21 is a schematic diagram representing the flow path for the primary drainage of crude oil through the core. Valve #11, #5, #16 and #8 are kept opened for the purpose of this experiment while the remaining valves are closed. The ISCO pump is used to move the piston inside the transfer cylinder which pushes the crude oil into the core.

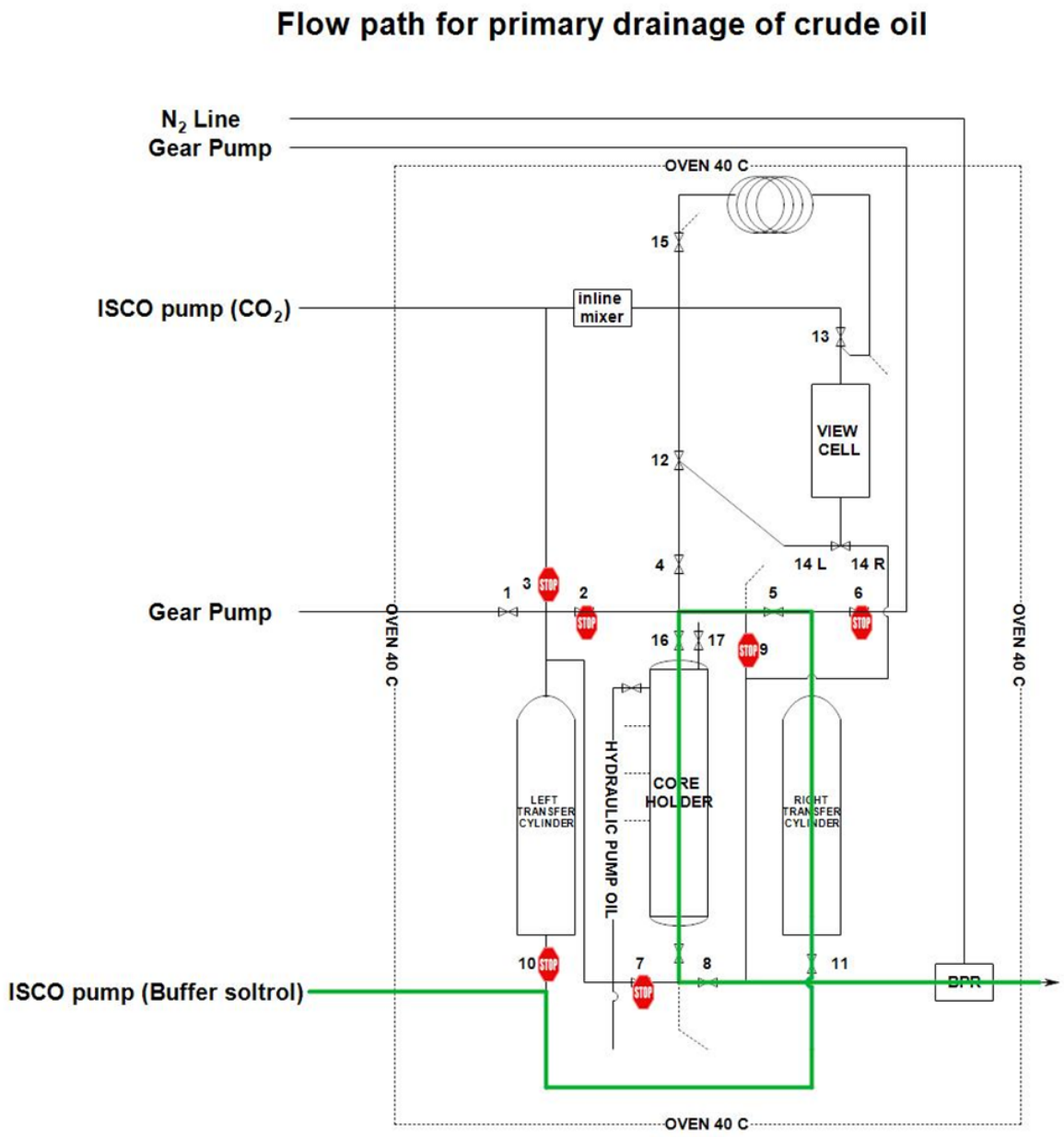

Figure 21 : Flow diagram representing the flow path in green for the primary drainage of crude oil through the core. The crude oil is filled in the right transfer cylinder as explained in Figure 18.

2. Water Flooding

Brine was injected at 0.5 CC/min till no more oil was produced. The volume of oil produced was noted and the residual oil left behind was calculated based on the volume of brine that replaced the oil. Ambient pressure and 500 psi of overburden pressure was applied. The temperature of the oven was maintained at 40 degrees Celsius. Figure 22 is the flow diagram for any aqueous phase injection through the core.

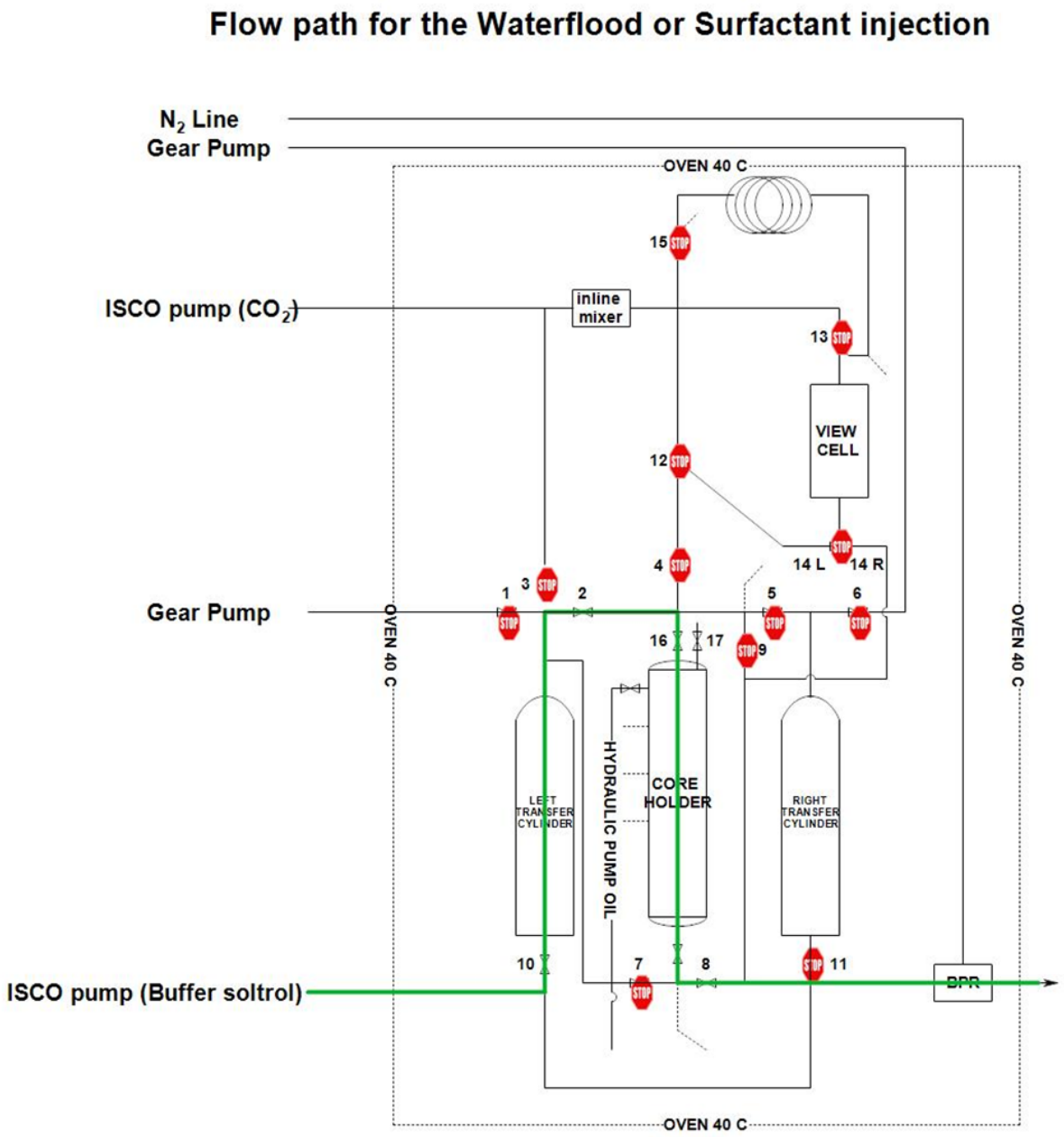

Figure 22: Flow diagram representing the injection of aqueous phase through the core. This flow path can be used for water flooding or surfactant flooding the core in the presence of crude oil or for the measurement of permeability in the absence of crude oil. It is the general flow path for any aqueos phase injection through the core.

3. CO_2 Foam Flooding

Prior to each new test with a new core, the transducers are flushed with transducer oil to clean the transducers. The system is water flooded with brine before the start of the CO_2 foam tests to pressurize the core up to 1300 psi. Typically no oil is produced during this waterflood since it is a continuation of the previous test. The aqueous phase (surfactant or PECNP-surfactant or PEI-surfactant) is mixed with supercritical CO_2 through an inline mixer before it passes through the core. The volume of oil produced along with other fluids are measured at the outlet. Each CO_2 foam test is followed with a waterflood with brine up to 5 PV to clean the core. The flow path for this test is the same as the CO_2 foam test without crude oil and can be represented by Figure 23. Table 4 summarizes the sequence of the tests that were conducted for each core along with the operating conditions.

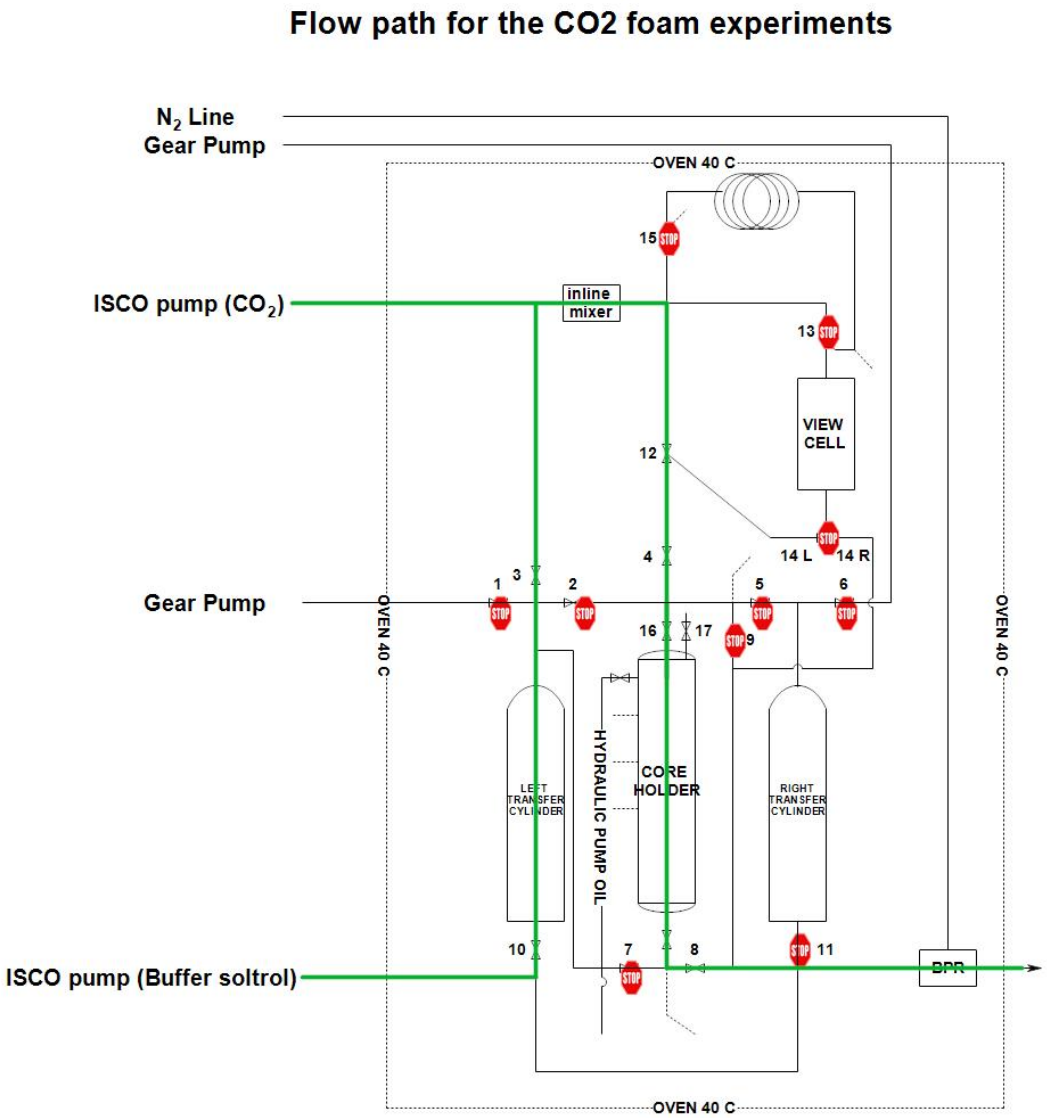

Figure 23: Flow diagram representing the flow path for the CO2 foam generation through the 7 micron inline filter followed by the injection through the core. This flow path can be followed after water flooding the core in the presence of crude oil or can be performed in the absence of crude oil to measure the average apparent viscosity of the foam.

Table 4: Sequence of the CO_2 foam tests conducted on each core along with their operating conditions [49].

Core #1		
Test	**Pressure (psi)**	**Temperature (Celcius)**
Primary Drainage	Ambient	40
Water flooding	Ambient	40
Water flooding	1300	40
CO2 foam , surfactant generated	1300	40
Water flooding	1300	40
CO2 foam ,NP-surfactant generated	1300	40
Water flooding	1300	40
CO2 foam ,PEI (1wt%, pH 8) -surfactant generated	1300	40
Water flooding	1300	40
Core #2		
Test	**Pressure (psi)**	**Temperature (Celcius)**
Primary Drainage	Ambient	40
Water flooding	Ambient	40
Water flooding	1300	40
CO2 foam ,NP-surfactant generated	1300	40
Water flooding	1300	40
CO2 foam ,PEI (1wt%, pH 8) -surfactant generated	1300	40
Water flooding	1300	40
CO2 foam , surfactant generated	1300	40
Water flooding	1300	40
Core #3		
Test	**Pressure (psi)**	**Temperature (Celcius)**
Primary Drainage	Ambient	40
Water flooding	Ambient	40
Water flooding	1300	40
CO2 foam ,PEI (1wt%, pH 8) -surfactant generated	1300	40
Water flooding	1300	40
CO2 foam ,NP-surfactant generated	1300	40
Water flooding	1300	40
CO2 foam , surfactant generated	1300	40
Water flooding	1300	40

Pressure Transducers

Four Validyne differential pressure transducers were used to measure the pressure drop across the core during the core flood experiments. Three of the pressure transducers had a maximum differential pressure rating of 125 psi and these were used to measure section wise pressure drops across the core. The last pressure transducer was used to measure the overall pressure drop across the whole core and had a higher differential pressure rating of 500 psi.

3.3.6 Core Flood to Measure Formation Damage

Apart from studying the stability of the foam and the final oil recovery, the damage to the core by the PECNP-surfactant is measured. It is possible for the oppositely charged ions to interact with the reservoir rock or for coagulation of the PECNP to plug the cores, thereby reducing the permeability. This could be detrimental for oil recovery. Different tests were done to prove that the permeability could be recovered after injecting the nanoparticles. Initially, the PECNP-surfactant solution was injected into the 10 inch core after the completion of core flood tests in the absence of oil and the pressure drops were monitored to determine any unusual changes. Also, the cores were flushed with brine after every CO_2 foam test to measure the permeability.

Since all these permeability recovery tests were conducted on a core that was already tested, the PECNP-surfactant used for this research was injected into a smaller new core of 3 inches in length. The experimental setup used for this test is shown in the figure below. The flow path for the injection of the PECNP-surfactant was relatively straight forward. Ten PV of brine (2wt% KCl) was injected to measure the initial permeability of the core. This was followed by the injection of 5 PV of PECNP-surfactant. Finally, 10 PV of brine was injected to flush the PECNP-surfactant solution from the core to recover the permeability. Three different flow rates were used to measure the permeability of the core.

A foam quality of 90% is used for all the core flood tests and hence only 10% of PECNP-surfactant is used. Therefore, the PECNP-surfactant solution was diluted further by 10 times and injected in another 3 inch core from the same block having similar initial permeability.

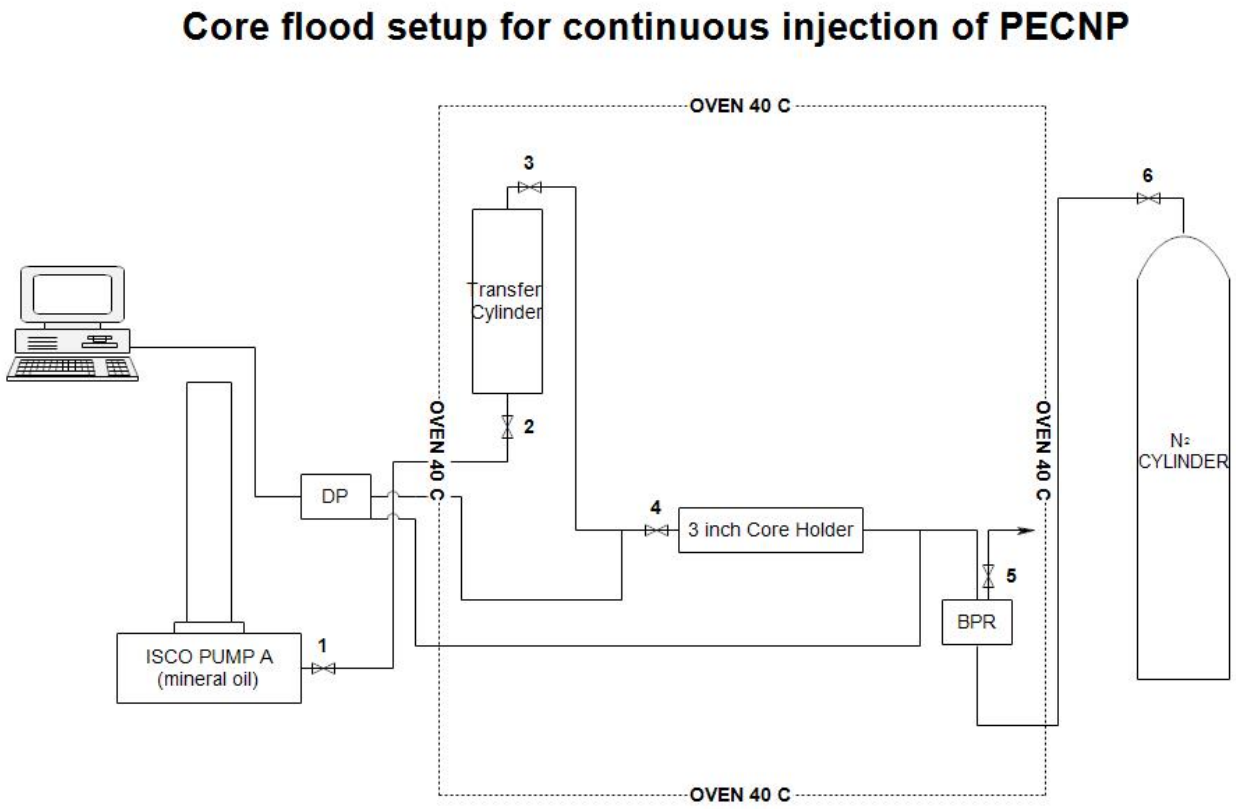

Figure 24: Schematic of the 3 inch core flood setup to measure the permeability recovered after the continuous injection of PECNP solution.

3.3.7 Viscometer and Densitometer

A Brookfield viscometer and an Anton Paar densitometer were used for measuring the viscosities and densities of the different samples that were used through the course of this research.

Working Principles

The viscometer comprises of a spindle (disk) that is submerged into the sample and the force applied to overcome the resistance against rotation or flow is measured. Based on the viscosity of the sample, the resistance to the movement of the sample changes with the speed of the spindle in use. Table 5 summarizes the densities and viscosities for the operating temperature.

Table 5: Summary of the viscosity and density at a particular temperature for the different samples used in this research [49].

Sample	Temperature (Ceclius)	Density (g/cc)	Viscosity (cP)
2wt% KCl	40.00	1.00	0.81
Surfactant	40.00	1.01	1.24
PEI(1WT%_Ph 8)-Surfactant	40.00	0.97	0.72
PECNP-Surfactant	40.00	1.06	0.71
PECNP-Surfactant diluted 10 times with 2wt% KCl	40.00	1.00	0.63
Light Mineral Oil	40.00	0.84	15.00
LKC Crude oil	40.00	0.83	5.86
Mississippian Crude oil	40.00	0.82	3.88
NP DIL 10 X IN 2WT% KCL	40.00	1.34	0.74

Chapter 4: Results and Discussion

4.1 Effect of Particle Size and Charge on the Overall Stability of the Systems

Foams are not thermodynamically stable but they possess some degree of kinetic stability [5]. Surfactants are used for the stabilization of the foams by increasing the electrostatic repulsive forces [17]. However the surfactants dynamically leave and enter the interface thereby making the foam film unstable [34]. The zeta potential and particle size for the different batches of the nanoparticles are summarized below. As described in chapter 3, the different batches of nanoparticles represent the ratio of the PEI: DS and the different pH of PEI used. Zeta potential values provide a good indication of the magnitude of the interaction between the interfaces. The stability of the system can be assessed based on the values. A large zeta potential value represents higher repulsive forces and a lower zeta potential value lacks any force that could prevent the interfaces from interacting with each other. Thus, the best combination with a smaller particle size and most importantly a high zeta potential value along with a lower polydispersity is chosen as the optimized batch of nanoparticle with the ideal pH of PEI. Batch number 3 with PEI of pH 8 was selected as it generated a more stable nanoparticle. Table 6 summarizes the values of the zeta potential and effective mean diameter for the different batches of PECNP-surfactant.

The stability of the nanoparticle system differed between RO water and 2wt% KCl. The best nanoparticle system in the RO water base had a 2:1 ratio of PEI: DS whereas the nanoparticle that was prepared in 2wt% KCl base had a 3:1 ratio of PEI: DS. It should be noted that the PEI and DS were also prepared in 2wt% KCl base and hence the salinity would have influenced the particle size and charge of the nanoparticle system. Figure 25 represents the effect of salinity on PECNP-surfactant system for different pH of PEI used. For an RO Water based system the change in zeta

potential with pH is very steep compared to the 2wt% KCl based system. For the purpose of this analysis, the PECNP-surfactant was prepared using 2:1:0.1 of PEI: DS: RO water/ 2wt% KCl. The stability of the PECNP-surfactant in an RO water based system is much more stable for a given pH of PEI used compared to the 2wt% KCl system.

Table 7, Table 8, Table 9 and Table 10 provides the zeta potential values and mean effective diameter for the PECNP, PECNP diluted 4 times and 8 times in RO water and PECNP-surfactant solutions for an RO water based system. It can be observed that the zeta potential values are the highest with a small mean effective diameter for the PECNP-surfactant solution with PEI of pH 8.

Table 6: Summary of the effective diameter, polydispersity and zeta potential values for the different batches of PECNP synthesized in 2wt% KCl [49].

PECNP-SURFACTANT						
Batch	**pH of PEI (1 wt %)**	**Mean Diameter (nm)**	**Polydispersity**	**Average Count Rate (kcps)**	**Mean Zeta Potential (mV)**	**Mobility**
1	8	442.00	0.36	462.50	8.73	0.68
1	8.5	234.53	0.20	464.00	14.26	1.11
1	9	327.28	0.21	93.60	8.66	0.68
2	8	167.35	0.21	450.00	1.14	0.09
2	8.5	140.47	0.19	465.90	10.29	0.80
2	9	215.78	0.33	466.50	8.73	0.68
3	**8**	**155.00**	**0.17**	**375.40**	**22.20**	**1.73**
3	8.5	162.17	0.19	383.00	21.47	1.68
3	9	146.58	0.21	385.30	13.68	0.75
4	8	190.59	0.22	472.80	9.59	0.75
4	8.5	175.62	0.21	410.00	9.72	0.76
4	9	173.63	0.22	445.00	15.36	1.20

Table 7: Summary of the zeta potential values and effective diameter of the PECNP, solution prepared in RO water

pH of PEI	Effective Diameter (nm)	Average Count Rate (kcps)	Zeta Potential(mV)
7.5	969.1	534.4	46.06
8	826.5	400.2	38.24
8.5	503	472.3	43.3
9	292.7	249.9	31.65

Table 8: Summary of the zeta potential values and effective diameter of the PECNP diluted 4 times prepared in RO water

pH of PEI	**Effective Diameter (nm)**	**Average Count Rate (kcps)**	**Zeta Potential(mV)**
7.5	297.9	28.8	56.25
8	579.7	486	48.54
8.5	494.8	402.6	50.82
9	253.5	376.6	29.31

Table 9: Summary of the zeta potential values and effective diameter of the PECNP diluted 8 times prepared in RO water

pH of PEI	**Effective Diameter (nm)**	**Average Count Rate (kcps)**	**Zeta Potential(mV)**
7.5	514.1	427	53.32
8	554.7	320.7	45.35
8.5	566.3	470.8	39.99
9	264.1	73.6	28.83

Table 10: Summary of the zeta potential values and effective diameter of PECNP-surfactant solution prepared in RO water

pH of PEI	Effective Diameter (nm)	Average Count Rate (kcps)	Zeta Potential(mV)
7.5	1068.3	188.7	63.28
8	396.5	15.4	58.21
8.5	920.7	14.9	43.29
9	537.8	490.9	31.8

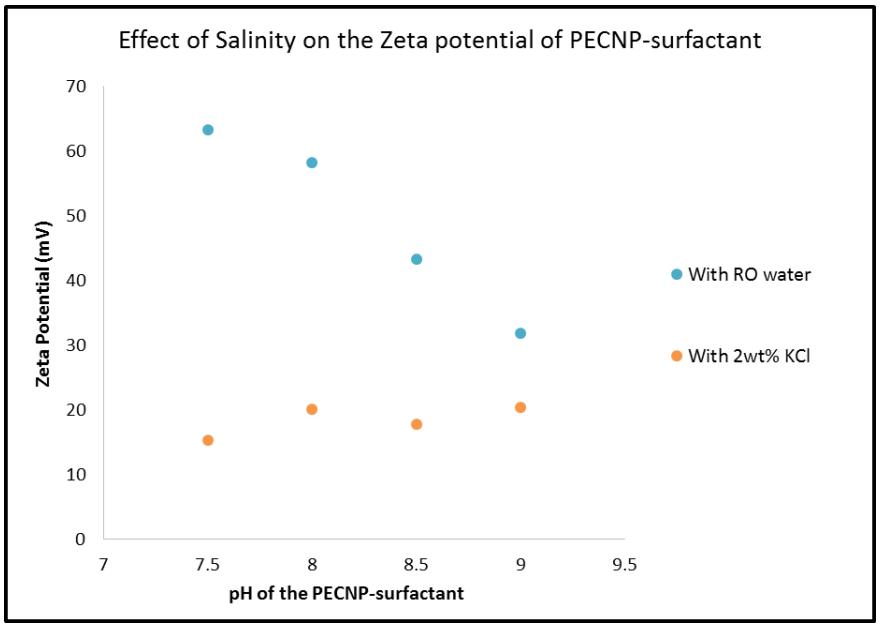

Figure 25: Effect of Salinity on the Zeta potential of PECNP-surfactant can be observed. PECNP is highly influenced by the charge of the solution and the electrostatic interactions.

PEI-surfactant did not yield a favorable count rate in both the RO water and 2wt% KCl and hence the stability of the system could not be assessed as much as the PECNP-surfactant. In conclusion, the PEI-surfactant system does not yield a complex whereas a complex formation could be inferred for the PECNP-surfactant system. However, the PEI-surfactant yielded a durable foam during the view cell tests in the absence of oil which will be discussed in the next few sections.

4.1.1 Interfacial Tension

The lamella in a foam has two gas-liquid interfaces that are separated by a layer of fluid thin film. Interfacial tension arises due to the imbalance of forces between the molecules particularly in the interfacial region [17]. Surfactants tend to lower the interfacial tension through their adsorption at the interface. The decrease in interfacial tension would facilitate the foam formation by reducing the amount of mechanical energy required [17]. The following paragraphs explain the results obtained by the addition of PEI and PECNP to the surfactants and their impact on the interfacial tension, critical micelle concentration and critical aggregate concentration.

Table 11 is the baseline IFT measured for the surfactant in 2wt% KCl. The IFT is calculated as described in chapter 7, (7.6) using the correction factors. By plotting the interfacial tension for the baseline surfactant versus the concentration of the surfactant, the critical micelle concentration (CMC) is obtained. The sudden change in slope in Figure 26 is characterized by the CMC. Based on this plot, the surfactant concentration is maintained below the CMC for all the preparations of solutions. Similar tests were conducted for the PEI-surfactant solutions as well as the PECNP-surfactant solutions.

It can be observed from Figure 25 and Figure 28 that the addition of PEI and PECNP to the surfactant results in a decrease in CMC and thus would reduce the burden on the surfactan

Table 11: Summary of Interfacial tension for different concentrations of Surfactant in 2wt% KCl.

Concentration (wt %)	IFT (dynes/cm)
0.025	3.24
0.05	2.8
0.075	2.65
0.1	2.57
0.15	2.13
0.2	2.09
0.25	2.05

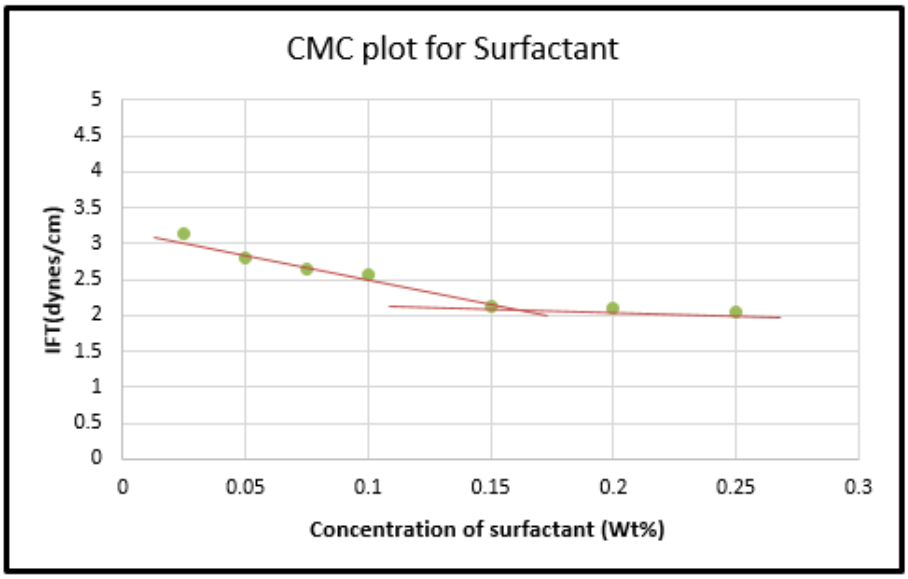

Figure 26: Critical Micille Concentration plot for Surfactant (N120 – 0.1wt%) prepared in 2wt% KCl.

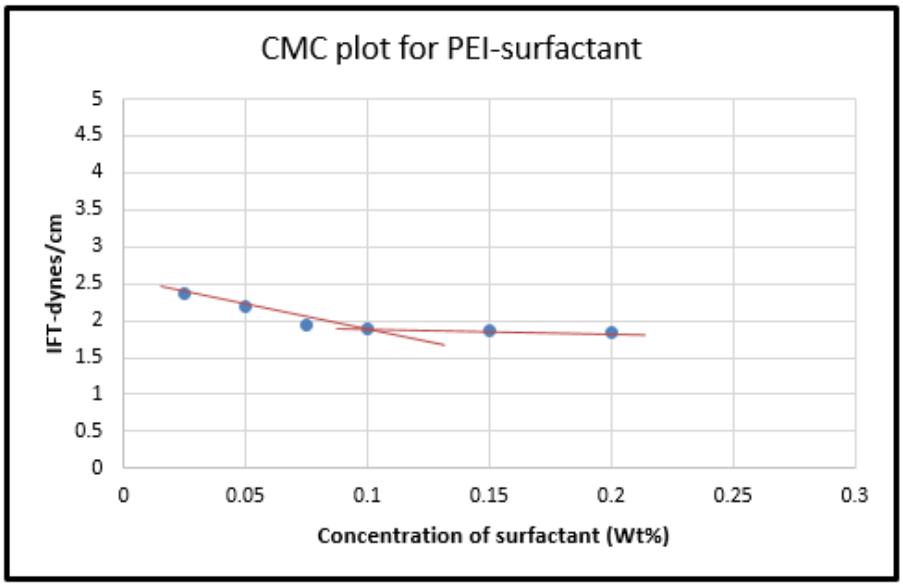

Figure 27: Critical Micelle Concentration plot for PEI-Surfactant (PEI- 1wt%, pH -8). Final concentration of surfactant is maintained at 0.1wt%. The ratio of the PEI:surfactant is also maintained at 1:9. The solution is prepared in 2wt% KCl.

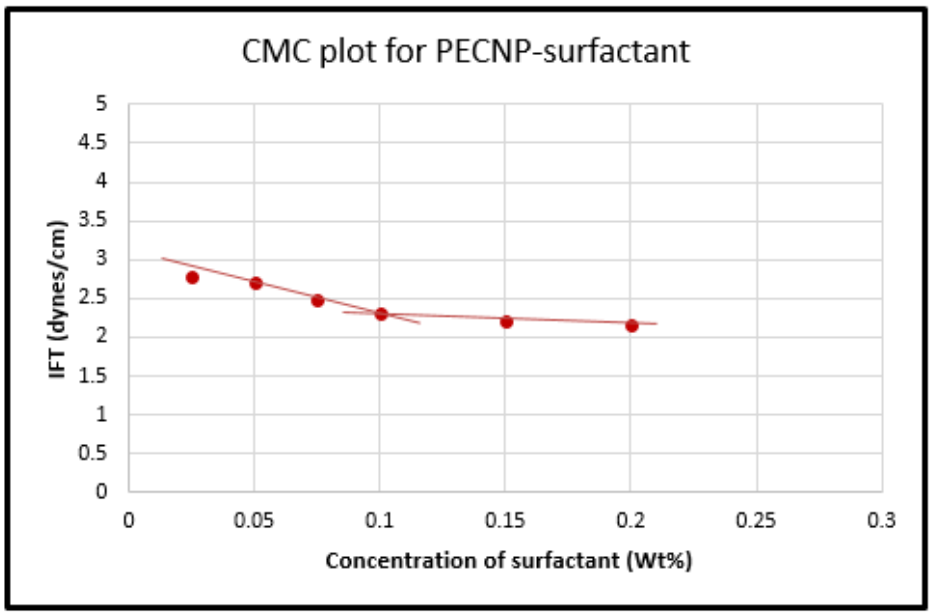

Figure 28 : Critical Micille Concentration plot for PECNP-Surfactant. The final concentration of surfactant is maintained at 0.1wt% and PECNP is prepared using PEI(1wt%, pH-8). The ratio of the PECNP:surfactant is also maintained at 1:9. The solution is prepared in 2wt% KCl.

Apart from knowing the CMC of the surfactant, polyelectrolytes are characterized by two other important parameters: CAC and overlap concentration (c*) which were discussed in chapter 2. The concentration of the branched PEI is maintained at 1wt% which is below the overlap concentration from literature . Also, the ratio of the surfactant to PEI/PECNP is maintained at 9:1 which is also below the CAC. Table 12 represents the IFT values for different concentrations of PEI having the same pH of 8.

Table 12: Summary of the IFT measured for the different concentrations of PEI prepared in 2wt% KCl.

PEI (Concentration wt %)	IFT (dynes/cm)
0.5	1.89
1	1.89
2	2.25

To avoid stratification of the foam film, the concentration of the surfactant is maintained below the CMC, the polyelectrolyte concentration is well below the overlap concentration and the ratio of the PEI/PECNP to surfactant is mixed such that it is below the CAC to prevent formation of aggregates. This helps in the creation of homogenous films without the formation of aggregates.

4.2 Foam Durability and Stability

Foam durability and stability is also measured through static view cell tests. These tests help understand the durability of the foam in the presence of the different types of oil. The addition of polyelectrolyte to surfactant results in the creation of either a thin newton black film or a thick common black film. The charge of the foam film created plays an important role in determining the stability of the foam based on the different forces that dominate. As discussed in chapter 2, the thickness of the common black film is controlled by the DVLO forces and the thin newton black film is controlled by the steric repulsion. The thin newton black film does not contain any free solvent molecules [22].

The foam durability tests that were conducted using the setup as shown in Figure 12 did not generate any foam. The view cell was filled with the PECNP-surfactant solution leaving 2 cm from the top of the view cell which was later filled with light mineral oil. The foam was not pre generated

and the CO_2 bubbles were injected from the bottom, similar to the IFT measurement tests. Therefore, the setup was later modified to generate a better foam column to study the interaction of the resultant foam with crude oil by filling the view cell with crude oil initially and allowing the foam column to push some of the oil. This could be viewed as a more realistic approach similar to foam injected into the reservoir. Once a considerable volume of foam column is generated, the view cell was isolated to observe the interaction of the foam and crude oil.These results are discussed in the next few sections.

4.2.1 Initial Screening of Foams

The CO_2 foam for the different systems prepared in RO water were screened to determine the foam durability and decay with time. Figure 29 is a graph showing the foam decay in terms of the foam column height with time for the three CO_2 foam systems. It can be observed that the PEI-surfactant and the PECNP-surfactant diluted 10 times have a more stable and durable foam for a longer period of time in the absence of oil and salinity.

It should be noted that the PEI-surfactant and the PECNP-surfactant were mixed in the ratio 1:9. The ratio of the PEI (pH 8): DS for generating the PECNP was maintained at 2:1 and the PECNP was further diluted 10 times with RO water.

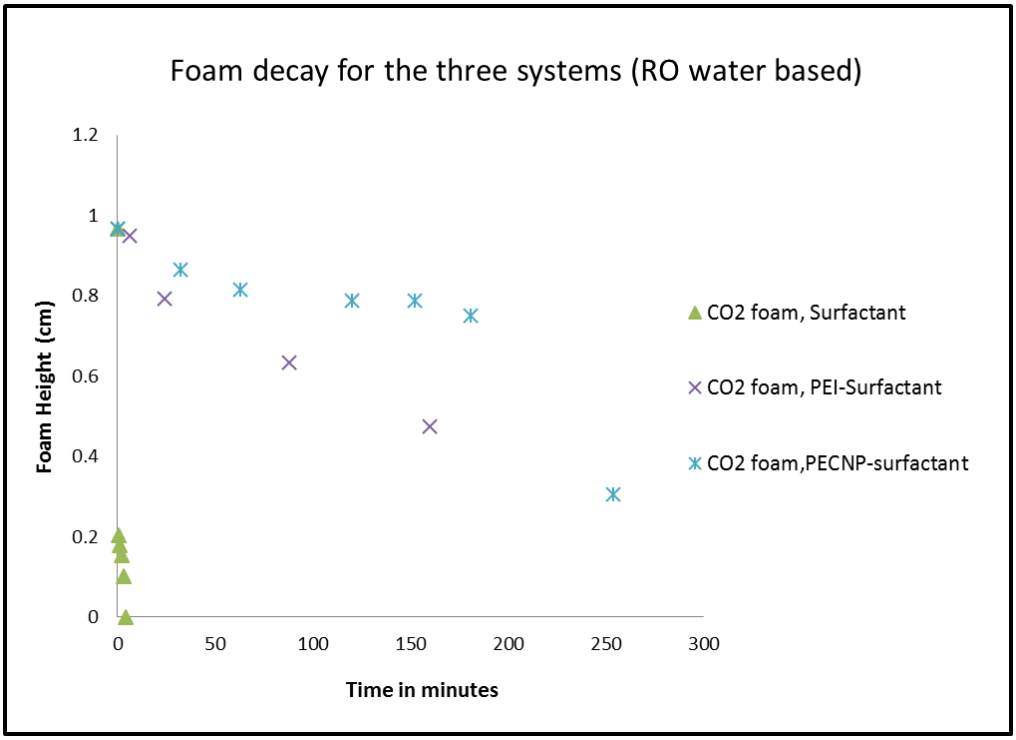

Figure 29: Comparison of the foam column height for the different CO_2 foam systems at a given time. The PECNP used is diluted 10 times with RO water before mixing with surfactant.

4.2.2 Influence of Salinity and Crude Oil on Foams

The final application of the CO_2 foam stabilized by PECNP-surfactant and PEI-surfactant is for enhanced oil recovery. Thus, it is imperative to understand the behavior of these foams in the presence of reservoir conditions. The static view cell tests in the presence of crude oil is a visual depiction of the interaction between the foam and the crude oil. Since the foam is injected into a view cell that is already filled with crude oil, it can be considered as a process closer to the real well conditions. Table 13 summarizes the results of the CO_2 foam tests in the presence of Lansing Kansas city crude oil, Mississippian crude oil, light mineral oil and no oil for brine based systems.

Table 13: Summary of view cell tests for the three CO_2 foam systems in the presence of three different types of oils and the absence of oil for brine based systems [49].

System injected	Without oil in the cell (minutes)	With light mineral oil (minutes)	With LKC crude oil (minutes)	With Mississippian crude oil (minutes)
CO_2 foam, surfactant generated	75	24	8	1
CO_2 foam, PEI-surfactant generated	86	16	3	1
CO_2 foam, NP-surfactant generated	60	31	20	10

In the absence of crude oil, the PEI-surfactant (in 2wt% KCl) foam has the highest foam durability and takes the longest time to decay completely. However, in the presence of different types of oil the PEI-surfactant foam has the least foam durability and stability compared to the other two foam systems.

A decreasing trend in the foam decay with time is observed with the decreasing viscosities of the oils. This could imply that the more viscous oils would emulsify slowly compared to the other oils with higher viscosity and this slow emulsification could retard the rate of foam lamella rupture. Alternatively, the three different oils have different components in them and hence more analysis needs to be done on the composition of the different oils to validate this point. However, if lighter hydrocarbons are present in the oil, it would have a more destabilizing effect on the foam and a heavier molecular weight hydrocarbon would have a lesser impact on the rupture of the foams [5].

The influence of salinity on the durability of foam was studied as well. From Table 14, it can be observed that the PECNP-surfactant when diluted 10 times in RO water created a very stable and a longer lasting foam. The PEI used for the best PECNP-surfactant foam system in RO water also had a pH of 8. However, when the PECNP-surfactant was diluted 10 times in 2wt% KCl, the foam

durability significantly reduced. Thus, the PECNP-surfactant in the ratio 1: 9 was used without diluting for all the remaining brine based tests. The zeta potential values were also measured for the PECNP-surfactant in 2wt% KCl and the optimum ratio of 3:1 of PEI (pH 8): DS was found to be the most stable due to the large zeta potential value. Thus, for the RO water based system, the PECNP-surfactant could be further diluted in RO water and generated a stable nanoparticle but for the 2wt% KCl system, the PECNP-surfactant system could not generate a stable nanoparticle when diluted in 2wt% KCl. Also, a higher ratio of PEI:DS is required for a stable PECNP-surfactant solution when prepared in 2wt% KCl compared the RO water PECNP system which had a 2:1 ratio of PEI:DS by volume.

Table 14: Comparison of the dilution effect on the PECNP-surfactant in RO water versus 2wt% KCl system.

System	pH of PEI used	RO water	2wt% KCl
		Foam decay (minutes)	Foam decay (minutes)
PECNP-surfactant	8	22	38
PECNP-surfactant diluted 10 times	8	80	20

Images of the surfactant foam, PEI-surfactant foam and PECNP-surfctant foam for the brine system in the absence and presence of light mineral oil and crude oil are presented for different time intervals from Figure 30 to Figure 56.

Surfactant without Oil:

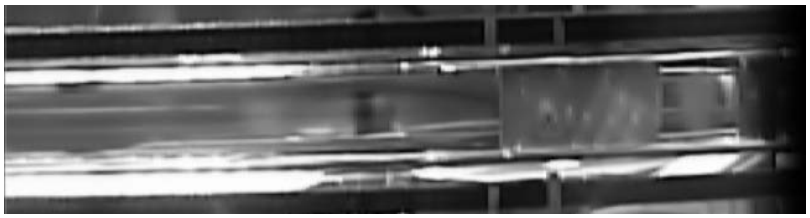

Figure 30: Surfactant foam column in the absence of oil after 5 seconds. The surfactant foam is injected from the right. The actual orientation of the view cell is vertical but is represented horizontal as a picture here.

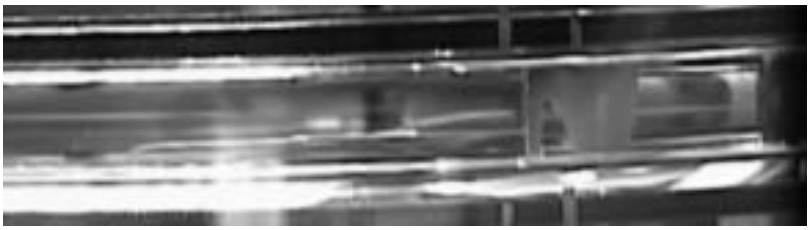

Figure 31: Surfactant foam column in the absence of oil after 20 minutes. The surfactant foam is injected from the right. The actual orientation of the view cell is vertical but is represented horizontal as a picture here.

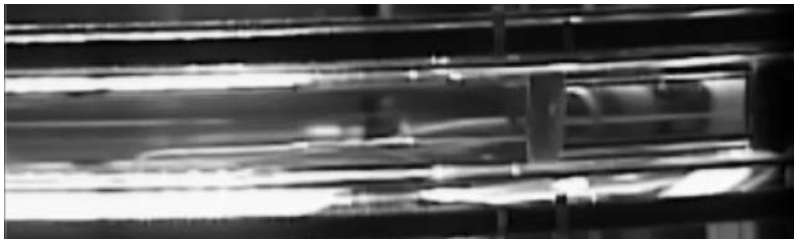

Figure 32: Surfactant foam column in the absence of oil after 75 minutes. The surfactant foam is injected from the right. The actual orientation of the view cell is vertical but is represented horizontal as a picture here.

Surfactant with Light Mineral Oil:

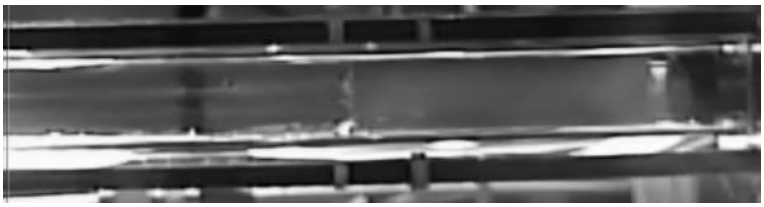

Figure 33: Surfactant foam column in the presence of light mineral oil after 5 seconds. The surfactant foam is injected from the right. The actual orientation of the view cell is vertical but is represented horizontal as a picture here.

Figure 34: Surfactant foam column in the presence of light mineral oil after 20 minutes. The surfactant foam is injected from the right. The actual orientation of the view cell is vertical but is represented horizontal as a picture here.

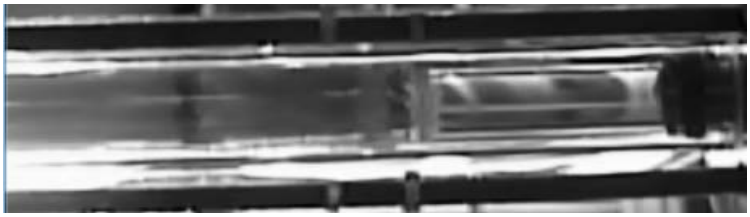

Figure 35: Surfactant foam column in the presence of light mineral oil after 60 minutes. The surfactant foam is injected from the right. The actual orientation of the view cell is vertical but is represented horizontal as a picture here.

Surfactant with Mississippian Crude Oil:

Figure 36: Surfactant foam column interacting with Mississippian crude oil after 20 seconds. The foam is injected from the right. The actual orientation of the view cell is vertical but is represented horizontal as a picture here.

Figure 37: Surfactant foam column interacting with Mississippian crude oil after 50 seconds. The foam is injected from the right. The actual orientation of the view cell is vertical but is represented horizontal as a picture here.

Figure 38: Surfactant foam column interacting with Mississippian crude oil after 1 minute. The foam is injected from the right. The actual orientation of the view cell is vertical but is represented horizontal as a picture here.

PEI-Surfactant without Oil:

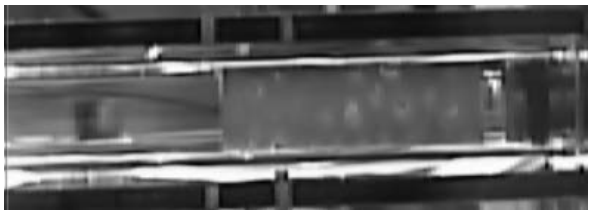

Figure 39: PEI-Surfactant foam column in the absence of oil after 5 seconds. The surfactant foam is injected from the right. The actual orientation of the view cell is vertical but is represented horizontal as a picture here

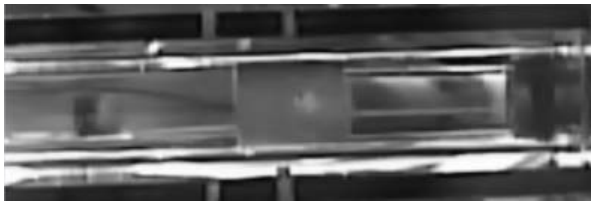

Figure 40: PEI-Surfactant foam column in the absence of oil after 15 minutes. The surfactant foam is injected from the right. The actual orientation of the view cell is vertical but is represented horizontal as a picture here

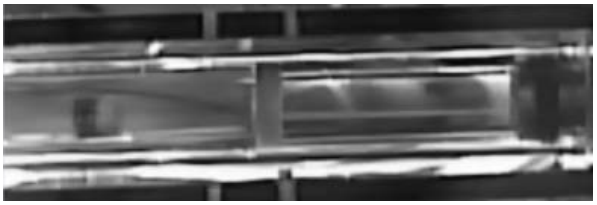

Figure 41: PEI-Surfactant foam column in the absence of oil after 86 minutes. The surfactant foam is injected from the right. The actual orientation of the view cell is vertical but is represented horizontal as a picture here

PEI-Surfactant with Light Mineral Oil:

Figure 42: PEI-Surfactant foam column in the presence of light mineral oil after 5 seconds. The surfactant foam is injected from the right. The actual orientation of the view cell is vertical but is represented horizontal as a picture here

Figure 43: PEI-Surfactant foam column in the presence of light mineral oil after 8 minutes. The surfactant foam is injected from the right. The actual orientation of the view cell is vertical but is represented horizontal as a picture here

Figure 44: PEI-Surfactant foam column in the presence of light mineral oil after 16 minutes. The surfactant foam is injected from the right. The actual orientation of the view cell is vertical but is represented horizontal as a picture here

PEI-Surfactant with Missisipian Crude Oil

Figure 45: PEI-Surfactant foam column interacting with Mississippian crude oil after 5 seconds. The foam is injected from the right. The actual orientation of the view cell is vertical but is represented horizontal as a picture here

Figure 46: PEI-Surfactant foam column interacting with Mississippian crude oil after 47 seconds. The foam is injected from the right. The actual orientation of the view cell is vertical but is represented horizontal as a picture here

Figure 47: PEI-Surfactant foam column interacting with Mississippian crude oil after 1 minute. The foam is injected from the right. The actual orientation of the view cell is vertical but is represented horizontal as a picture here

PECNP-Surfactant Without Oil

Figure 48: PECNP-Surfactant foam column in the absence of oil after 5 seconds. The surfactant foam is injected from the right. The actual orientation of the view cell is vertical but is represented horizontal as a picture here

Figure 49: PECNP-Surfactant foam column in the absence of oil after 20 minutes. The surfactant foam is injected from the right. The actual orientation of the view cell is vertical but is represented horizontal as a picture here

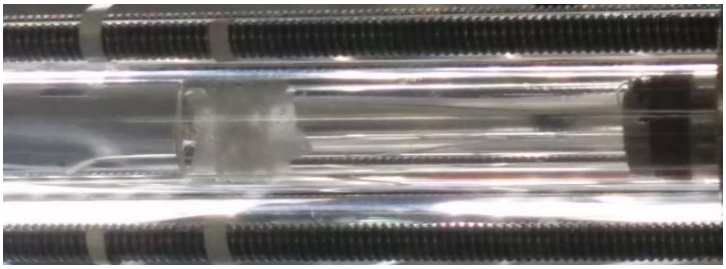

Figure 50: PECNP-Surfactant foam column in the absence of oil after 60 minutes. The surfactant foam is injected from the right. The actual orientation of the view cell is vertical but is represented horizontal as a picture here

PECNP-Surfactant with Light Mineral Oil

Figure 51: PECNP-Surfactant foam column in the presence of light mineral oil after 5 seconds. The surfactant foam is injected from the right. The actual orientation of the view cell is vertical but is represented horizontal as a picture here

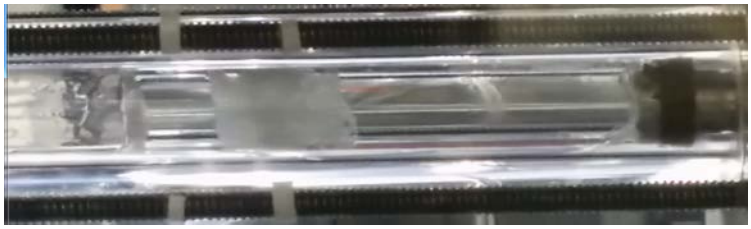

Figure 52: PECNP-Surfactant foam column in the presence of light mineral oil after 15 minutes. The surfactant foam is injected from the right. The actual orientation of the view cell is vertical but is represented horizontal as a picture here

Figure 53: PECNP-Surfactant foam column in the presence of light mineral oil after 32 minutes. The surfactant foam is injected from the right. The actual orientation of the view cell is vertical but is represented horizontal as a picture here

PECNP-Surfactant Mississippian Crude Oil:

Figure 54: PECNP-Surfactant foam column interacting with Mississippian crude oil after 5 seconds. The foam is injected from the right. The actual orientation of the view cell is vertical but is represented horizontal as a picture here

Figure 55: PECNP-Surfactant foam column interacting with Mississippian crude oil after 4 minute. The foam is injected from the right. The actual orientation of the view cell is vertical but is represented horizontal as a picture here

Figure 56: PECNP-Surfactant foam column interacting with Mississippian crude oil after 11 minutes. The foam is injected from the right. The actual orientation of the view cell is vertical but is represented horizontal as a picture here

4.3 Rheology of the CO_2 Foam Systems

Surfactant monolayer at the foam interface can be expanded and compressed. Thus the dynamic surface tension that is created is due to the surface dilatational viscosity, surface shear viscosity and elastic forces [5]. It is hard to measure the interfacial viscosity separately since the CO_2 phase is a supercritical. Thus, the bulk viscosities are measured. As mentioned earlier in the literature review chapter, bulk viscosities and surface viscosities act as resistances to the thinning and rupturing of the foam film [5]. Bulk viscosity influences the thinning of the thick common black films while the surface viscosity controls the thinning of the thin newton black film [5]. Generally the foam dilatational viscosity occurs due to the viscous flow within the thin films and the interfacial tension gradients that act along the foam bubble surface. This results in an increase in foam viscosity and act as a resistance to flow. Foams have higher resistance to flow compared to just a liquid or a gas and hence this makes them a more viable option for mobility control in enhanced oil recovery applications.

In a porous medium such as the reservoir, it is important to understand the effect of shear on the average apparent viscosity of the foam. Shearing is an important factor required for the formation of foams. Low superficial velocities of CO_2 foam injection for foam formation might not result in the formation of foams since insufficient force is provided [50]. The mobility increases and becomes similar to that of CO_2 thereby defeating the purpose of foam injection. Hence it is essential to study the effect of both the shear as well as the influence of injection rate on the viscosity of the foam. These results can be validated by the dynamic and static rheology tests.

Thus, the study of the viscosity of foam film is important as it provides resistance to the rupture of the foam and the effect of shear on viscosity is also essential to determine the minimum required

superficial velocity. Finally, the increased viscosity is also necessary to achieve mobility control of CO_2.

4.3.1 Dynamic Rheology Test Results

The different flow rates chosen for the dynamic tests were 0.5, 1, 3 cc/minute. Two forces act on the foam during the dynamic test. The first one is the torque that is applied to the measuring cup to shear the foam inside the annulus while the second force is perpendicular to it and is provided by the continuous injection of fluids at a given velocity for the generation of foam. The viscosity increases continuously as the fluids are being injected and the following inferences can be made:

1. As the flow rate increases, the viscosity increases and this could translate to the superficial velocity that is required for the foam generation in a porous medium.
2. The PEI-surfactant foam has the highest viscosity compared to the other two systems.
3. All the three systems have an increasing viscosity trend under a constant shear thus proving that a constant external force is required for the existence of foam. It is important to understand that at any given time, 30 ml of foam or fluid is present inside the annulus. At any given time, the old foam is withdrawn while the new foam is being injected into the measuring cup. Figure 57 is a schematic that represents the viscosity measured with time for the three different foam systems during the dynamic test.

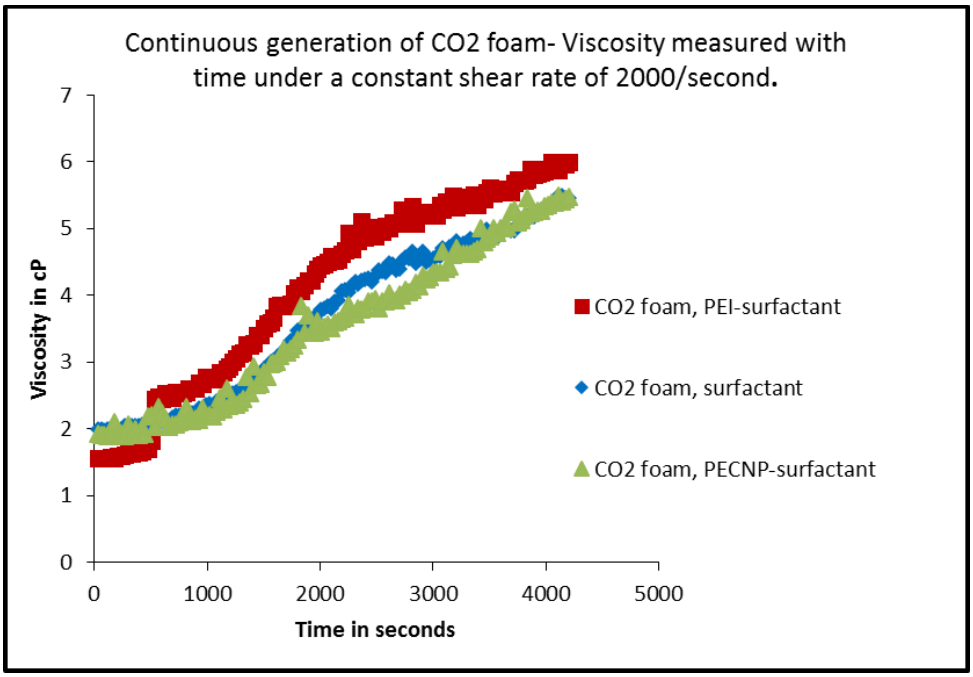

Figure 57: Graph representing the viscosity measured with time under a constant shear for a dynamic test where the foam is continuously being generated at 3cc/minute. The three different foam systems are plotted together to compare their viscosity [49].

4.3.2 Static Rheology Test Results

The static tests were conducted right after the dynamic generation of foam. The valves were closed to isolate the measuring cup and the foam present inside the annulus was sheared continuously at 2000 s^{-1}.The objective of this test was to measure the change in viscosity with time under constant shear rate of 2000 s^{-1} but without the continuous generation of foam. Thus only one external force is provided for shearing the foam. The following inferences are made from these tests:

1. The viscosity of the foam for all three systems are reduced significantly after the continuous generation of foam is halted.
2. From the dynamic tests, it was observed that the viscosity increases as the flow rate increases. Though the viscosity isn't as high as the dynamic test, the same order is

maintained for the static tests, i.e. for foams that were generated at a higher flow rate, the viscosity is higher and is maintained through the completion of the static test.

3. At lower flow rates, the PECNP surfactant foam has the highest viscosity under shear compared to the other two systems. At 3cc/min flow rate, the PEI-surfactant foam has the highest viscosity followed by the PECNP-surfactant. This suggests that a minimum velocity is required for the generation of the foam which is equivalent to the superficial velocity in a porous medium.

For a foam generated at 3cc/minute velocity there is a clear distinction between the PEI-surfactant, PECNP-surfactant and surfactant only foams as observed from Figure 60. Thus, this flow rate is chosen for the core flood tests moving forward. The different static tests that were conducted after different flow rates of dynamic tests are graphically represented in Figure 58, Figure 59 and Figure 60.

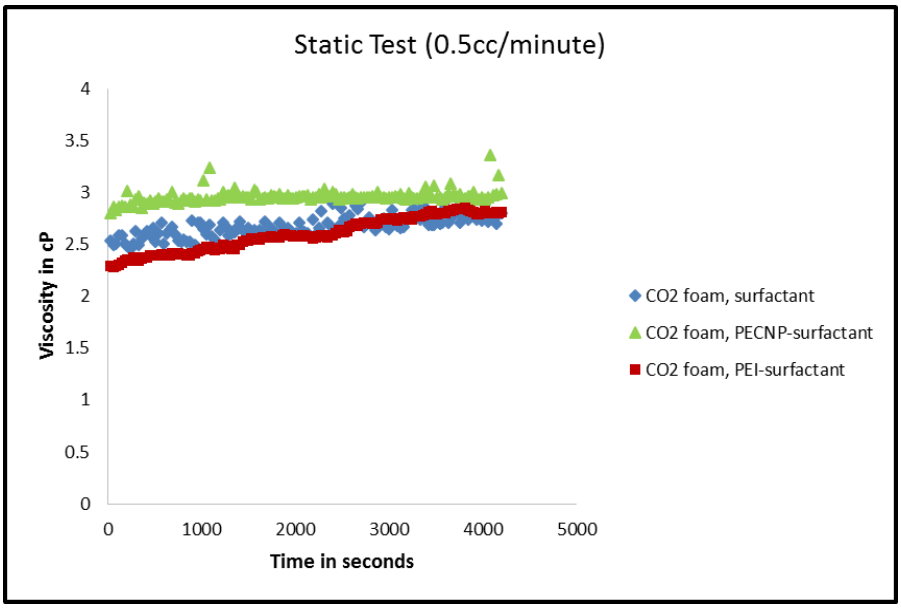

Figure 58: Graph representing the change in viscosity with time for the static test. The dynamic test that was conducted prior to the static test generated foam at 0.5 cc/minute.

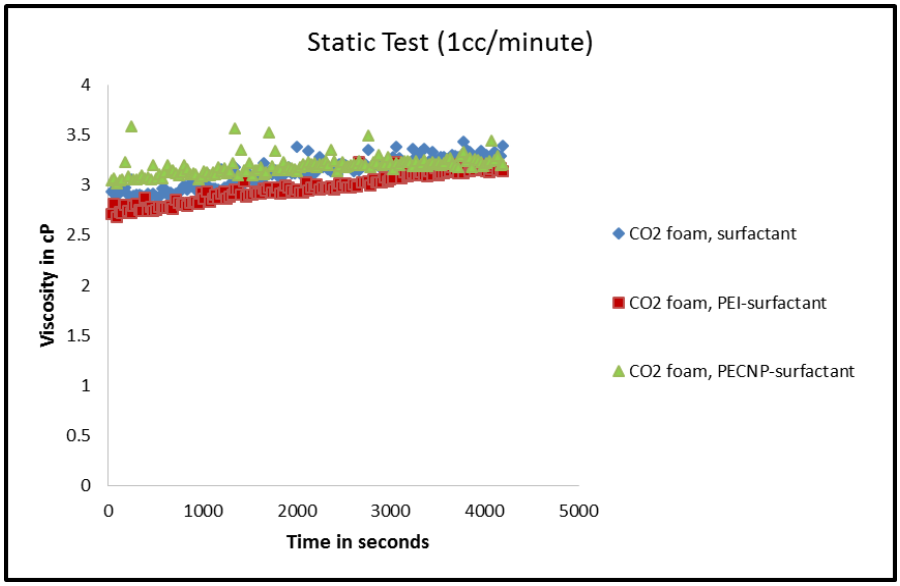

Figure 59: Graph representing the change in viscosity with time for the static test. The dynamic test that was conducted prior to the static test generated foam at 1 cc/minute.

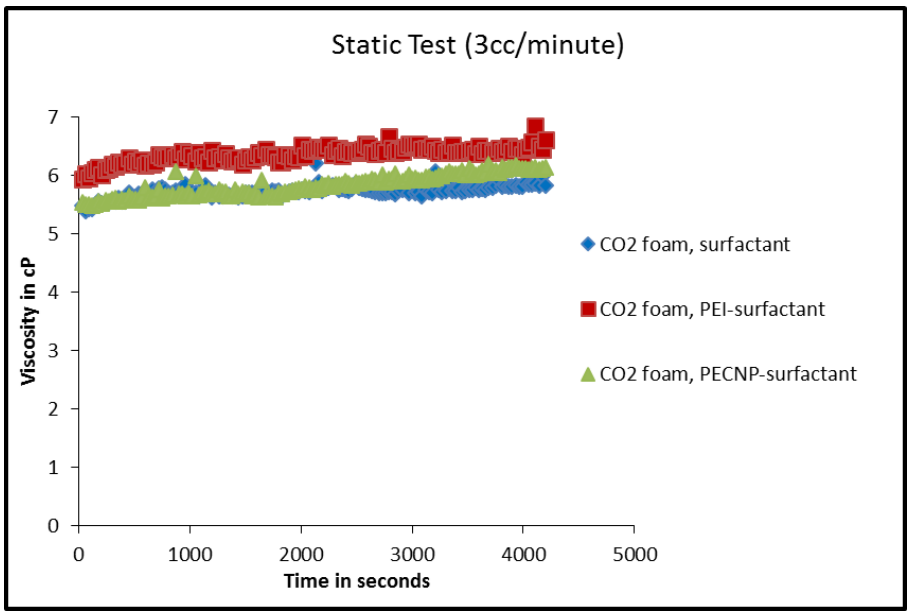

Figure 60: Graph representing the change in viscosity with time for the static test. The dynamic test that was conducted prior to the static test generated foam at 3 cc/minute [48].

A shear sweep test was conducted to observe the effect of shear on the CO_2 foam for the different systems. The power law model attributed by Ostwald and de Waele [51], provided a relationship between shear stress and shear rate which could be applied for non-Newtonian fluids.

$$\tau = K\gamma^n$$

The above equation is the power law model and K represents the flow consistency index, n is flow behavior index or the power law exponent. Following this, the apparent viscosity of the foams could be determines as:

$$\mu_{app} = K\gamma^{n-1}$$

Table 15 summarizes the values of the power law exponent and consistency index for the three different CO_2 foam systems. The foams are pseudo plastic in nature and it can be seen that the flow consistency index is the highest for the CO_2 foam generated by the PECNP-surfactant system

and the power law exponent is the highest for the CO_2 foam generated using PEI (1wt%, pH 8)-surfactant system. The average apparent viscosity calculated at a shear rate of 2000 s^{-1} is found to be the highest for the PEI-surfactant foam. This phenomenon is believed to occur as a result of generating a more stable interface using polyelectrolytes and nanoparticles. The more shear thinning the foam, the higher the viscosity would be when the foam enters a fracture and lower inside a matrix.

Table 15: Summary of the flow consistency index , power law exponent for the three CO_2 foam systems and average apparent viscosity at 2000 s^{-1}, obtained from the ramping tests [49].

System	n	K	R^2	μ_{app}
CO_2 foam, surfactant generated	0.38	0.57	0.98	0.07
CO_2 foam, PEI-surfactant generated	0.38	0.60	0.97	0.12
CO_2 foam, PECNP-surfactant	0.34	0.80	0.98	0.07

4.3.3 Influence of Salinity in the Rheology of the Foam

The surfactant, PEI-surfactant and PECNP-surfactant were prepared in RO water and in 2wt% KCl. The results summarized till now were for the foam systems that were prepared in 2wt% KCl. Although it is sufficient to understand these results for a brine based foam system since the real reservoir conditions would include some amount of salinity, it is worthwhile to observe the influence of salinity in the rheology of the foam systems.

From Figure 61, Figure 62 and Figure 63, it is interesting to note that the viscosity of all the three foam systems increase when salinity is introduced. The PECNP-surfactant foam increases by a greater degree followed by the PEI-surfactant foam when salinity is introduced. This shows that

the PEI and PECNP are highly influenced by charge and hence the bulk rheology of the foam is dependent on the charge of the components.

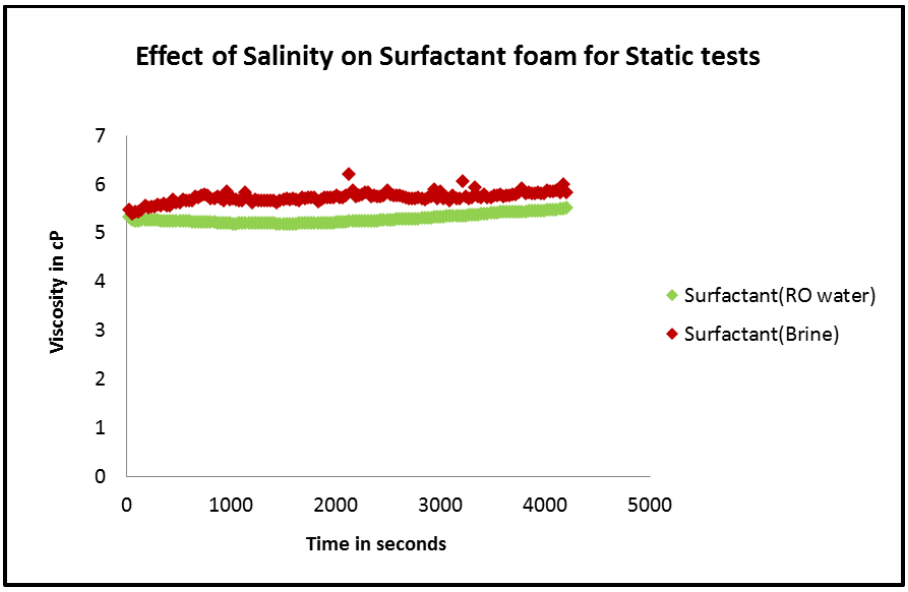

Figure 61: Comparison of the viscosity with time for the surfactant foam generated in RO water versus 2wt% KCl

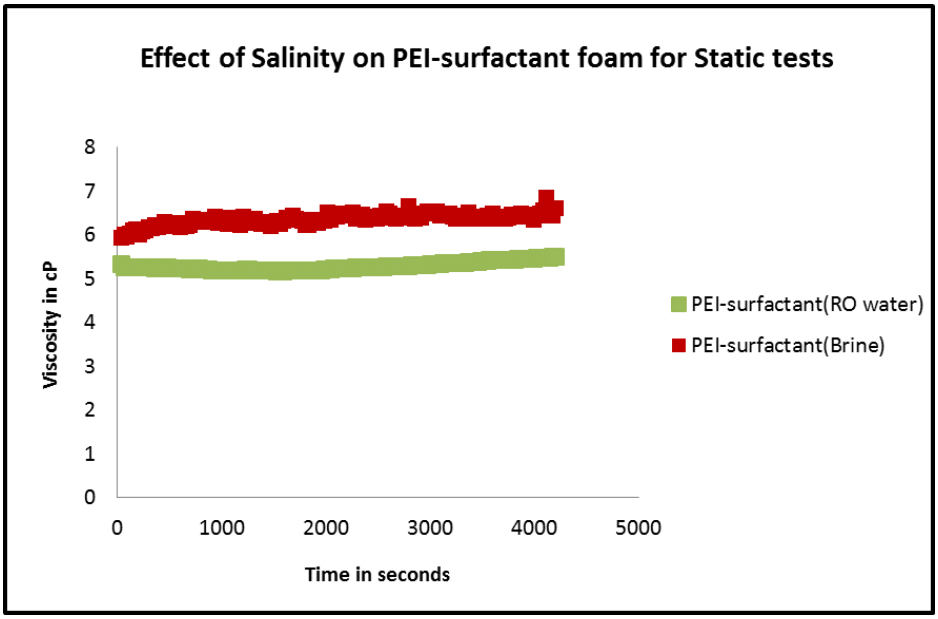

Figure 62: Comparison of the viscosity with time for the PEI-surfactant foam generated in RO water versus 2wt% KCl.

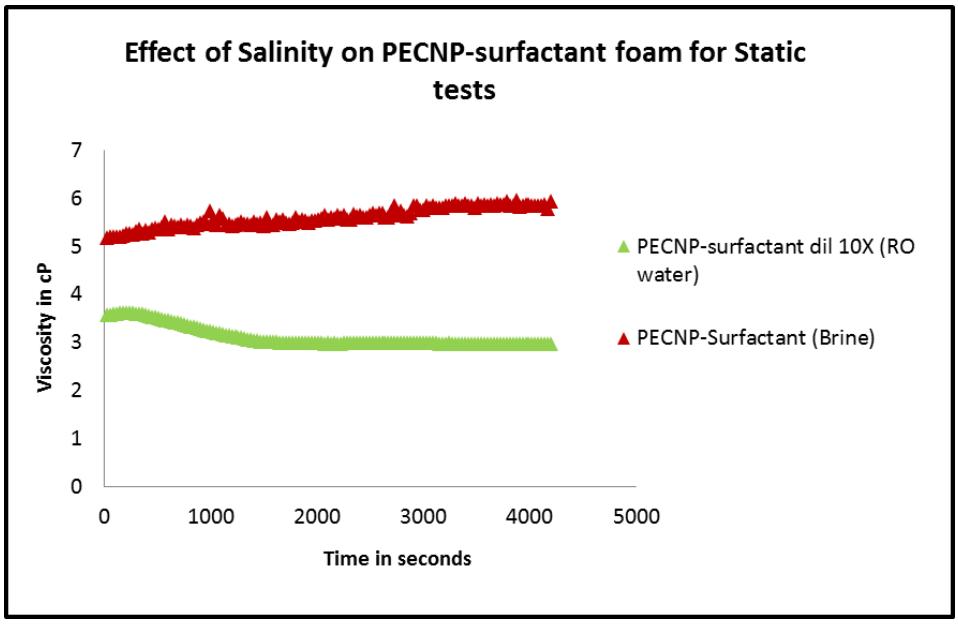

Figure 63: Comparison of the viscosity with time for the PECNP-surfactant foam generated in RO water versus 2wt% KCl.

4.3.4 Influence of Foam Quality in the Rheology of Foam

Additionally, the influence of foam quality on the viscosity of the foam was also studied during these tests. The rheology of the different foam systems discussed till now have a 90% foam quality. Generally, foams with 90% foam quality have reduced mobility since they are composed primarily of the gaseous phase [1] . Thus the film is composed of just 10% of the aqueous phase and is challenging to obtain a more stable foam film with such a low aqueous composition. Foam mobility typically reaches a minimum value approximately in the 50-80% quality range [52].

It can be observed that for the surfactant used in this research, the 90% foam quality has the highest viscosity with shear and the viscosity is reduced as the foam quality decreases as represented in Figure 64. The influence of temperature is also observed from these tests. As the temperature increases, the foam viscosity reduces thereby indicating a sensitivity to higher temperatures. This is represented in Figure 65.

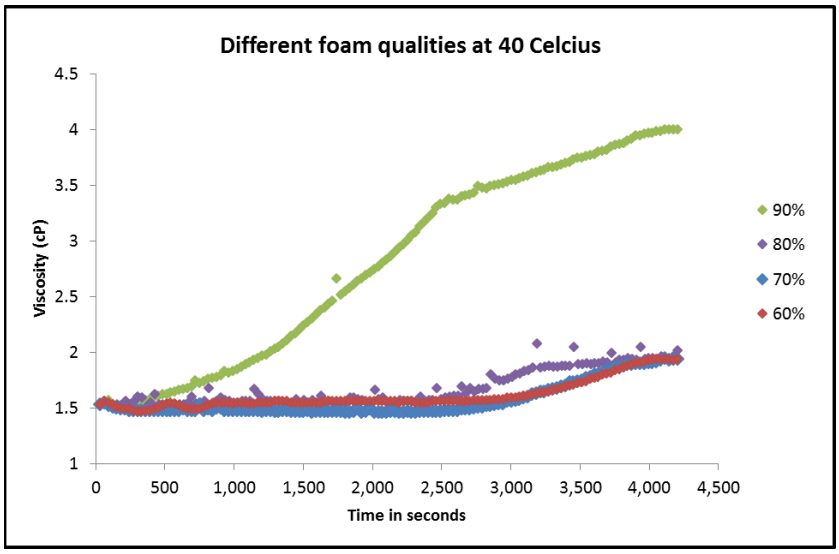

Figure 64: : Graph representing the influence of different foam qualities on the viscosity for the surfactant foam at 40 degrees Celsius during a Dynamic test.

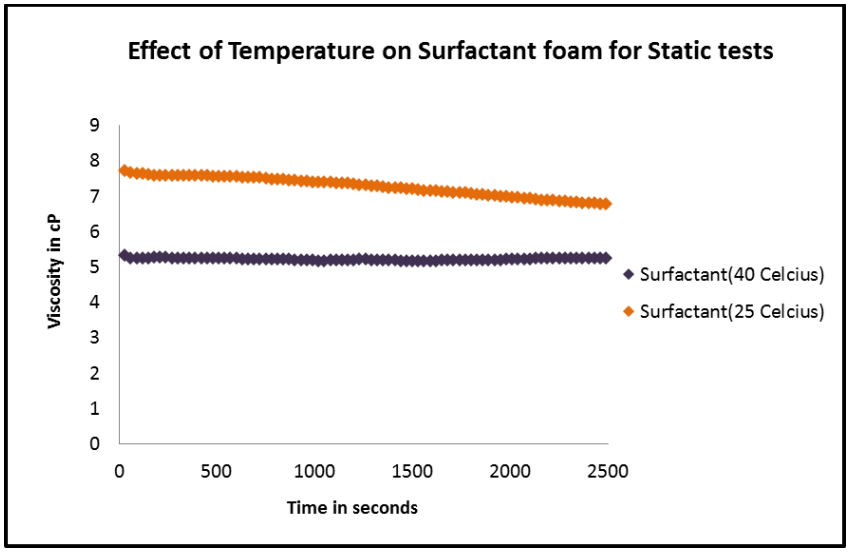

Figure 65: : Graph representing the effect of temperature on the viscosity of surfactant foam during a static test.

The rheology and view cell tests have proved that the PECNP-surfactant and PEI-surfactant foams have a slightly favorable viscosity and are significantly more durable as a foam system compared to the surfactant foam. The core flood tests in the presence and absence of crude oil will be

discussed in the next few sub-sections. The pressure transducers used to measure the pressure drop across the core were calibrated and their sensitivity to different operating conditions were tested before the start of the core flood tests. The core flood setup is designed to perform different tests. A few tests that were conducted prior to the foam tests are summarized as well. Finally, the CO_2 foam tests in the absence of oil is conducted to determine the average apparent viscosity of the foams and determine the most stable foam front.

4.4 Core Flood Testing Without Crude Oil

The rheology and view cell tests have proved that the PECNP-surfactant and PEI-surfactant foams have a favorable viscosity and are more durable as a foam system compared to the surfactant foam. The core flood tests in the presence and absence of crude oil will be discussed in the next few sub-sections. The pressure transducers used to measure the pressure drop across the core were calibrated and their sensitivity to different operating conditions were tested before the start of the core flood tests. The core flood setup is designed to perform different tests. A few tests that were conducted prior to the foam tests are summarized as well. Finally, the CO_2 foam tests in the absence of oil is conducted to determine the average apparent viscosity of the foams and determine the most stable foam front.

4.4.1 Transducer Calibrations

The four Validyne pressure transducers that were used for the core flood experiments were calibrated and their sensitivities to changes in system pressure and overburden pressure were observed. The table below summarizes the changes in the transducer pressure as the system pressure is increased. It can be observed that the transducer values drift when left overnight and when the system pressure is increased. The term calibration here refers to resetting the transducer values to close to 0. Thus, it was decided to reset the transducer values once the desired system

pressure of 1300 psi was obtained. There after the transducers could be used to measure the pressure drop across the sections of the core. Figure 66 represents the numbering of the different pressure transducers in the core holder to better understand or visualize the pressure drops across the different sections of the core.

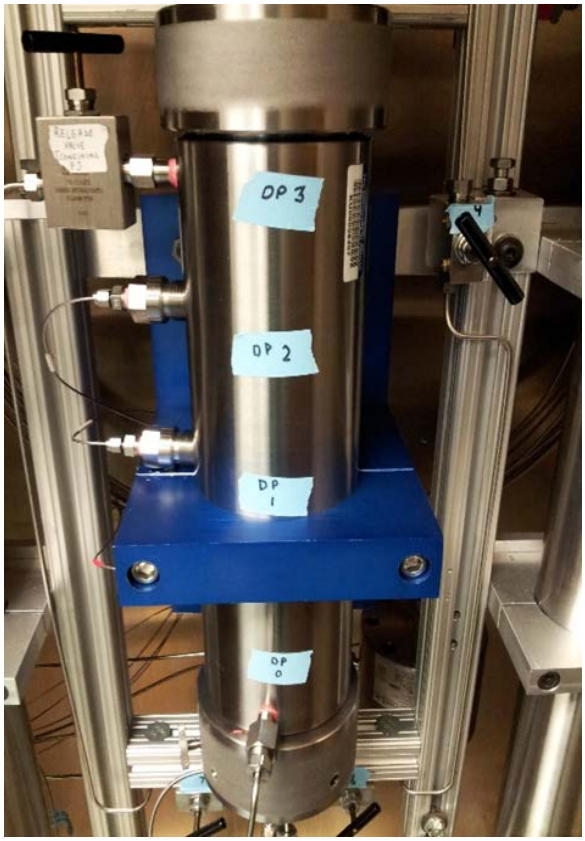

Figure 66: Image of the core holder showing the different pressure taps and the numbering of each transducer.

Table 16: Summary of the transducer pressure drops at different system pressures to determine the magnitude of measurement error.

Before the start of the Experiment						
	DP 0	**DP 1**	**DP 2**	**DP 3**	**DP 4**	**Sum (DP 0-3)**
	psi	**psi**	**psi**	**psi**	**psi**	**psi**
Calibrated values previous night	0.04	0.02	0.06	0.03	0.37	0.15
Drifter values the next day	0.33	0.04	0.13	0.45	0.53	0.95
At 100 psi system Pressure						
	DP 0	**DP 1**	**DP 2**	**DP 3**	**DP 4**	**Sum (DP 0-3)**
	psi	**psi**	**psi**	**psi**	**psi**	**psi**
Flow rate of 0.5 cc/min	0.77	3.75	3.94	1.70	9.88	10.16
Static (No flow)	0.09	0.04	0.11	0.16	0.33	0.40
Calibrated values	Did not calibrate					
At 500 psi system Pressure						
	DP 0	**DP 1**	**DP 2**	**DP 3**	**DP 4**	**Sum (DP 0-3)**
	psi	**psi**	**psi**	**psi**	**psi**	**psi**
Flow rate of 0.5 cc/min	1.04	3.23	3.21	0.02	6.87	7.50
Static (No flow)	0.19	0.13	0.03	1.49	1.73	1.85
Calibrated values	0.05	0.04	0.03	0.05	0.25	0.16
At 1000 psi system Pressure						
	DP 0	**DP 1**	**DP 2**	**DP 3**	**DP 4**	**Sum (DP 0-3)**
	psi	**psi**	**psi**	**psi**	**psi**	**psi**
Flow rate of 0.5 cc/min	1.36	3.34	3.01	0.37	6.38	8.08
Static (No flow)	0.87	0.58	0.22	1.19	1.37	2.86
Calibrated values	0.03	0.07	0.09	0.10	0.13	0.29
At 1300 psi system Pressure						
	DP 0	**DP 1**	**DP 2**	**DP 3**	**DP 4**	**Sum (DP 0-3)**
	psi	**psi**	**psi**	**psi**	**psi**	**Psi**
Flow rate of 0.5 cc/min	0.83	2.66	2.63	0.91	6.60	7.03
Static (No flow)	0.51	0.07	0.16	0.80	1.11	1.53
Calibrated values	0.03	0.02	0.05	0.07	0.10	0.16
Pressure drop after calibrating at 1300 psi						
	DP 0	**DP 1**	**DP 2**	**DP 3**	**DP 4**	**Sum (DP 0-3)**
Flow rate (cc/min)	**psi**	**psi**	**psi**	**psi**	**psi**	**Psi**
0.50	0.63	2.83	2.86	1.54	7.72	7.85
1.00	1.22	6.08	6.13	3.38	16.51	16.80
1.50	1.81	9.38	9.45	5.24	25.58	25.87

4.4.2 Permeability Measurements

Three different core flood tests are conducted using cores of different lengths. The core flood experiments conducted without oil used 10-inch core, core flood experiments that were used for enhanced oil recovery experiments used three cores measuring 9 inches each and the core flood experiments that were conducted to measure the extent of damage caused by the PECNP injection used two 3-inch cores. The permeabilities of each of these cores were measured according to the procedure outlined in chapter 3.

Table 17 summarizes the permeability calculation for the core plugs used for the core flood tests without oil. The pressure drops for the different flow rates are tabulated and the slope of pressure drop versus flow rate is calculated from the graph as plotted. The graph should pass through the origin as represented in Figure 67.

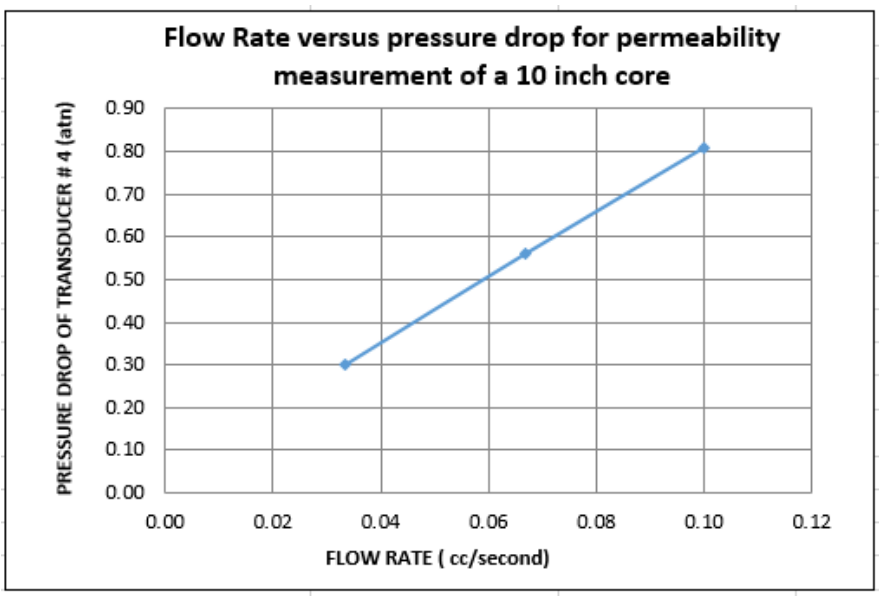

Figure 67: Graph of flow rate versus pressure drop to obtain the permeability of the 10 inch Indiana limestone core for core flood tests without oil.

Table 17: Summary of the permeability measurement for the 10 inch Indiana limestone core.

Permeability Calculation for the 10 inch Indiana limestone core							
q (cm^3/sec)	**Pressure drop (atm)**	**Slope**	**Length (cm)**	**Diameter (cm)**	**Area (cm^2)**	**Viscosity, 2% KCL (cp)**	**Permeability, (md)**
0.03	0.30		25.40	3.81	11.40	0.89	260.24
0.07	0.56	0.13					
0.10	0.81						

Table 18: Summary of the permeabilities measured for the 9 inch cores. Three of the cores with the closest permeability were chosen for the core flood tests in the presence of crude oil. Core #1, #2 and #3 were chosen for the furture tests.

Core #	Permeability (mD)	Porosity (%)	Pore volume (ml)	Bulk volume (ml)
1	292.00	0.19	50.16	260.62
2	356.00	0.16	42.00	260.62
3	387.00	0.17	45.00	260.62
4	257.13	0.20	52.00	260.62
5	213.00	0.17	44.00	260.62

Table 19: Summary of the permeabilities of the 3 inch cores used for measuring the extent of damage caused by the continuous injection of PECNP-surfactant.

Core #	Length (inches)	Bulk Volume (ml)	Porosity	Pore Volumes (ml)	Permeability (mD)
1	3	83.79	0.15	12.27	169.61
2	3	83.79	0.15	12.61	224.24

4.4.3 Surfactant Injection in the Absence of Crude Oil

When pure aqueous phase is injected into the 10 inch core, the pressure drop across the core and section-wise pressure drops for different flow rates were analyzed. A pure surfactant injection has a higher pressure drop followed by the PECNP-surfactant and PEI-surfactant. This can be observed in Figure 68, Figure 69 and Figure 70. Thus, the average apparent viscosity of the pure surfactant is the highest followed by PECNP-surfactant and PEI-surfactant. The order of the viscosities follow an interesting trend which will further be discussed after observing the CO2 foam results.

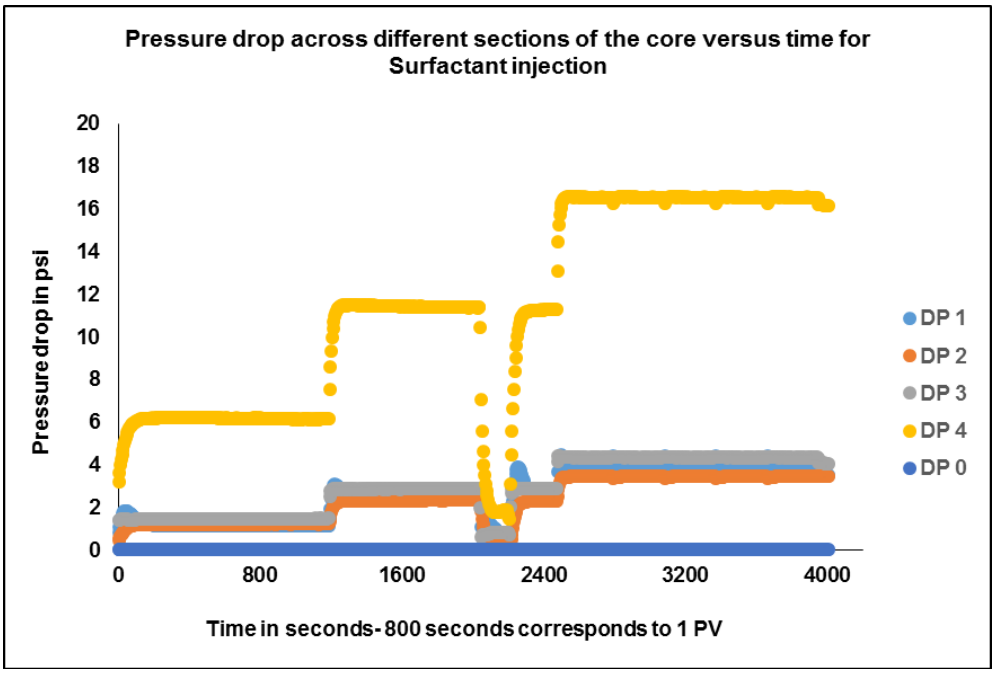

Figure 68: Pressure drop across the different sections of the core with time for the surfactant injection in the absence of oil. Transducer #0 was closed during this test.

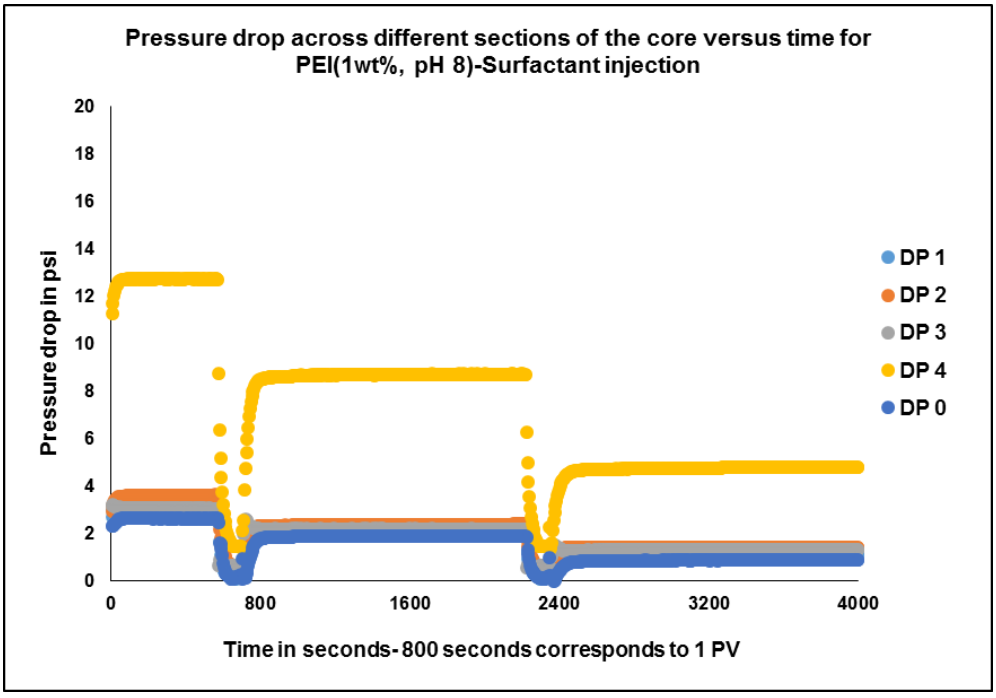

Figure 69: Pressure drop across the different sections of the core with time for the PEI-surfactant injection in the absence of oil.

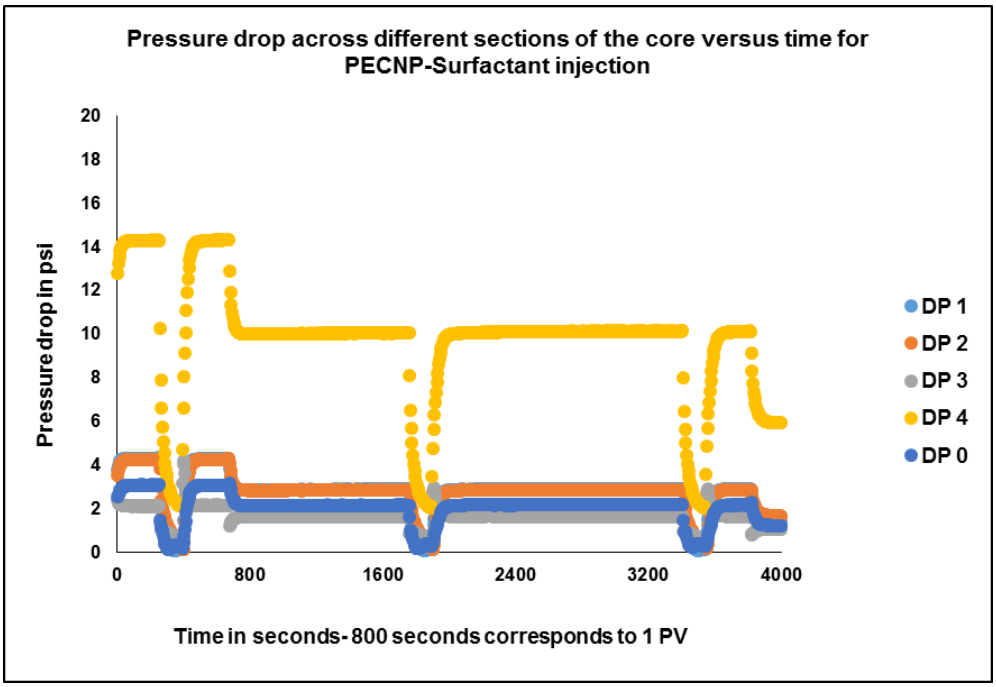

Figure 70: Pressure drop across the different sections of the core with time for the PECNP-surfactant injection in the absence of oil.

4.4.4 CO_2 Foam Flooding in the Absence of Crude Oil

The three different CO_2 foam systems are injected into the core and the pressure drop with time is measured. The pressure drop can translate to the average apparent viscosity of the foam systems. The increase in pressure drop corresponds to a stable foam front with high average apparent viscosity. Figure 71, Figure 72 and Figure 73 represent the pressure drops for the different foam systems with time. Injection time of 800 seconds corresponds to 1 PV of foam injection. The PEI-surfactant foam has the highest pressure drop followed by the PECNP-surfactant and surfactant foam. This implies that the average apparent viscosity of the PEI-surfactant foam is the highest as well. The foam injected has a 90% foam quality. Also, from the rheology testing, it was observed that the foam quality of 90% yielded the highest viscosity compared to foams that had higher aqueous phase content. This suggests that the surfactant becomes unstable when used by itself in

generating the foam and can be stabilized by the addition of PECNP and PEI which probably increase the interfacial viscosity and along with the bulk viscosity of the foam thereby preventing the rupture of the foams. A high apparent viscosity and pressure drop is typically indicative of a stable foam front. It can also be noted that during the rheology tests, the PECNP-surfactant viscosity was slightly higher than the surfactant foam and the same trend is observed in the core flood tests. Figure 71, Figure 72 and Figure 73 represent the change in pressure drop with time or pore volumes of foam injected for the different foam systems. Figure 74 is a graph that combines the total pressure drops with time and compares them for all the three CO_2 foam systems.

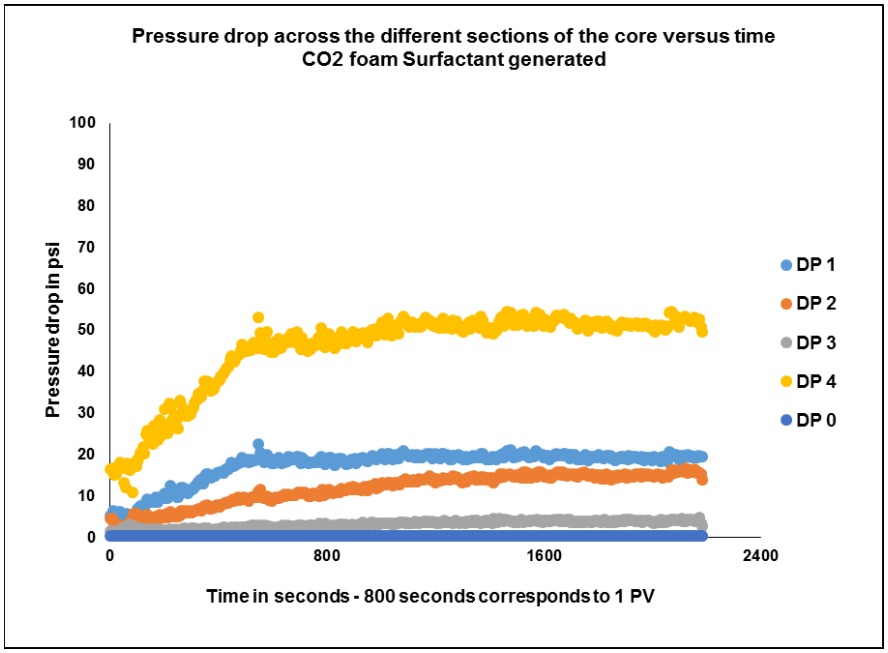

Figure 71: Pressure drop across the different sections of the core with time for the surfactant CO_2 Foam Injection in the Absence of Oil.

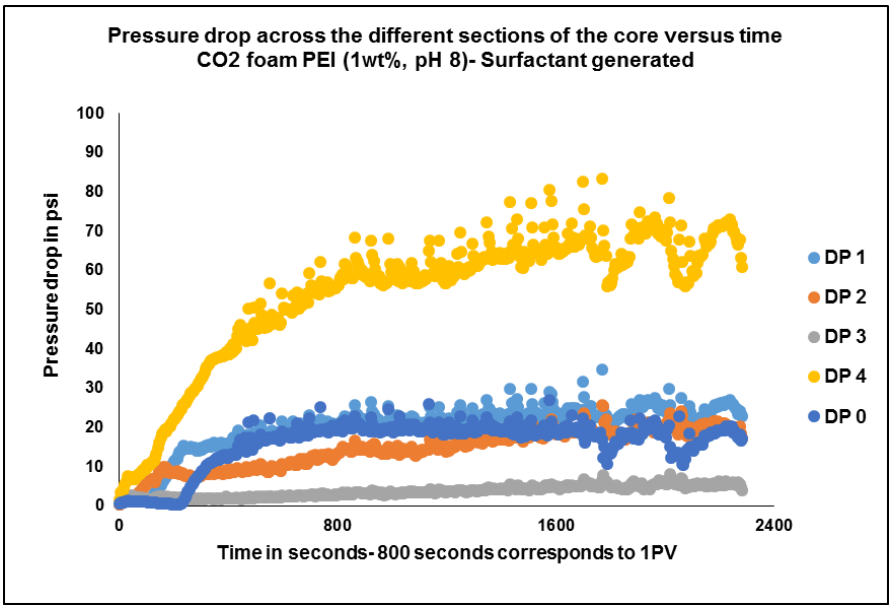

Figure 72: Pressure drop across the different sections of the core with time for the PEI-surfactant CO_2 foam injection in the absence of oil.

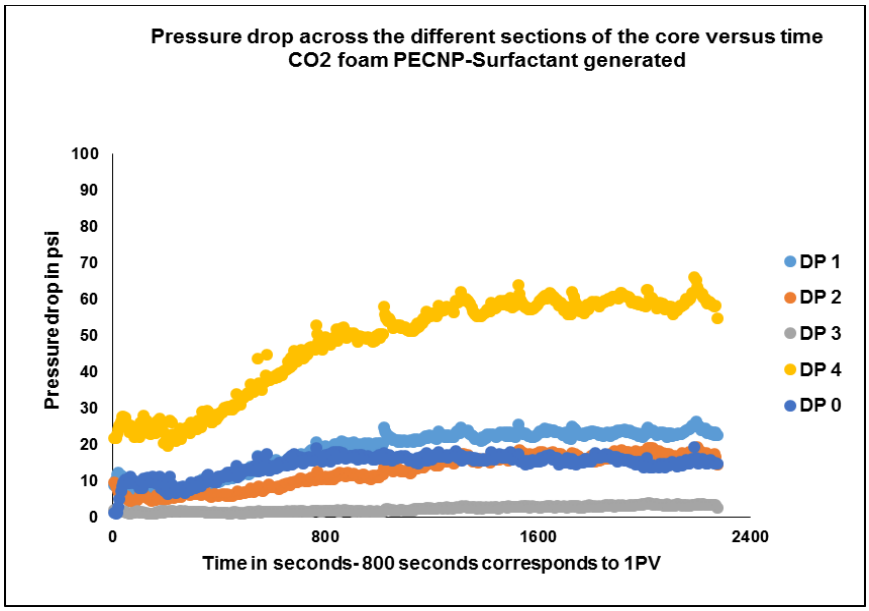

Figure 73: Pressure drop across the different sections of the core with time for the PECNP-surfactant CO_2 foam injection in the absence of oil.

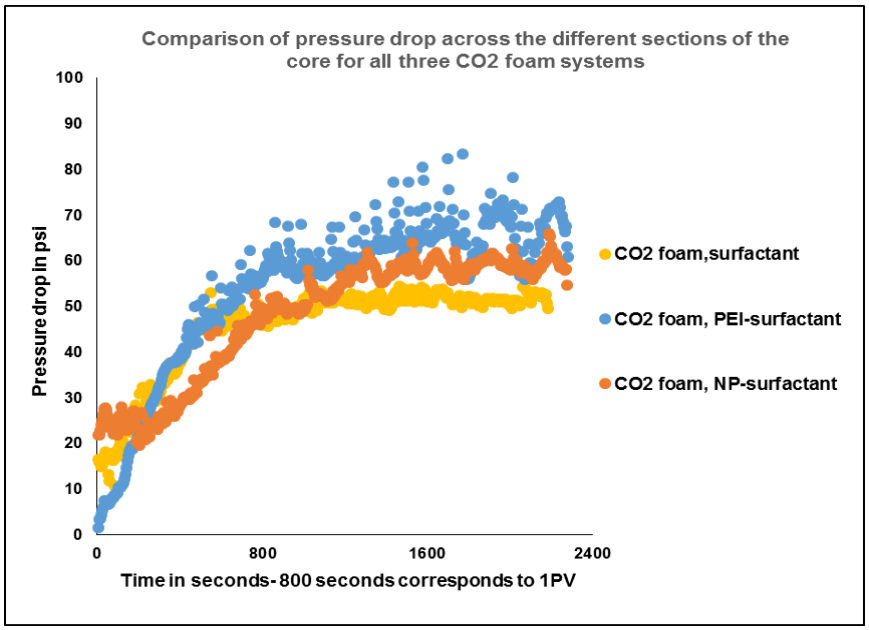

Figure 74: Total pressure drop across the whole core for the three different CO_2 foam systems in the absence of crude oil in the core [49].

4.5 Enhanced Oil Recovery Tests

The ability of foams to be generated at higher permeability reservoir rocks is very useful since it can help in the mobility control of CO2 in these rocks. Thus, foams are considered to be selective or smart since they have the ability to divert the flow based on the permeability thereby recovering more oil from the oil rich zones as opposed to the watered out thief zones [1]. Therefore, cores that have high permeability were chosen for the oil recovery tests.

Table 18 summarizes the cores that were obtained from the same block. The permeability, porosity and pore volume were measured for each of the five cores. Three cores that had the closest permeability, porosity and pore volume were selected for the rest of the tests. This included cores #1, #2 and #3.

The initial oil saturation and the residual oil saturations were measured after the primary drainage, water flood and CO2 foam tests. The values for each of the cores are summarized in Table 20 along with the percentage of oil recovered after each test. The analysis of the tests between the different cores are discussed initially followed by the analysis of the tests within each core.

4.5.1 Comparison of Oil Recovery between different Foam Systems:

The three cores were saturated with Mississippian crude oil during the primary drainage and this was followed by a water flood. Every core is then flooded with different CO_2 foam systems. The PECNP-surfactant foam recovers the highest amount of oil after water flooding from core #2. The surfactant foam recovers the second highest amount of oil (47.62%) from core #1. However, the PEI-surfactant foam does not recover as much oil from core #3 though it has very similar initial oil saturation to core #1. Figure 75 graphically represents the amount of oil recovered after

injecting the different CO_2 foam systems into each of the cores with PECNP-surfactant foam recovering the highest amount of oil.

For any tertiary oil recovery process, the capillary forces are reduced in order to recover the oil that is restrained by these forces in the pores. The capillary number is defined as the ratio of the viscous forces to capillary forces [6]. Thus, either a reduction in the capillary forces or an increase in the viscous forces would enhance the oil recovery [6]. In order to implement this, the viscosity and velocity of the displacing fluid would have to be increased or the interfacial tension of the fluid would have to be low enough to displace the oil from the pores [6].

From the rheology tests, the viscosity of the PEI-surfactant foam was slightly increased followed by the PECNP-surfactant foam system. The PEI-surfactant foam had the highest average apparent viscosity or total pressure drop across the core was the highest for the core flood tests in the absence of oil. The injection flow rate was also determined from the rheology tests by trying different flow rates and the most suitable flow rate with high viscosity was found to be equivalent to 12.4 feet/day. Additionally, the IFT of the PEI-surfactant foam was the lowest at 0.1wt% concentration followed by the PECNP-surfactant foam and surfactant foam. However the foam durability tests in the presence of crude oil and the core flood tests do not yield favorable results for the PEI-surfactant foam but in the absence of oil proved to be highly durable. Ideally, the PEI-surfactant foam should have been the best foam but upon interacting with the crude oil the foam collapses.

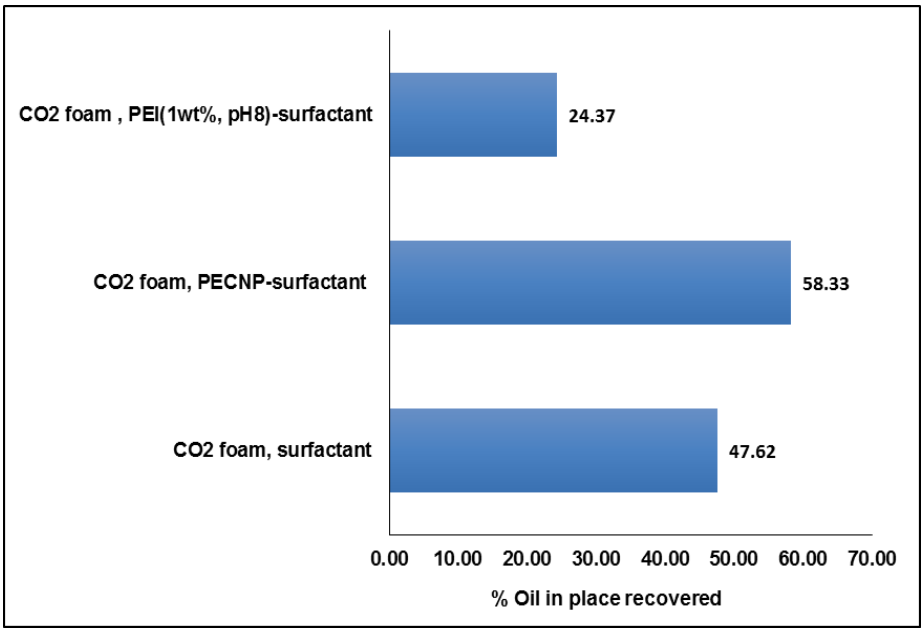

Figure 75: Bar graph showing the percentage of oil recovered by the different CO_2 foam systems for each core. The PECNP-surfactant foam recovers the maximum amount of oil from the 9 inch Indiana limestone core # 2 followed by surfactant foam(core #1) and PEI-surfactant foam (core # 3).

4.5.2 Comparison of Oil Recovery using different Foam Systems:

Followed by each CO_2 foam displacement test, the core is sequentially flooded with a second and third different foam system. The purpose of this sequential flooding is to determine if any additional oil could be recovered after the first CO_2 foam flood. For core #1, the surfactant foam flood is followed by PECNP-surfactant and PEI-surfactant foams. Approximately 9.1 % of oil is recovered by the injection of PECNP-surfactant foam even after the surfactant foam recovered 47% of the oil. An additional 2% of oil is further recovered by the PEI-surfactant after the PECNP-surfactant foam injection.

For core #2, PECNP-surfactant foam is injected as the first tertiary oil recovery technique and recovers 58.33% of oil. This is followed by the injection of PEI-surfactant foam that recovers

4.34% of the remaining oil and finally completed by the surfactant foam injection that recovers only 0.5% of the oil. Thus, compared to core #1's sequence, the injection of PECNP-surfactant foam as the first tertiary oil recovery technique proves to be more efficient in terms of recovering the maximum amount of oil. In the case of core#1, when the surfactant foam was injected as the first tertiary oil recovery technique, the PECNP-surfactant and PEI-surfactant could still recover the additional 9% and 2% of remaining oil respectively. In contrast to that, the surfactant foam could barely recover 0.5% of the remaining oil when injected after the PEI-surfactant foam for core #2. For core #3, the PEI-surfactant when injected as the first tertiary oil recovery technique, recovers 24.37% of oil when used as the first tertiary oil recovery technique. This is the lowest oil recovery compared to the other two cores. Similar results were observed in the view cell tests in the presence of crude oil and hence suggests the instability of the PEI-surfactant foam in the presence of crude oil. However, the PECNP-surfactant foam is followed right after the PEI-surfactant foam in core #3 and it recovers 6.38% of the remaining oil in place. From the three cores, it can be observed that after the surfactant foam injection, the PECNP-surfactant foam and PEI-surfactant foam can always recover additional oil. When the PECNP-surfactant foam is injected as the first tertiary oil recovery technique, it recovers the highest amount of oil compared to the three cores as well. However, the surfactant foam fails to recover a significant amount of additional oil when used after the PEI-surfactant or PECNP-surfactant foam. Although the PEI-surfactant foam does not recover a substantial amount of oil when used as the first tertiary oil recovery technique, it has the potential to recover additional oil after the surfactant foam or PECNP-surfactant foam. Thus, the sequential flooding performed on the three cores further validate the success of using PECNP-surfactant foam and PEI-surfactant foams over the conventional surfactant foams for enhanced oil recovery.

There are a few reasons for the incremental oil recovery attained by the PECNP-surfactant and PEI-surfactant. For the PECNP-surfactant, the foam interface is stabilized by the electrostatic forces and remain stable even in the presence of crude oil. Thus, the surfactant is prevented from leaving the interface and is available for continuous foam generation. In the case of the PEI-surfactant, the electrostatic forces are deterred by the addition of crude oil. This suggest that the PEI is affected by the charge of the crude oil and tends to destabilize in its presence.

The ability of foams to be generated at higher permeability reservoirs rocks is very useful since it can help in the mobility control of CO_2 in these rocks. Thus, foams are considered to be selective or smart since they have the ability to divert the flow based on the permeability thereby recovering more oil from the oil rich zones as opposed to the watered out thief zones [1]. Therefore, cores that have high permeability were chosen for the oil recovery tests.

Table 18 summarizes the cores that were obtained from the same block. The permeability, porosity and pore volume were measured for each of the five cores. Three cores that had the closest permeability, porosity and pore volume were selected for the rest of the tests. This included core #1, #2 and #3.

The initial oil saturation and the residual oil saturations were measured after the primary drainage, water flood and CO_2 foam tests. The values for each of the cores are summarized in Table 20 along with the percentage of oil recovered after each test. The analysis of the tests between the different cores are discussed initially followed by the analysis of the tests within each core.

Table 20: Summary of the oil saturation and % oil recovered after the series of CO2 foam tests conducted on each of the three cores [49].

Core 1		
System	**Oil Saturation values**	**% Oil recovered**
After Primary drainage	0.600	-
After waterflood	0.420	30.00%
After CO2 foam, surfactant generated	0.220	47.62%
After CO2 foam, NP-surfactant generated	0.200	9.10%
After CO2 foam, PEI-surfactant generated	0.196	2.00%
Core 2		
After Primary drainage	0.460	-
After waterflood	0.285	38.52%
After CO2 foam, NP-surfactant generated	0.119	58.33%
After CO2 foam, PEI-surfactant generated	0.107	4.34%
After CO2 foam, surfactant generated	0.106	0.50%
Core 3		
After Primary drainage	0.577	-
After waterflood	0.455	21.11%
After CO2 foam, PEI-surfactant generated	0.344	24.37%
After CO2 foam, NP-surfactant generated	0.322	6.38%
After CO2 foam, surfactant generated	0.321	0.33%

4.6 Permeability Recovery

The extent of damage caused by the continuous injection of PECNP-surfactant and PECNP-surfactant diluted 10 times with 2wt% KCl is summarized below in Table 21. It can be observed that the continuous injection of the pure PECNP-surfactant results in a 4.24% change in the permeability while the dilution of the PECNP-surfactant results in a 1.25% change in the permeability. Therefore, the change in the permeability is almost negligible. The pressure drop as a function of time for the different tests are shown in Figure 76. For a given core, the initial pressure drop during brine injection followed by the pressure drop of the PECNP-surfactant diluted 10 times with brine and the pressure drop during the flushing out period are represented in the same graph. Three different flow rates were used to determine the initial and final permeability of the core. Figure 76 is a graph of the pressure drop measured with time for all the three tests that include the

initial permeability measurement, the injection of PECNP-surfactant diluted 10 times with brine and the flushing of the core with brine to measure the recovered permeability. It can be observed that the pressure drop for the different flow rates when repeated after the injection of the PECNP-surfactant diluted 10X, are similar to the initial pressure drop measurements. Thus, no damage would be observed due to the injection of PECNP-surfactant foam since the foam comprises of 90% of gas and 10% of aqueous phase (of which only 1% is the PECNP).

Table 21: Summary of the permeability, viscosity and operating conditions for the 3 inch Indiana limestone core #1 during the PECNP-surfactant injection to measure the permeability recovery.

System injected	System Temperature (Celcius)	System Pressure (psi)	Viscosity (cP)	Permeability (mD)
Brine	40	1300	0.81	169.61
NP-Surfactant	40	1300	0.71	160.47
Brine	40	1300	0.81	162.32

Table 22: Summary of the permeability, viscosity and operating conditions for the 3 inch Indiana limestone core #2 during the PECNP-surfactant (diluted 10X in 2wt% KCl) injection to measure the permeability recovery.

System injected	System Temperature (Celcius)	System Pressure (psi)	Viscosity (cP)	Permeability (mD)
Brine	40	1300	0.81	224.24
PECNP-Surfactant Diluted 10X	40	1300	0.63	189.86
Brine	40	1300	0.81	220.97

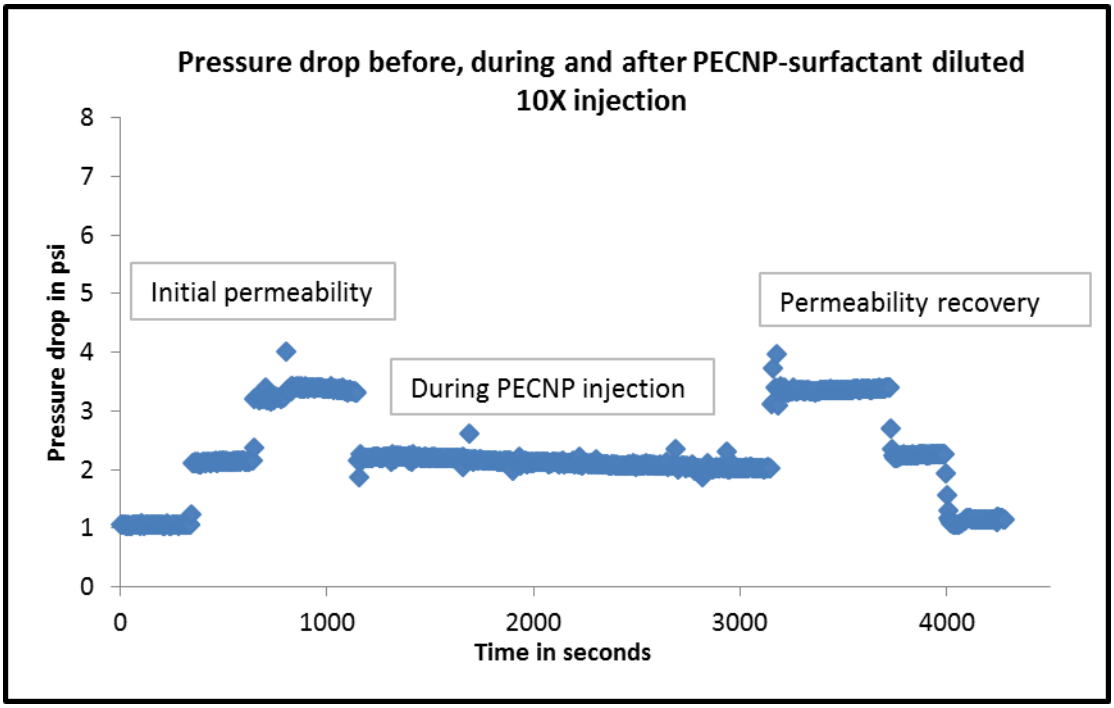

Figure 76: Graph representing the pressure drop measured across core # 2 during the initial permeability measurement, PECNP-surfactant diluted 10X injection and permeability recovery tests.

Chapter 5: Conclusions

This research elaborately explains the microscopic as well as macroscopic behavior of foams through the design of three high pressure high temperature systems. Understanding further, the bulk viscosity is known to reduce the rate of bubble coalescence and rupture of foam film and hence understanding the rheology of the foam and comparing them against the different systems help us better visualize the performance of foams under shear. The final application of the stable foam is for enhanced oil recovery operations and a core flood performed in the lab provides an insight for a scaled up pilot study. Additionally, the impact of the nanoparticles on the rock is studied to determine if core plugging occurs and if there is any permeability reduction due to the injection of the nanoparticle stabilized foam. This research proves that the addition of just 1 vol% of nanoparticles to 9 vol% of the surfactant solution can stabilize a system of 90% foam quality. From an environmental stand point, the volume of nanoparticle used is very low compared to the foams stabilized by nanoparticles only. Also the presence of surfactants aids in the continuous generation of foam due to their surface active properties and the addition of polyelectrolyte complex nanoparticles to their interface reduces their dynamic instability.

The following important conclusions can be drawn from this research:

1. **Particle size and Surface potential measurements**: The PECNP-surfactant system that had the lowest particle size and the highest zeta potential values were considered to be the most stable systems. Different pH of PEI and ratios of PEI: DS were used for preparing the PECNP-surfactant. Finally, PEI of pH 8 and a 3:1 ratio of PEI: DS was used for preparing the PECNP-surfactant. However, for the PEI-surfactant system, the average count rate for the system was very low and hence the zeta potential could not be measured accurately.

From initial screening tests conducted using the view cell, the PEI-surfactant foam using PEI of pH 8 and ratio 1:9 of PEI: surfactant was found to be stable and durable.

2. **Bulk rheology**: PEI-surfactant foam was found to have the highest viscosity under a constant shear of 2000 $s^{-1.}$ The PECNP-surfactant foam had the second highest viscosity and the shear sweep test indicated the PECNP-surfactant foam would be more stable due to the fact that it has a lower power law exponent and hence the foam film doesn't become as thin with shear compared to the other two foam systems. Additionally, the PECNP-surfactant foam has a better stability due to the higher flow consistency compared to the PEI-surfactant.The influence of foam quality, temperature and salinity were observed on the rheology of the foam as well. It was found that as the foam quality increased, the viscosity of the foam system increased and hence a 90% foam quality was found to be the best foam quality to proceed for future tests. The temperature of the system influenced the viscosity negatively by lowering the viscosity under shear as the temperature increased. The addition of 2wt% KCl to the foam systems increased the viscosity of the foam systems to a greater degree, especially the PECNP-surfactant and PEI-surfactant foam system. These results indicate the charge dependence of PECNP and PEI and their influence on the bulk and interfacial foam film rheology.

3. **Foam stability and durability**: The initial screening tests with RO water indicated that the PECNP-surfactant foam diluted 10 times in RO water had the most durable foam and lasted for a longer time followed by the PEI-surfactant foam. The pH of the PEI used for all the systems was 8. The influence of salinity was observed when the dilution of the PECNP-surfactant foam in 2wt% KCl resulted in a weak foam due to the early foam decay. Thus, the stability of PEI and PECNP are highly influenced by the charge of the solution.

In the 2wt% KCl based systems, the PEI-surfactant foam yielded the best foam with a longer lasting foam in the absence of oil. However in the presence of oil , the PECNP-surfactant foam yielded a more stable and longer lasting foam upon interacting with all three different types of oil. Additionally, as the viscosity of the oil increased, the stability of the foams improved. Thus, for less viscous or lighter hydrocarbon chains present in the oil, the foams destabilized.

4. **Core flood tests without oil**: The injection of pure aqueous phase (surfactant, PEI-surfactant and PECNP-surfactant) into the core showed that the average apparent viscosity of the pure surfactant was higher than the PECNP-surfactant and PEI-surfactant. These results are completely reversed when the CO_2 foam flood tests are conducted. Thus, the interfacial and bulk rheological properties are improved when the two phases are combined with each other to form foams. The PEI-surfactant foam has the highest pressure drop and hence corresponds to the highest average apparent viscosity followed by the PECNP-surfactant foam. Typically, the higher the pressure drop, the more stable the foam front is considered to be inside the core. However, the stability of the foam front needed to be analyzed further in the presence of crude oil.

5. **Core flood tests with oil:** Mississippian crude oil has the lowest viscosity and the foam durability tests conducted using the sapphire view cell showed that all three foam systems had lower foam durability upon interacting with this crude oil. The lower the viscosity the faster the foam decay occurred for all the three foam systems. The core flood tests using the Mississippian crude oil still showed significant results using the three foam systems. Three different cores were saturated with crude oil and water flooded up to the residual oil saturation after water flood. Each of the core was then sequentially flooded with the three

CO_2 foam systems. The PECNP-surfactant foam recovered 58% of the oil in place when it was injected after water flooding the core. This was the highest amount of oil recovered amongst the three foam systems when injected right after the water flooding. In the sequential flooding of the foams, it was observed that the injection of PECNP-surfactant foam and PEI-surfactant foam recovered additional oil after the surfactant foam was injected. However, the surfactant foam system when injected after the PECNP-surfactant and PEI-surfactant did not recover more than 0.5% of the oil in place. This implies that the PECNP-surfactant and PEI-surfactant foam are more stable in the presence of crude oil and efficiently mobilize the oil compared to the surfactant foam. However, the PEI-surfactant foam recovers only 24% of the oil in place when it was injected after water flooding the core. This result is similar to the foam durability tests that were conducted in the sapphire view cell in the presence of crude oil. The PECNP is hypothesized to form a strong layer around the surfactant thereby creating a more stable foam lamella and avoiding rupture of the foam film in the presence of crude oil.

6. **Permeability recovery:** The extent of damage caused by the injection of PECNP into the core along with the foam system was studied. The foam quality was maintained at 90% throughout the study of this thesis. The ratio of the PECNP: surfactant was maintained at 1: 9 and this constituted only 1% of the foam system. The continuous injection of the PECNP and the PECNP diluted 10 times using 2wt% KCl was observed in a 3 inch core. It was found that the permeability changed by 1.25% upon diluting the PECNP solution 10 times with 2wt% KCl and by 4.24% upon injecting pure PECNP-surfactant solution. Thus, it can be found that the PECNP does not plug the core and the permeability could be recovered.

Finally, the following hypothesis could be derived for the stability of the PECNP-surfactant and PEI-surfactant foams. The PECNP-surfactant system is stabilized by the electrostatic forces and the foam lamella is considered to be highly stable in the presence of different types of oil compared to surfactant foam itself. The PECNP is believed to form a layer around the surfactant thereby preventing the loss of surfactant and maintaining the stability of the foam film in the presence of crude oil. The PECNP could be entrapping the surfactant similar to the enzyme entrapment observed by Barati et al and Tiyaaboonchai ([44] and [42]. Another hypothesis could be considered for the PECNP-surfactant foam and this could be the formation of a pseudo emulsion. If a pseudo emulsion is formed, it is probably stable due to the PECNP binding the surfactant.

The PEI-surfactant foam seems to have a different behavior compared to the PECNP-surfactant foam. The ratio of the PEI: surfactant is maintained below the CAC and the c*. Thus, the process of stratification should not be present. Hence, the only possible way for stabilizing the foam would be through interfacial properties. The bulk viscosity of the PEI-surfactant foam is high but the stability is lower compared to the PECNP-surfactant due to the lower flow consistency index and higher power law exponent. The stability of PEI-surfactant is highly influenced by the charge and becomes destabilized in the presence of any type of oil.

Chapter 6: References

[1] R. M. Enick and D. K. Olsen, "Mobility and Conformance Control for Carbon Dioxide Enhanced Oil Recovery (CO2-EOR) via Thickeners, Foams, and Gels – A Detailed Literature Review of 40 Years of Research," U.S.Department of Energy, 2012.

[2] R. Barati, S. Pennell, L. Schoeling and M. Linroth, "Overview of CO2 Injection and WAG Sensitivity in SACROC," in Twentieth SPE Improved Oil Recovery Conference, April 9-13, 2016., Tulsa, Oklahoma, USA, 2016.

[3] J. Christensen, E. Stenby and A. Skauge, "Review of WAG Field Experience," SPE, pp. 97-106, 2001.

[4] D. Espinosa, F. Caldelas, . K. Johnston, L. Bryant and C. Huh, "Nanoparticle-stabilized supercritical CO2 foams for potential mobility control applications," in SPE Improved Oil Recovery Symposium, Tulsa, 2010.

[5] L. L. Schramm, FOAMS, Fundamentals and Applications in the Petroleum Industry, Washington D.C: Advances in Chemistry Series 242, 1994.

[6] D. W. Green and G. P. Willhite, Enhanced Oil Recovery, Richardson, Texas: SPE, 1998.

[7] R. Long and A. Yost, "Development of Novel Methods for CO2," E&P Focus, Spring 2012 Oil & Natural Gas Program Newsletter, 2012.

[8] W. R. Rossen, R. K. Prud'homme and S. A. Khan, "Chapter 11: Foams in Enhanced Oil Recovery," in Foams: Theory, Measurements and Applications, New York, Marcel Dekker Inc, 1996, pp. 413-465.

[9] J. Novosad and L. Schramm, "Micro-visualization of foam interactions with a crude oil," Colloids and Surfaces, no. 46, pp. 21-43, 1990.

[10] T. Ransohoff and C. Radke, "Mechanisms of Foam Generation in Glass-Bead Packs," SPE, vol. 3, no. 02, pp. 573-585, 1988.

[11] S. H. Talebian, R. Masoudi, I. M. Tan and P. Zitha, "Foam assissted CO2- EOR; Concepts, Challenges and Applications," in SPE EOR conference, 2-4 July 2013, Kuala Lumpur, Malaysia, 2013.

[12] R. Farajzadeh, A. Andrianov and P. Zitha, "Investigation of Immiscible and Miscible Foam for Enhancing Oil Recovery," Industrial & Engineering Chemistry Research, vol. 4, no. 49, pp. 1910-1919, 2010.

[13] D. Huh, T. Cochrane and F. Kovarik, "The Effect of Microscopic Heterogeneity on CO2/ Foam Mobility: Part 1- A mechanistic study," in SPE/ DOE EOR Symposium, Tulsa, 1988.

[14] K. Raterman, F. Suffridge and G. Russell, "Foam Performance Under Reservoir Conditions," in SPE Annual Technical Conference and Exhibition, 8-11 October, San Antonio, 1989.

[15] S. Thibeau, D. Broseta and P. Chiquet, "Wettability alteration of caprock minerals by carbon dioxide," Geofluids, vol. 7, no. 2, pp. 112-122, 2007.

[16] J. Sanchez and R. Hazlett, SPE Reservoir Engineering, vol. 1, no. 7, pp. 91-97, 1992.

[17] L. L. Schramm, Surfactants: Fundamentals and Applications in the Petroleum Industry, Cambridge, United Kingdom: Cambridge University Press, 2000.

[18] R. Petkova, S. Tcholakova and N. Denkov, "Foaming and foam stability for mixed polymer-surfactant solutions: effects of surfactant type and polymer charge," Langmuir, ACS Publications, pp. 4996-5009, 2012.

[19] R. Hunter, Zeta Potential in Colloid Science, New York: Academic Press, 1981.

[20] A. A. Eftekhari, R. Krastev and R. Farajzadeh, "Foam stabilized by Fly-Ash nanoparticles for Enhanced Oil Recovery," in SPE Kuwait oil and gas show and conference, Kuwait, 2015.

[21] Y. Gao, "Fundamental Studies of Refined Polyelectrolyte/Surfactant Nanoparticles-Bulk and Interfacial properties," University of Kansas, Lawrence, 2014.

[22] N. Kristen and R. v. Klitzing, "Effect of polyelectrolyte/surfactant combinationon the stability of foam films," Soft Matter, The Royal Society of Chemistry, no. 6, pp. 849-861, 7 January 2010.

[23] W. J. McLendon, "Mobility reduction of CO2 using CO2 soluble surfactants," UNiversity of Pittsburgh, 2012.

[24] G. Bernard and L. Holm, "Method for recovering oil from subterranian formations". USA Patent 3,342,256, 19 September 1967.

[25] N. Liu, Nanoparticle-Stabilized CO2 Foam for CO2 EOR Application, New Mexico: U.S. Department of Energy, National Energy Technology Laboratory, 2015.

[26] B. Binks, "particles as surfactants-similarities and differences," Current Opinion in Colloid & Interface Science, no. 7, pp. 21-41, 2002.

[27] B. Brinks and T. Horozov, "Aqueous foams stabilized solely by silica nanoparticles," Angew Chem. International, vol. 24, no. 44, pp. 3722-3725, 2005.

[28] B. Binks, J. Dickston and K. Johnston, "Stabilization of carbon dioxide-in-water emulsions with silica nanoparticles," Langmuir, no. 20, pp. 7976-7983, 2004.

[29] T. N. Huntera, R. J. Pughb, V. G. Franks and G. J. Jameson, "The role of particles in stabilising foams and emulsions," Advances in Colloid and Interface Science, vol. 137, no. 2, pp. 57-81, 18 March 2008.

[30] A. Worthen, H. Bagaria, Y. Chen, S. L. Bryant, K. P. Johnston and C. Huh, "Nanoparticle Stabilized Carbon Dioxide in Water Foams for Enhanced Oil Recovery," in SPE, Tulsa, 2012.

[31] R. D. Shah, "Application of Nanoparticle Saturated Injectant Gases for EOR of Heavy Oils," in SPE Annual Technical Conference and Exhibition, 4-7 October, Louisiana, 2009.

[32] R. Singh, A. Gupta, K. K. Mohanty, C. Huh, H. Cho and D. Lee, "Fly Ash Nanoparticle-Stabilized CO2 in Water Foams for Gas Mobility Control Applications," in SPE Annual Technical Conference and Exhibition, 28–30 September 2015., Houston, Texas, USA, 2015.

[33] Z. Cui, C. Cui, Y. Zhu and B. Binks, "Multiple phase inversion of emulsions stabilized by in situ surface activation of CaCO3 nanoparticles via adsorption of fatty acids," Langmuir, 2012, vol. 1, no. 28, p. pp 314–320, 2011.

[34] J. Koetz and S. Kosmella, Polyelectrolytes and Nanoparticles, Springer Laboratory Manuals in Polymer Science, 2006.

[35] J. Koetz, S. Kosmella and T. Beitz, "Self assembled polyelectrolyte systems," Elseiver, Progress in Polymer Science, pp. 1199-1232, 2001.

[36] D. Li, "Towards rational design of polyelectrolyte-surfactant complexes: Thermodynamics, Microstructure and property," University of Delaware, 2013.

[37] Y. Lapitsky, M. Parikh and E. Kaler, in Journal of Physical Chemistry B,, 2007, pp. 111(29), p. 8379-8387..

[38] C. Wang and K. Tam, in Journal of Physical Chemistry B, 2004, pp. 108(26), p. 8976-8982..

[39] J. Israelachvili, Intermolecular and Surface Forces, Second Edition: With Applications to Colloidal and Biological Systems (Colloid Science). 2nd ed, London: Academic Press: London Second ed., 1991.

[40] K. Hayakawa and J. Kwak, in Journal of Physical Chemistry, 1982, pp. 86(19): p. 3866-3870..

[41] E. D. Goddard, "Application of Polymer surfactant systems," in Polymer-Surfactant Systems, vol. 71, New York, Marcel Dekker Inc, 1998, pp. 21-60.

[42] W. Tiyaboonchai, "Development of a New Nanoparticle Delivery Vehicle Based on an Aqueous Polymer System: Polyethylenimine and Dextran Sulfate," The University of Kansas, Lawrence, 2003.

[43] T. J. Waree, R. C. Sims and R. Middaugh, "Insulin Containing Polyethylenimine-Dextran Sulfate Nanoparticles.," International Journal of Pharmaceutics, pp. 139-151, 2003.

[44] R. B. Ghahfarokhi, "Fracturing Fluid Cleanup by Controlled Release of Enzymes from," University of Kansas, Lawrence, 2005.

[45] R. Barati, S. Johnson, S. Mc Cool, D. Green and J. Liang, "Polyelectrolyte complex nanoparticles for protection and delayed release of enzymes in alkaline pH and at elevated temperature during hydraulic fracturing of oil wells," Journal of Applied Polymer Science, pp. 587-592, 2012.

[46] C. B. Chempakathinal, B. Alshatti, L. Swartz, A. Gupta and R. Barati, "Dual Application of Polyelectrolyte Complex Nanoparticles as Enzyme Breaker Carriers and Fluid Loss Additives for Fracturing Fluids," in SPE/CSUR Unconventional Resources Conference – Canada, 30 September–2 October, Calgary, 2014.

[47] R. B. Ghahfarokhi, "Fracturing Fluid Cleanup by Controlled Release of Enzymes from," University of Kansas, Lawrence, 2005.

[48] L. L. Schramm, FOAMS, Fundamentals and Applications in the Petroleum Industry, Washington D.C: Advances in Chemistry Series 242, 1994.

[49] N. Kalyanaraman, C. Arnold, A. Gupta, J. S. Tsau and R. Barati, "Stability Improvement of CO2 Foam for Enhanced Oil Recovery Applications Using Polyelectrolytes and Polyelectrolyte Complex Nanoparticles," in SPE Asia Pacific Enhanced Oil Recovery Conference, 11-13 August, Kuala Lumpur, Malaysia, 2015.

[50] L. Pilon and R. Viskanta , "Minimum superficial gas velocity for onset of foaming," Elsevier, vol. 49, pp. 149-160, 2003.

[51] W. Ostwald, Kolloid Zeitschrift, vol. 2, no. 47, pp. 176-187, 1929.

[52] A. Moradi-Aghari, E. Johnston, Z. D.R. and J. Harpole, "Laboratory Evaluation of Surfactants for CO2-Foam Applications at the South Cowden Unit," in SPE International Symposium on Oilfield Chemistry, Houston, February 16-21, 1997.

[53] A. W. O'Connell, "Titration of nonionic surfactants with potassium tetrakis(4-chlorophenyl)borate," Analytical Chemistry, vol. 3, no. 58, pp. 669-670, 1986.

[54] D. Green and P. Willhite, Enhanced Oil Recovery, SPE , 1998.

[55] D. Taylor, R. Thomas and J. Penfold, "Polymer/surfactant interactions at the air/water interface," Advances in Colloid and Interface Science 132 (2007) 69-110, pp. 70-110, 2007.

[56] S. J. Johnson, R. Barati, S. Mc Cool, D. W. Green, G. P. Willhite and J.-T. Liang, "Polyelectrolyte complex nanoparticles to entrap enzymes for hydraulic fracturing fluid cleanup," in ABSTRACTS OF PAPERS OF THE AMERICAN CHEMICAL SOCIETY, 2011.

[57] D. E. Alejandro, F. M. Caldelas, K. P. Johnston, S. L. Bryant and C. Huh, "Nanoparticle-Stabilized Supercritical CO2 Foams for Potential Mobility Control Applications," in SPE Improved Oil Recovery Symposium, Tulsa, 2010.

[58] P. Nguyen , H. Fadaei and D. Sinton, "Nanoparticle Stabilized CO2 in water foam for Mobility Control in Enhanced Oil Recovery via Microfluidic Method," in SPE Heavy oil conference-Canada, Toronto, 2014.

[59] K. He, Z. Yue, C. Fan and L. Xu, "Minimizing Surfactant Adsorption Using Polyelectrolyte Based Sacrificial Agent: a Way to Optimize Surfactant Performance in Unconventional Formations," in SPE International Symposium on Oilfield Chemistry, Woodlands, 2015.

[60] D. Matulis, I. Rouzina and V. Bloomfield, in Journal of the American Chemical Society, 2002, pp. 124(25): p. 7331-7342..

[61] D. S. Schechter and R. B. Grigg, "Improved efficiency of miscible CO2 floods and Enhacned prospects for CO2 flooding heterogenous reservoirs," U.S. Department of Energy, Socorro, 1998.

[62] J. Yu, N. Liu and R. Lee, "Generation of Nanoparticle-Stabilized Supercritical CO2 Foams," in Carbon Management Technology Conference, Orlando, 2012.

[63] D. C. Bond and O. C. Holbrook, "Gas Drive Oil recovery process". United States of America Patent 2866507, 30 December 1958.

[64] J. Yu, C. An, D. Mo, N. Liu and R. Lee, "Foam Mobility Control for Nanoparticle-Stabilized CO2 Foam," in SPE Improved Oil recovery symposium , Oklahoma, 2012.

[65] S. R. I. Mahesh Shrichand Picha, "Enhanced Oil Recovery By Hot CO2 Flooding," in SPE Middle East Oil and Gas Show and Conference, 11-14 March, Manama, Bahrain, 2007.

[66] C. Berkland, M. Cordova, J. Liang and G. Willhite, "Delayed Hpam Gelation Via Transient Sequestration of Chromium in Polyelectrolyte Complex Nanoparticles," Macromolecules, ACS Publications, vol. 12, no. 41, pp. 4398-4404, 2008.

[67] D. X. Micha, B. Wei, Y. Sung, J. Eastoe, K. Trickett and A. Mohamed, "CO2 soluble surfactants for Improved Mobility Control," in SPE Improved Oil recovery symposium 2010, Oklahoma, 2010.

[68] K. Chambers and C. Radke, "Capillary Phenomena in Foam Flow through Porous Media," in Interfacial Phenomena in Oil Recovery, vol. 36, New York, Marcel Dekker Inc, 1990, pp. 191-257.

[69] E. D. Goddard, Journal of the American Oil Chemists Society, vol. 71, 1994.

Chapter 7: Appendix

This chapter provides results of the CO_2 WAG test, titration of nonionic surfactant, vial tests, code snippets of the pressure head calculation for the core flood setup and IFT measurement calculations.

7.1 CO_2 WAG

1.2 Pore volume of Supercritical CO_2 and 1.2 Pore volume of 2wt% KCl were injected at intervals of 18 minutes. After the 6 cycles were complete, the core was flushed with 4.2 PV of brine. CO_2 breakthrough was observed at the end of the brine injection during cycle 6. Outlet temperature of the CO_2 was 26 Celsius and the outlet pressure was 14.15 atm. Flow rate was measured at the outlet and was found to be 0.5 cc/minute. Table 23 summarizes the results obtained during the WAG test. This test was performed in the absence of oil to observe the changes in pressure drops during the alternate injection of two phases.

Table 23: Summary of the pressure drops measured during the CO_2 WAG test. Supercritical CO_2 is represented as sc CO_2

Flow rate (cc/min)	Cumulative PV injected	Fluid	Cycle	DP 0	DP 1	DP 2	DP 3	DP 4	Sum (DP0-DP3)
0.50	0.20	brine	cycle 1	1.02	1.95	2.59	4.29	7.86	9.85
0.50	0.20	sc co2		0.09	2.69	0.36	4.74	4.46	7.88
0.50	0.40	brine	cycle 2	0.81	1.63	5.08	10.21	10.56	17.74
0.50	0.40	sc co2		0.11	2.60	0.33	4.64	4.52	7.68
0.50	0.60	brine	cycle 3	0.77	1.17	4.47	9.34	8.76	15.75
0.50	0.60	sc co2		0.12	2.59	0.34	4.65	4.46	7.71
0.50	0.80	brine	cycle 4	0.75	0.99	4.21	9.11	8.04	15.05
0.50	0.80	sc co2		0.19	2.29	0.67	5.05	3.36	8.19
0.50	1.00	brine	cycle 5	0.73	0.83	4.03	8.97	7.56	14.56
0.50	1.00	sc co2		0.59	0.03	4.52	7.97	6.18	13.10
0.50	1.20	brine	cycle 6	0.71	3.04	9.41	9.22	15.40	22.37
0.50	1.20	sc co2		1.05	3.49	7.02	8.21	12.67	19.76

7.2 Titration of Non Ionic Surfactant

The nonionic surfactant used in this research (N120) provided by Huntsman was titrated using potassium tetrakis (4-chlorophenyl) borate [53]. The end point was observed in the form of a color change from blue to intermediate purple.

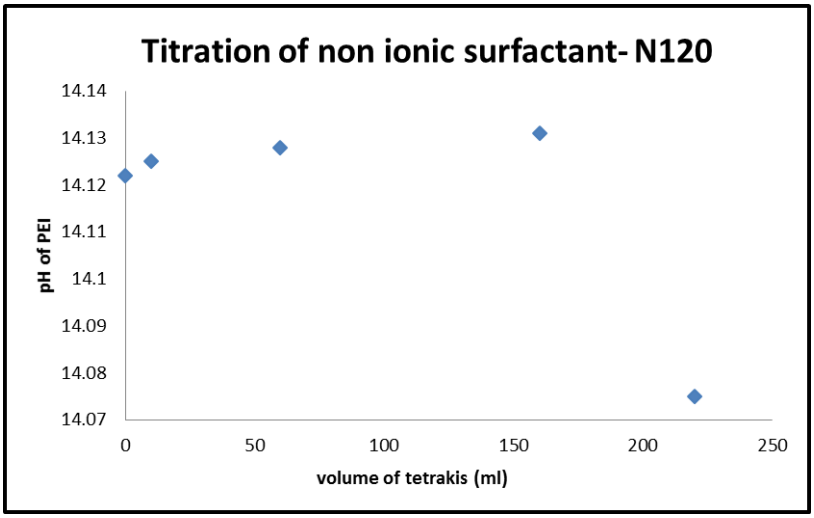

Figure 77: Titration curve of N120 using potassium tetrakis (4-chlorophenyl) borate

7.3 Titration Curves

The titration curve for PEI (1wt %) prepared in 2wt% KCl is presented in Figure 78.

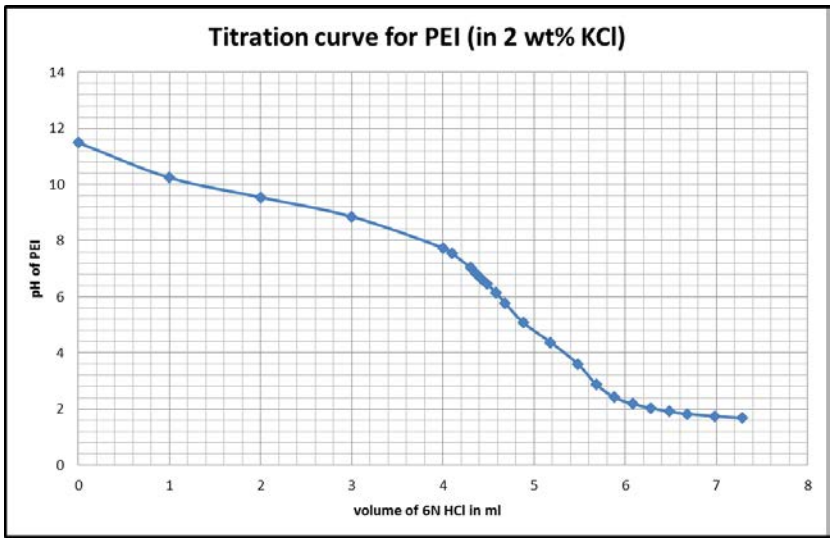

Figure 78: Titration curve for PEI (1wt %) in 2wt% KCl

7.4 Vial tests

PECNP-surfactant, PEI-surfactant, surfactant and 2wt% KCl solutions are mixed with soltrol and Mississippian crude oil in small vials each. The vials are hand shaken and left to sit on the table

top for a day inside the oven maintained at 40 degrees Celsius. The images of vials can be seen in Figure 79. It can be observed that the PEI-surfactant and 2wt% KCl solutions do not form an emulsion whereas the PECNP-surfactant forms a pseudo emulsion with soltrol and Mississippian crude oil.

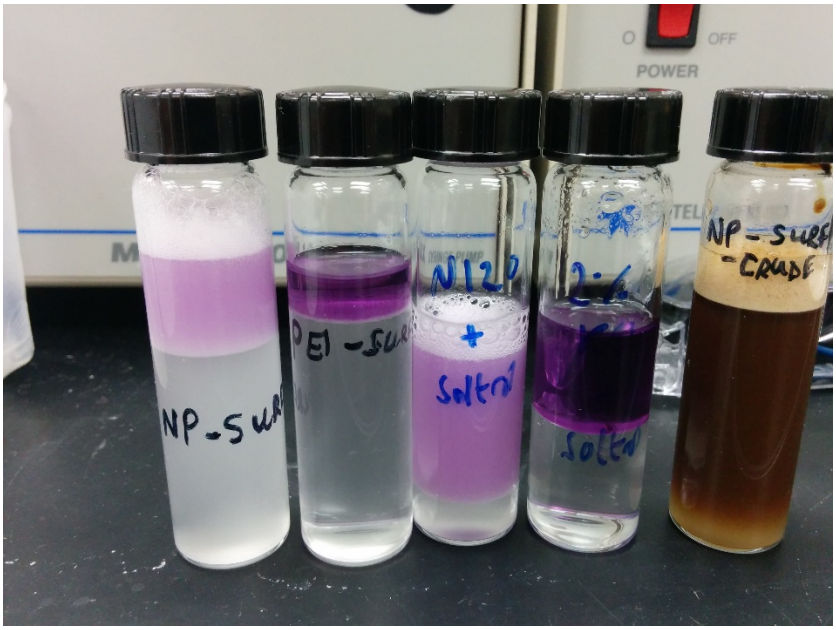

Figure 79: Images of viles containing different solutions interacting with soltrol and crude oil. Starting from the left, PECNP-surfactant with soltrol in the first vial, PEI-surfactant with soltrol, surfactant with soltrol, 2wt% KCl with soltrol and PECNP-surfactant with Mississippian crude oil.

7.5 Pressure head calculation code snippets

1. PECNP-surfactant CO_2 foam

```
Sub blah()


Dim j, k, l, m As Integer



For j = 2 To 858 Step 1
Cells(j, 9) = Cells(j, 8) + 0.0468
Next j

For k = 2 To 858 Step 1
Cells(k, 11) = Cells(k, 10) + 0.0468
Next k

For l = 2 To 858 Step 1
Cells(l, 13) = Cells(l, 12) + 0.2432
Next l

For m = 2 To 858 Step 1
Cells(m, 15) = Cells(m, 14) + 0.561
Next m

End Sub
```

Figure 80: Code for calculating the pressure head for the PECNP-surfactant foam

2. PEI-surfactant foam

```
Sub blah()


Dim i, j, k, l, m As Integer

For i = 2 To 858 Step 1
Cells(i, 7) = Cells(i, 6) + 0.170861
Next i

For j = 2 To 858 Step 1
Cells(j, 9) = Cells(j, 8) + 0.044963
Next j

For k = 2 To 858 Step 1
Cells(k, 11) = Cells(k, 10) + 0.044963
Next k

For l = 2 To 858 Step 1
Cells(l, 13) = Cells(l, 12) + 0.233809
Next l

For m = 2 To 858 Step 1
Cells(m, 15) = Cells(m, 14) + 0.53956
Next m

End Sub
```

Figure 81: Code for calculating the pressure head for the PEI-surfactant foam.

3. Surfactant foam

```
Sub surf()


Dim i, j, k, l, m As Integer

For i = 2 To 858 Step 1
Cells(i, 7) = Cells(i, 6) + 0.170861
Next i

For j = 2 To 858 Step 1
Cells(j, 9) = Cells(j, 8) + 0.044963
Next j

For k = 2 To 858 Step 1
Cells(k, 11) = Cells(k, 10) + 0.044963
Next k

For l = 2 To 858 Step 1
Cells(l, 13) = Cells(l, 12) + 0.233809
Next l

For m = 2 To 858 Step 1
Cells(m, 15) = Cells(m, 14) + 0.53956
Next m

End Sub
```

Figure 82: Code for calculating the pressure head for surfactant foam

4. PECNP-surfactant

```
Sub blah()


Dim j, k, l, m As Integer


For j = 2 To 1293 Step 1
Cells(j, 9) = Cells(j, 8) + 0.0952
Next j

For k = 2 To 1293 Step 1
Cells(k, 11) = Cells(k, 10) + 0.0952
Next k

For l = 2 To 1293 Step 1
Cells(l, 13) = Cells(l, 12) + 0.495
Next l

For m = 2 To 1293 Step 1
Cells(m, 15) = Cells(m, 14) + 1.1424
Next m

End Sub
```

Figure 83: Code for calculating the pressure head for the PECNP-surfactant solution.

5. PEI-surfactant

```
Sub blah()


Dim j, k, l, m As Integer


For j = 2 To 1174 Step 1
Cells(j, 9) = Cells(j, 8) + 0.08604491
Next j

For k = 2 To 1174 Step 1
Cells(k, 11) = Cells(k, 10) + 0.0872
Next k

For l = 2 To 1174 Step 1
Cells(l, 13) = Cells(l, 12) + 0.4536
Next l

For m = 2 To 1174 Step 1
Cells(m, 15) = Cells(m, 14) + 1.0467
Next m

End Sub
```

Figure 84: Code for calculating the pressure head for the PEI-surfactant solution.

6. Surfactant

```
Sub blah()


Dim i, j, k, l, m As Integer

For i = 2 To 1174 Step 1
Cells(i, 7) = Cells(i, 6) + 0.03595
Next i

For j = 2 To 1174 Step 1
Cells(j, 9) = Cells(j, 8) + 0.0898
Next j

For k = 2 To 1174 Step 1
Cells(k, 11) = Cells(k, 10) + 0.0898
Next k

For l = 2 To 1174 Step 1
Cells(l, 13) = Cells(l, 12) + 0.4674
Next l

For m = 2 To 1174 Step 1
Cells(m, 15) = Cells(m, 14) + 1.0608
Next m

End Sub
```

Figure 85: Code for calculating the pressure head for the surfactant foam

7.6 IFT calculation – Correction factor table

The Harking-Browns correction factor table is summarized in Table 24. Depending on the flow rate and duration of CO2 injection, the volume of CO_2 injected can be calculated. Linear interpolation is used to calculate the correction factor for the exact ratio of the radius of the needle to the volume of the CO_2 bubbles injected.

Table 24: Summary of the correction factor for the different ratios of radius of the needle to the volume of the CO_2 bubble.

Radius of needle/(Volume of CO2 injected)^1/3	Correction factor (f)
0.000	1.000
0.300	0.726
0.350	0.701
0.400	0.683
0.450	0.667
0.500	0.652
0.550	0.636
0.600	0.625
0.650	0.617
0.700	0.609
0.750	0.603
0.800	0.600
0.850	0.599
0.900	0.600
0.950	0.603
1.000	0.610
1.050	0.618
1.100	0.628
1.150	0.641
1.200	0.654

The radius of the needle was estimated to be 0.15875 cm. Using the correction factor obtained by linear interpolation, the IFT can be calculated by using the formulas below.

$$\text{Avg Bubble radius} = (3/4 * \pi * \text{volume of bubble})^{1/3}$$

$$IFT = \frac{Avg\ Bubble\ radius * 981 * (correction\ factor - radius\ of\ needle)}{2 * \pi * radius\ of\ needle * correction\ factor}$$